MASTER THESIS
MECHANICAL ENGINEERING

Development of patient-specific finite element models for the simulation of strain adaptive tibial bone remodeling after total knee replacement

I.N. (Inger) van Langen
Student number: 2359251

Faculty of Engineering Technology
Department of Biomechanical Engineering

Examination committee

prof. dr. ir. N. Verdonschot	ET, Biomechanical Engineering	Chair
dr. ir. R. Fluit	ET, Biomechanical Engineering	Supervisor UT
prof. dr.ir. C. Slump	EEMCS, Robotics and Mechatronics	External member UT
dr. ir. D. Janssen	Orthopaedic Research Lab, Radboudumc	Supervisor Radboudumc
dr. ir. T. Bitter	Orthopaedic Research Lab, Radboudums	Supervisor Radboudumc

UNIVERSITY OF TWENTE. **Radboud**umc

i – Abstract

An important factor in failure of total knee replacement (TKR) is periprosthetic bone loss, due to post-operative bone remodeling. An implant in the knee changes the stresses and strains within the knee. As bone adapts to changes of these mechanical loads, according to Wolff's law, TKR will thus lead to bone remodeling.

In this project, the bone remodeling after TKR was studied by finite element (FE) modeling. The first goal was to develop a workflow in which available CT patient data can be used to create patient-specific FE models of the pre- and post-operative tibia which can be simulated with an existing strain adaptive remodeling algorithm. The second goal was to compare the outcomes of these remodeling simulations with clinical dual energy X-ray absorptiometry (DEXA) data.

For this project, 5 patient's pre- and post-operative CT scans from a Japanese dataset were used. For the creation of FE models, an existing workflow was largely adapted. The implant position and orientation in the post-operative scans were extracted and used to resemble the clinical situation in the model. By using the image intensities in the pre-operative CT scans, bone material properties could be assigned to all elements of the models. The loads used to resemble daily activities were from the OrthoLoad dataset and scaled to bodyweight for each of the patients.

The post-operative bone remodeling was simulated to resemble 5 years of clinical time after surgery. The resulting bone mineral densities at 0 weeks, 2 weeks, 6 months, 12 months, 24 months, 3 years and 5 years post-surgery were studied. Virtual DEXA scans were created out of the BMD data and DEXA values of three regions of interest (ROI) were obtained. Those virtual DEXA values were compared to clinical DEXA data at all 7 time points.

In the clinical data the BMD in the medial ROI on average decreased from 0.97 to 0.57 g/cm^2, while in simulations each of the models showed different behavior. Three of the simulations showed an increase in BMD over time and two of the simulations showed a decrease over time. The distal ROI on average had an almost constant BMD value in the clinical data around 0.75 g/cm^2 but did increase from 0.53 to 0.72 g/cm^2 in the simulation results. For the lateral ROI, the clinical data on average showed a decrease of 0.71 to 0.58 g/cm^2 although each of the patients showed different behavior. In the simulations an average decrease from 0.35 to 0.20 g/cm^2 was observed.

The results of patient-specific models used in the strain adaptive remodeling algorithm do not compare with clinical remodeling data. The remodeling algorithm has thus not been proven to work for these models. This can be attributed to a number of uncertainties and assumptions in both the clinical data, like unknown patient activity and measurement errors in the BMD data and in the FE model, like the bone remodeling algorithm, the applied boundary conditions, used alignments and used implant orientations.

Table of Contents

ii – List of Abbreviations

AP	anteroposterior
BMC	bone mineral content
BMD	bone mineral density
BW	bodyweight
CoCr	cobalt-chrome
CPD	coherent point drift
CT	computed tomography
CTU	computer time unit
DEXA	dual energy x-ray absorptiometry
ERC	European Research Council
FE	finite element
FTA	femorotibial angle
HKA	hip knee ankle
HU	Hounsfield units
LCL	lateral collateral ligament
ML	mediolateral
OA	osteoarthritis
PCL	posterior cruciate ligament
PD	posterior-distal
PS	posterior stabilized
ROI	region of interest
RP	rotating platform
SED	strain energy density
THR	total hip replacement
TKR	total knee replacement
UHMWPE	ultra high molecular weight polyethylene
VV	varus-valgus

iii – List of Used Programs

During this project, the following programs were used:

- 3D Slicer (Harvard Medical School, Boston, MA, USA) version 4.11.20210226

- HyperMesh (Altair Engineering, Troy, MI, USA) version 2020

- MATLAB® (The MathWorks Inc., Natick, MA, USA) version: R2020a

- MSC Marc Mentat (MSC Software Corp., Santa Ana, CA, USA): version 2020, models created in version 2007

1 – Introduction

Primary osteoarthritis

Osteoarthritis (OA) is the most common form of arthritis (CDC, 2013). It is a degenerative and progressive disease that affect the joints and because of that causes functional impairment and disability (Mora et al., 2018).Two types of osteoarthritis exist; primary osteoarthritis, which is idiopathic or non-traumatic and secondary osteoarthritis, which is often traumatic or caused by mechanical misalignment (Mora et al., 2018). In this research, all data used was of patients who underwent surgery due to symptoms caused by primary osteoarthritis.

As the knee is a frequently used joint in which loads are high, especially during dynamic activities, where peak loads can be up to 346 %BW while descending stairs and 253 %BW during knee bending (Kutzner et al., 2010), the knee joint is a site on which OA occurs frequently. As the OA advances many structures in and around the knee are affected, causing, among other symptoms, breakdown of cartilage, bone remodeling, weakening of periarticular muscles and degeneration of the ligaments and menisci. It thus affects the complete joint structure. The clinical features are pain, deformity and joint dysfunction (Mora et al., 2018). OA is a progressive and degenerative disease and, currently, there is no treatment to prevent it or slow it down. So at some point, the severity of the symptoms command for joint replacement (Robinson et al., 2016). Elderly females and patients with obesity have the highest risk of developing OA (Jordan et al., 2009). As the trend is that people live longer and the presence of obesity in the population is rising, it is likely that the prevalence of OA will increase in the coming years (Mora et al., 2018).

Total knee replacement

Total knee replacement (TKR) can be performed to relieve pain and improve stability and mobility of the joint. It is performed to improve the quality of life for patients with severe knee osteoarthritis. This procedure is, in most cases, reserved for people with chronic (pain) symptoms that persist after all types of conservative treatments (Cross et al., 2006; Hungerford & Krackow, 1985). Total knee replacement is one of the most successful orthopedic surgical procedures (Sharkey et al., 2014). During the procedure the articular surfaces of the femur and the tibia are removed and replaced by implants. The patella can also be resurfaced.

Failure of total knee replacement

As the total number of total knee replacement rises, so does the number of revision surgeries. In the USA, the number of TKR procedures in 2008 was more than 615.000 and the number of revisions was more than 75.000. It was predicted that the demand for TKR procedures would increase with 673% to a total of more than 3.48 million in 2030 and that the demand for revision surgeries would rise with 601%, also in 2030 (Kurtz et al., 2007). The rising number of TKR surgeries and revision surgeries is due to the aging population and the fact that younger, active patients are also accepted for TKR surgery (Sharkey et al., 2014). Causes of failure of knee replacements are aseptic loosening, instability, infection, polyethylene wear, arthrofibrosis and malalignment, of which aseptic loosening is the dominant cause of failure (Schroer et al., 2013; Sundfeldt et al., 2006). Revision surgery is a time-consuming and expensive procedure. Moreover, it can be dangerous for the patient (Sundfeldt et al., 2006). So, it is desirable to study the mechanisms of failure and improve the success rate of TKR.

Among other factors, the alignment of the knee is found to be a key factor for successful TKR on the long term, since it determines the functional outcome of and survivorship after TKR on the long-term (Barrett et al., 2011; Berend et al., 2004). Implants can be placed in different orientations to create different alignments of the knee. One of the most common alignments is mechanical alignment, in which the post-operative alignment of the knee is neutral, regardless of the pre-operative alignment of the knee. Another common option is kinematic alignment, in which the post-operative alignment is more similar to the pre-operative knee, including deformities. In kinematic alignment the pre-operative situation is thus maintained, while in mechanical alignment the situation is

different from the pre-operative situation and thus load distributions in the bone change. In the past, mechanical alignment has been the standard used in TKR. Mechanical alignment has been shown to lead to medial bone resorption with the risk of failing implants (Jaroma et al., 2016). Also because of that, the placement of implants to get kinematic alignment has been rising in the past years (Cherian et al., 2014) (Rivière et al., 2017). In all patients used in this project, mechanical alignment was applied during surgery (Ueyama et al., 2020).

Implants

In total knee replacement, several types of implants can be used. The tibial component of the implant consists of two parts, the tray and the insert. Those two components and the femoral components can be made of multiple materials. Also, the type of implant can vary, it can be chosen use a cruciate retaining (CR) implant, or a posterior stabilizing (PS) implant. Moreover, the insert can be fixed to the tray or be able to rotate. Also, the tibial and femoral component can be either fixed to the corresponding bones by cementing the component, or using uncemented techniques like press-fitting. Those implants often have a porous surface to improve bone tissue ingrowth (Hanzlik & Day, 2013; Kim et al., 2014).

Total knee replacement can be performed in a cruciate retaining manner, in which, as is in the name, the posterior cruciate ligament (PCL) is retained. The other option is to resect the PCL and use a posterior-stabilized implant, to take over the stabilizing function of the PCL in the knee joint. When retaining the PCL, balance in the joint, kinematics and proprioceptic functions can be maintained (Swanik et al., 2004). However, as total knee replacement is performed on patients with osteoarthritis, the PCL is often also degenerated or even broken (Rajgopal et al., 2014). This demands for a posterior stabilizing solution. A disadvantage of PS TKR is that it may be more vulnerable to laxity of the knee joint compared to CR TKR, which leads to an increased wear of the implant (Perkins et al., 2020). Studies, however, have not shown significant superiority of either the posterior-stabilizing or cruciate retaining procedure (Clark et al., 2001; Jiang et al., 2016; Migliorini et al., 2019; Swanik et al., 2004).

The tibial insert can be either fixed to the tibial tray and be a so-called fixed bearing or have an insert which can rotate in the tray, a mobile bearing. Some mobile bearing implants can move in both anterior-posterior translation and internal-external rotation, but the mobile bearing design used in the data used in this study, a rotating platform (RP) design, can only rotate in internal-external rotation (McEwen et al., 2005; Ueyama et al., 2020). Fixed-bearing implants in combination with cement have shown good survival rates and functional results (Gill & Joshi, 2001; Pavone et al., 2001). However, polyethylene wear, osteolysis and patellar tracking issues are associated with this type of implant (Killen et al., 2020). The use of mobile-bearing implants allow the insert to rotate a maximum of 8.4° to 10.3° degrees, which leads to less contact stresses in the bone (Dennis et al., 2005), improves patellar tracking and allows for self-alignment of the tibial component with the femoral component, allowing for a more anatomical motion (Sawaguchi et al., 2010). For mobile-bearings however, it is required to have well-functioning ligaments and soft tissue structures around the knee (Killen et al., 2020). Concluding, currently, comparable studies between fixed-bearing and mobile-bearing implant have not demonstrated a significant advantage of either of those (Bailey et al., 2015; Killen et al., 2020; Kim et al., 2012).

If the tibial implant is cemented to the bone, two techniques are available, full cementation and surface cementation. Full cementation consists of the cementation of both the tibial cut surface and the stem, whereas surface cementation only covers the tibial cut surface only (Cawley et al., 2012). There is no consensus on which of those techniques works best. Researchers have claimed that surface cementing would be better since the stem is left uncemented, which avoids stress shielding around the keel and therefore the bone mineral density (BMD) is maintained (Hofmann et al., 2006; Skwara et al., 2009). Others argued that full cementing is better as cementing the keel decreases the possibility for micromotions around the stem and thus creates more stability on the long term (Bert & McShane, 1998; Luring et al., 2006).

Apart from the discussion on how to cement implants, one can also use completely uncemented techniques to fix the implant to the bone. The pre-operative bone quality is important for the chosen fixation of the implant (Li & Nilsson, 2000b). For uncemented implant, good metabolite properties and high quality bone is needed (Matassi et al., 2014) A drawback of this technique is that it is three times more expensive than cemented implants (Matassi

et al., 2014). Cemented implants ensure a greater stability and can be used for the delivery of antibiotics, but it also has some drawbacks. Wear of the cement can occur, resulting in release of particles in the joint (Matassi et al., 2014). Also, during the polymerization of the cement, the surrounding tissue can be damaged because of the exothermal reaction (Khandaker & Meng, 2015) and surgeries with cemented implants take more time than those without cement as the cement has to be prepared (Matassi et al., 2014). It is not proven that either cemented or uncemented implantations are better in terms of clinical outcomes or looking at long term survival rates (Matassi et al., 2014). In the patient population of this project all implants were fully cemented (Ueyama et al., 2020).

For the used bone cement and implant components, several choices in materials and for the implant also in design can be made. Multiple studies have been performed, using the finite element (FE) method, on what material properties are desirable to transfer the loads through the implant into the bone optimally and avoid stress-shielding. Stress shielding is the phenomenon in which the post-operative periprosthetic bone is unloaded compared to the preoperative situation. Since the implant material has a higher Young's modulus than bone, the periprosthetic bone surrounding the implant is unloaded relative to the preoperative situation. Au et al. found that a relative high Youngs modulus of the implant material compared to bone is not the primary cause of stress shielding, but that the loading condition, load placement, implant geometry and load pattern are more important factors (Au et al., 2007). Another FE study, however, showed that the material was more important than the implant geometry (Zhang et al., 2016). In this study, it was found that use of an all polyethylene implant was favorable for the bone mineral density, especially just below the tibial tray. In metal backed implants the stress shielding occurred significantly whereas in the all-polyethylene implant, the stress shielding was mostly low. However, it was also found that metal-backed design performs better during more active behavior compared to all-polyethylene implants (Brihault et al., 2016). In another FE study, Enab et al. showed that a new material with gradually changing Young's modulus in vertical direction is favorable over the standard implant materials titanium and cobalt-chrome, as it gave better stress distributions in the bone (Enab & Bondok, 2013). The effect of material and implant design on periprosthetic bone resorption was also studied by Yoon et al. They found that implants of cobalt chrome led to more bone resorption in comparison with titanium implants, when the implant designs were equal. Also medial tibial bone resorption was found to be greater in cobalt chrome implants than in titanium implants (Yoon et al., 2018). As shown by these studies, the optimal material to use was not found yet. The tibiae used in this project all contained a rotating platform mobile-bearing implant (Ueyama et al., 2020).

Bone, bone remodeling and bone mineral density

Bone is a mineralized connective tissue which is capable of adapting itself to circumstances. According to Wolff's law, the bone adapts to external mechanical loads. This adaptation, called bone remodeling, can be in the form of either bone resorption or bone formation. If there is an increase in load, the bone is formed and if the load decreases the bone is resolved (Stock, 2018). The bone in the proximal tibia is crucial to provide mechanical support to the tibial tray and bearing after TKR. This bone should thus have enough strength to provide fixation for the tibial components of the implant (Li & Nilsson, 2000b). However, as post-operatively stress-shielding can occur, and loads in the periprosthetic bone decrease, the bone can be resorbed. This can result in aseptic loosening or fracture of the bone (Sundfeldt et al., 2006). So, studies investigating the causes of stress-shielding and how to prevent it are crucial.

The bone mineral density (BMD) [g/cm^2] is a bone quality measure. The minerals hydroxyapatite and calcium make up about 60-70% of the bone composition and the density of these minerals is used to measure the quality of the bone (Boskey, 2013). The bone mineral density measured in the bone mineral content (BMC) per area, so [g/cm^2]. Bone quality is an important factor for a successful TKR. The bone mineral density of the bone after TKR can be assessed with dual energy x-ray absorptiometry (DEXA) scans.

Dual energy x-ray absorptiometry (DEXA) is a technique to quantify the bone mineral density (BMD).The BMD in the proximal tibia is of interest since it can be used to study bone remodeling after total knee replacement (TKR). A change in BMD shows bone adaptation, possibly an effect of the TKR. The use of DEXA scans is favorable over the use of x-ray to quantify BMD, since DEXA can be used to quantify changes in bone density in its

evolution over years whereas x-ray can only detect those changes when 40% of the bone is left (Engh et al., 2000).

A limitation of DEXA is that the scans are two-dimensional. DEXA does not show the actual bone mineral density values, but the sum of all values in the scanned area (Herrera et al., 2007) and thus, the volume of the scanned bone, is influenced by the volume and size of the bone.

DEXA is the preferred method for assessing the BMD in clinical practice. It is precise, accurate and scans are easy and fast to make (Li & Nilsson, 2000b). Also, studies have shown strong correlation between BMD in human trabecular bone and bone strength (Carter & Hayes, 1976; Mosekilde et al., 1987)

Bone remodeling theories

There are several bone remodeling theories that describe how the bone reacts to stresses and loads, like described in Wolff's law. One theory from Bingzhi et al. uses the strain energy density as optimality criteria method (Bingzhi et al., 2009). Strain energy density was used as a feedback mechanism for bone remodeling in the theory of Huiskes et al., 1987. Other factors for bone remodeling, for example the stress (Carter et al., 1996) and strain (Hart et al., 1984; Stülpner et al., 1997; Zhang et al., 2016) were also studied. Also, non-uniformity in stress distribution is considered in bone remodeling theory (Adachi et al., 1997). S. C. Cowin & Hegedus, 1976 proposed a theory in which bone is seen as an elastic porous solid which reacts to local strains and remodels by normalizing these local strains. Each of those theories describe factors that could influence the bone remodeling process, but there is no consensus about what factor or combination of factors really affect bone remodeling.

Computational bone remodeling simulation

With finite element (FE) models, the effect of each of these mechanical factors can be examined. In this project, strain energy density (SED) is taken as mechanical stimulus for remodeling of both the surface of the tibia as for the internal remodeling, as was proposed by Huiskes et al., 1987. Research has not shown the effect of only SED on bone remodeling, but the SED values can be considered to represent the recent loading history (Huiskes et al., 1992). Using a strain adaptive finite element model, the bone remodeling of tibiae after TKR will be modelled and compared with bone mineral density (BMD) data from DEXA scans.

The model created is a finite element model. These models can be used to simulate the effect of bone alignment and implant size, design, material and orientation on bone remodeling (García et al., 2002; Park et al., 2021). Also, these models are used to test various bone remodeling theories to see which of those theories resembles the biology best (Gong et al., 2014; Stülpner et al., 1997; Turner et al., 2005). Simulations can be made patient-specific and can be used to find out what parameters are the best fit for each patient.

Strain adaptive remodeling

The used algorithm uses the strain energy density values per unit bone mass. In the algorithm, the local pre- and post-operative SED values are compared. The local pre-operative SED value is displayed as S_{ref} and the local post-operative SED as S. The difference between those is the stimulus for bone remodeling, displayed with $\left[\frac{\partial \rho}{\partial t}\right]$.

If the relative difference is smaller than 35% a dead-zone is reached and no remodeling takes place. If the relative change is more than 35%, in case S_{ref} is larger than S, bone resorption occurs and in case S is larger than S_{ref}, bone formation takes place. Also, the available surface, a, determined by porosity and specific surface, is of importance (Martin, 1984), since the remodeling takes place at the surface of bone. The used dead-zone of 35% was studied by Tarala et al., 2011. In that study, FE simulations of femoral hip implant periprosthetic bone remodeling were used. By fitting FE simulations with this strain adaptive remodeling algorithm to clinical data set of 2 years follow-up, they found that a dead-zone value of 35% in combination with a time unit of 60 gave the best simulation results. The time unit of 60 means that 60 computer time units (CTU) resemble the clinical time of 2 years. So each 30 CTU correspond to 1 year clinical reality. These time units were also used in this project.

In Equation 1, on the next page, the bone remodeling rate, according to the description above, is shown. This equation was adapted from Anijs et al., 2020. It follows the strain adaptive theory of Huiskes et al., 1987.

$$\left[\frac{\partial \rho}{\partial t}\right] = \begin{cases} 0 & if \quad |S/S_{ref} - 1| < 0.35 \\ a(\rho)\{S - 1.35 \cdot S_{ref}\} & if \quad S/S_{ref} - 1 \geq 0.35 \\ a(\rho)\{S - 0.65 \cdot S_{ref}\} & if \quad S/S_{ref} - 1 \leq -0.35 \end{cases} \tag{1}$$

Personalized models

In this project, patient-specific finite element models were created to research the effect of TKR on bone remodeling. Of all subjects pre- and post-operative computed tomography (CT) scans were available, as well as DEXA results to compare modeling results with clinical data. Since post-operative data of all subjects was available, the exact orientation, location and size of the implant was known. Thus, the patient-specific models could have the geometry and mechanical properties of the tibia and the location, orientation and size of the used implant could be extracted from the post-operative CT scans and applied in the model. Strain adaptive finite elements models were used to investigate the effect of the placement of an implant onto the tibia on bone remodeling in the proximal tibia. With the patient-specific finite element models and available DEXA data, the bone remodeling outcomes of the strain adaptive algorithm could compared to clinical data.

To the authors knowledge, strain adaptive remodeling FE models of the tibia in which the patient-specific implant orientation is used, were not validated before. Similar research on the strain adaptive remodeling algorithm was performed by Anijs et al., 2020 and Chong et al., 2011, before, but those results were not validated with clinical data, and the models were not patient-specific. Validation of the strain adaptive remodeling algorithm was performed by Anijs et al., 2021, but the patient-specific implant-orientation and DEXA values were not known in that study. To be able to create FE models of the tibiae of the patients with patient-specific implant orientation, the workflow that was created by Anijs et al., 2020, was largely adapted. To the authors knowledge, such a workflow did not exist yet.

Workflow

To create finite element (FE) models of the patient data and to be able to perform calculations on these models, a workflow was used to get the CT data to a FE model on which bone remodeling simulations could be performed. To do so, first the CT images were segmented to extract the tibial bone. Then, the segmentations were converted to surface meshes. The pre-operative mesh data was then rotated to the ERC reference frame and the post-operative mesh including the implant was registered over this rotated pre-operative mesh. In this way, the implant was on the correct place and orientation on the pre-operative tibial mesh. Lastly, the implant geometry was registered towards the segmented implant and as a result the implant geometry was placed in the correct place and orientation on the pre-operative tibial mesh, as was surgically done. Then some steps were taken to place the implant geometry on the tibial bone and remove the excess bone. Then, with air-fat-muscle calibration method (Eggermont et al., 2019), the BMD values were assigned to each of the elements. The models were completed by applying the loads of OrthoLoad (Bergmann et al., 2014), scaled to body weight to the models.

These models were then simulated with the strain adaptive remodeling algorithm. The resulting BMC values per element were converted to virtual DEXA scans and BMD values were extracted from those virtual DEXAs. Those BMD values were then compared to the clinical BMD data.

Study goals

This research project assessed two goals. These goals were:

1. To create patient-specific finite element models based on pre- and post-operative TKR CT data and use those models to study the effect of knee replacement on the bone remodeling in the proximal tibia.

2. To validate the computational remodeling algorithm by simulating bone remodeling in the created patient-specific models and comparing the results with the clinically measured bone mineral densities of the patients tibia, acquired with dual energy x-ray absorptiometry (DEXA).

2 – Methods

In this section the dataset used and the methods used for creating models out of the data are described. Furthermore, the methods for simulating the models used in this project and post-processing the simulation results are described.

Patient data

The data used in this research is obtained at the Osaka City University Graduate School of Medicine, Japan. The dataset consists of CT scans of 30 primary osteoarthritis patients who underwent simultaneous bilateral total knee replacement between December 2007 and September 2012. Pre-operatively, all patients had varus deformity. There were no patients with medical conditions that could affect bone metabolism, like diabetes mellitus or chronic kidney disease (Ueyama et al., 2020).

All operations were performed by the same surgical team and with the same surgical technique. During surgery all patients received one mobile-bearing implant (Vanguard RP; Zimmer-Biomet, Warsaw, IL, USA) and one fixed-bearing implant (Vanguard PS; Zimmer-Biomet, Warsaw, IL, USA). It was determined by the surgeons which implant was used in which knee. In all patients mechanical alignment was applied. All components were cemented (Ueyama et al., 2020).

Due to time restrictions, it was decided to focus on the mobile-bearing implant. Of all 30 patients, the data of 13 patients could have been used. For these 13 patients, pre- and post-operative CT scans of the tibia in which the mobile bearing implant was placed were available. For the other patients, either the pre-operative or the post-operative CT scan or neither were available. In this project, five tibiae from this dataset were used, all with a mobile-bearing implant. In Table 1 information about the used data is displayed.

Table 1: Parameters of the five tibiae used in this project

Number of knees	5 [-]
Laterality (Left / Right)	3 / 2
Age	71.8 ± 6.5 [years]
Gender (Male / Female)	0 / 5
Height	149 ± 4 [cm]
Pre-operative body weight	60.9 ± 7.4 [kg]
Pre-operative scan, days before OR	102 ± 67 [days]
Pre-op FTA	187± 3 [°]
Pre-op HKA	13 ± 3 [°]
Post-operative scan, days after OR	17± 2 [days]
Post-op FTA	174 ± 2 [°]
Post-op HKA	2 ± 1 [°]
Follow-up period (operation day till final observational day)	64.4 ± 5.3 [months]

During the follow-up period of 5 years, there were no cases of loosening, migration or failure of the implant or periprosthetic fracture, aseptic loosening or infection in the tibia.

Implants used

In this research patient data in which the Vanguard® Complete Knee System (Zimmer-Biomet, Warsaw, IN, USA) was used, is evaluated. In this project only the tibiae with a mobile-bearing are studied.

Various tibial tray thicknesses and implant sizes have been used, see Table 2 :

Table 2: Sizes of used trays and insert per tibia

	Tray size [mm]	Insert size [mm] / thickness [mm]
No14	71	67.5 / 10
No15	67	62.5 / 12
No16	63	60 / 12
No19	71	60 / 12
No20	59	57.5 / 10

CT and DEXA data

The CT scans were taken with a wide variability of days before surgery, with 1 day as the shortest period before OR and 191 days the longest. The post-operative CT scans were taken at a more consistent moment, either 15 of 19 days post-surgery.

DEXA scans of the tibia were acquired 2 weeks, 6 months, 12 months, 24 months, 3 years and 5 years post-operatively. Several regions of interest were scanned. In this research two proximal regions of interest, one on the medial and one on the lateral side, and one distal region of interest were used.

Load cases

The load cases used in this project are from the Standardized Knee Loads OrthoLoad data set (Bergmann et al., 2014). In the OrthoLoad study, contact forces and moments in the knee joint during various activities were measured with instrumented implants in 8 patients. It was decided to choose three load cases to resemble the activity in daily living. The chosen activities are gait, knee bending and walking stairs down. For each of the activities, the peak load during the activity, averaged over all measured patients in the OrthoLoad study was used. For all activities the loads in anteroposterior, mediolateral and posterior-distal were applied, as well as the varus-valgus (VV) moment. The loads were scaled to the bodyweight of each of the patients.

Workflow

In this project a workflow was used to process all CT data and create patient-specific finite element models of the CT data. These models could be used to simulate bone remodeling. The simulation results could then be compared to post-operative patient data. In this workflow, the tibia was segmented out of the CT scan, then the correct implant orientation was found and the implant was placed onto the bone model in that orientation. Then the bone material properties were assigned to the model and, lastly, the load cases and boundary conditions were applied to the model. A complete overview of the practical steps taken in each step of the workflow can be found in Appendix A and an overview of all scripts needed to create models is given in Appendix B.

This workflow was created and used before by Anijs et al., 2020 and was largely adapted for this project.

1 – Segmentation

In the first step of the workflow, the tibiae geometries of the subjects were extracted from the CT data. In this step the pre-operative CT, post-operative CT including the implant and the implant itself are segmented.

First, the DICOM folders of each patient were converted to single files. In this conversion the CT image was cropped around the tibia to decrease computational time. The files used for the segmentation of the post-operative tibia and the segmentation of the implant were cropped in the exact same place, to make sure the implant was in the same position and orientation in both segmentations. All created cropped files were then automatically segmented via an auto segmentation program. This auto segmentation program is based on

methods described by Krčah et al., 2011. In this method, the bones are segmented with graph-cut segmentation and boundary enhancement. In this segmentation program, masks of the tibia geometries are created for each of the input files.

Each of the autosegmented masks was adjusted manually in 3D Slicer (Harvard Medical School, Boston, MA, USA) (Kikinis et al., 2014) so that any parts of the femur, fibula, patella or other unwanted parts were deleted from the mask and only the tibia will be segmented. This was done by means of intensity based segmentation.

The tibiae in these files were sometimes deformed since the resolution and slice thickness were not imported correctly by 3D Slicer. Therefore the file was more scaled in width than in the length of the tibia. The triangle elements created by 3D Slicer were also very small, about 0.5 mm. So both the scaling and the element size were adjusted in the third step of the workflow.

2 – Implant preparation

In the next step of the workflow, the implant models were prepared for use in the rest of the workflow. The models of the implant, called implant geometries from now on, were created by Zimmer-Biomet (Warsaw, IN, USA). The geometries of all used sizes and types of tibial trays, inserts and femoral components were supplied by Zimmer Biomet. These were used in the FE simulations of bone remodeling.

The tibial tray geometry was also used to create an artificial cement layer to resemble the actual post-operational situation in the model. To reconstruct the clinical tibia-implant combination after surgery in a FE model, the tibial mesh was cut proximally, to fit the implant and cement layer onto the tibia, see Figure 1. Appendix A.3 contains an in depth description of the preparation of these model components.
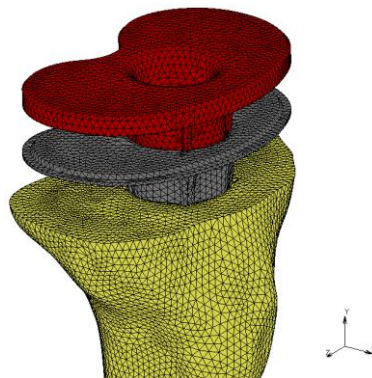
Figure 1: tibial tray (red), artificial cement layer (grey) and cut tibia (yellow)

3 – Rotation and Registration

In the third step of the workflow, the meshes were rotated to fit the implant on the pre-operative tibia. First, the mesh was scaled to its original size and remeshed to 1st order triangle elements with a size of 2 mm.

The tibia needed to be oriented in a correct reference frame to be able to correctly apply OrthoLoad loads to the tibia. To achieve this, the ERC reference frame was used. This mechanical reference frame, used the mechanical axis in line with findings of Grood & Suntay, 1983, and with the medial third of the tibial tuberosity in anterior direction as neutral rotational alignment (Lützner et al., 2010). In this frame, X points in anterior direction, axis, Y in superior, along the largest inertial direction and Z completes the right handed system, as is shown in Figure 2.
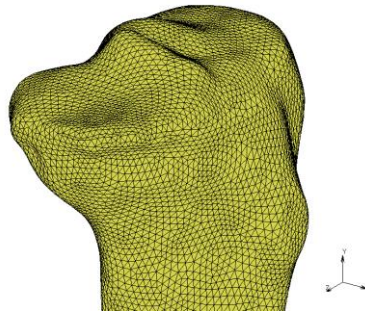
Figure 2: Tibial mesh oriented according to the ERC reference frame

To resemble the clinical orientation of the implant on the tibia of the patient, the implant orientation in the post-operative scan was used. By registering the post-operative model, including the segmented implant (Figure 3), onto the pre-operative model, the implant was placed in the correct orientation and position on the pre-operative tibia (Figure 4). Then, by registering the implant geometry to the segmented implant (Figure 5), the implant needed for the model was in the right position and orientation on the tibia (Figure 6). The registration of the post-operative tibia onto the pre-operative tibia and of the implant geometry onto the segmented implant was done with the coherent point drift (CPD) algorithm integrated MATLAB®. With the CPD algorithm two point clouds were registered to each other. In this case, the point cloud of post-operative tibia was registered to the point cloud of the pre-operative tibia. The registration was via a rigid transformation in this case. So, the spatial transformation applied to align the point clouds consisted of a rotation and a translation only.
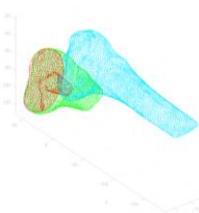
Figure 3: pre- (blue) and post-operative(green) bone including segmented implant (red)
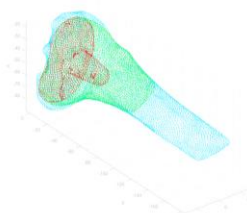
Figure 4: post-operative bone (green) including segmented implant (red), registered to pre-operative bone (blue)
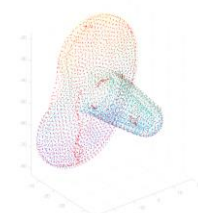
Figure 5: implant geometry (multicolor) registered to segmented implant (red)
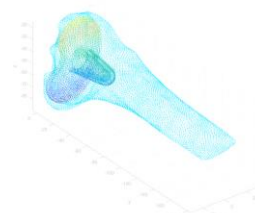
Figure 6: implant geometry (multicolor) in correct orientation on pre-operative bone (blue)

The result of this step was thus a file of the pre-operative tibia, oriented according to ERC standards and an implant model which was oriented in the correct position relative to the pre-operative tibial mesh.

4 – Bone cutting

In the fourth step of the workflow, the bone cutting was performed. In this part, the tibial mesh was cut both distally and proximally. For the proximal cut the rotated implant geometries were used, to create a cut with the correct shape for the artificial cement layer and implant geometry to fit. The distal cut was made 150 mm distal to

the proximal cutting line. The bone cutting was performed in HyperMesh (Altair Engineering, Troy, MI, USA). In model specific scripts, all commands for the bone cutting in HyperMesh were given automatically. The bone cutting resulted in two parts, the distal part of the tibia and the proximal part, together forming the tibia, which could be used for the pre-operative model. The proximal part was removed in the post-operative model for the placement of the implant geometry. The distal and proximal parts are shown in Figure 7.
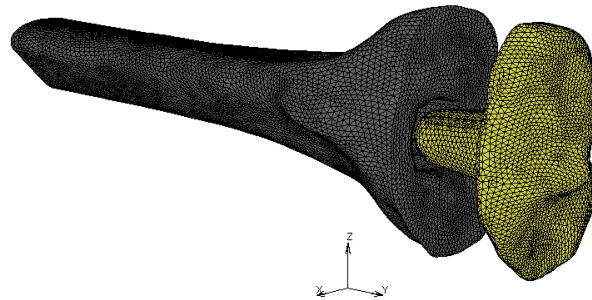
Figure 7: Distal part (grey) and proximal part (yellow), after bone cutting, proximal part is moved in Y direction for clarity.

5 – Material assignment

To perform optimal simulations, it was desirable that the patient-specific bone material properties were applied to the model. To do so, each element was given its own bone mineral density and Young's modulus. Since no calibration phantoms in the CT data were available, the air-fat-muscle calibration tool created by Eggermont et al., 2019 was used. With this tool, all elements in the pre-operative mesh got a BMD value, based on the corresponding CT intensities (Powell, 2015; Powell & Abel, 2015). By scaling the Hounsfield Units (HU) in the CT scan to the intensities of air, fat and muscle in the CT scan, the HU intensities could be linked to bone mineral densities. Moreover, with the bone mineral densities, the elastic modulus in each of the elements were calculated with modulus-density relationships as studied by Keller, 1994 for cortical bone and Morgan et al., 2003, for trabecular bone.

As both the pre- and post-operative models were made out of the pre-operative tibial mesh, the materials were assigned to the elements of the pre-operative mesh.

The mobile bearing tray used is made of cobalt-chromium-alloy (CoCr), for which an elastic modulus E of 210 GPa and a Poisson's ratio of 0.3 were used in the models. The insert is made of Direct Compression Molded Polyethylene Ultra High Molecular Weight Polyethylene (UHMWPE)(Xie, 2011), with an elastic modulus of 588 MPa and Poisson's ration of 0.49 used in this model. The material properties of the cement layer in the model were an elastic modulus E of 2551 MPa and a Poisson's ratio of 0.4.

6 – Model set-up

From this step in the workflow, the difference between the pre- and post-operative model was made. Both models were created in MSC Marc/Mentat (MSC Software Corp., Santa Ana, CA, USA).

To distribute the point load of the OrthoLoad data over the medial and lateral condyles in the pre-operative model, a control node was used. The control node was at the center of the keel and at the height of the lowest point in the condyle of the insert, if the insert was placed onto the tibia. This position was chosen since the origin of the OrthoLoad coordinate system is at that point, see Figure 10. Stiff springs (10e+09 [N/m]) were used between the control node and the medial and lateral surfaces of the pre-operative condyles to distribute the load over the condyles, see Figure 8.
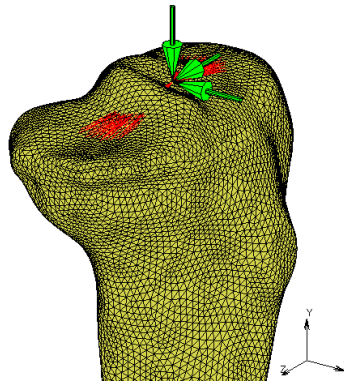
Figure 8: Pre-operative model with springs (red) distributing the point load (green)

In the post-operative situation, due to physically impossible results in simulations, it was chosen to leave out the tibial insert. The loads were placed directly onto the tibial tray with two point loads; one medial, in the center of the area in which the springs were attached in the pre-operative situation, see Figure 9.
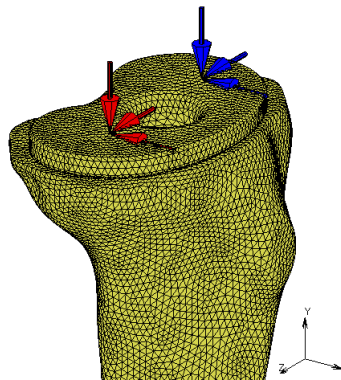
Figure 9:Post-operative model with two point loads, medial (red) and lateral (blue) directly on the tibial tray

As the OrthoLoad data is measured in the middle of an implant's keel at the height of the lowest point in the condyle of that implant, see Figure 10, the medial and lateral forces in the model had to be recalculated. The axial force in the medial condyle could be calculated with Equations 2 and 3, with F_z the total axial force on the tibia, M_y the moment around F_y, which is in anterior direction and l, the distance between F_z and the place of the medial force, F_{med} (Kutzner et al., 2010). The anteroposterior and mediolateral forces from OrthoLoad were spread evenly over both point loads. Note that this coordinate system is different from the ERC reference frame. The forces scaled to body weight applied to each model, which was in the ERC frame and thus has different orientations for X, Y and Z are displayed in Table 3. The absolute values are shown in Appendix C.

$$F_{med} = \frac{-F_z}{2} - \frac{M_y}{l} \tag{2}$$

The axial force in the lateral condyle was then calculated with

$$F_{lat} = F_z - F_{med} \tag{3}$$
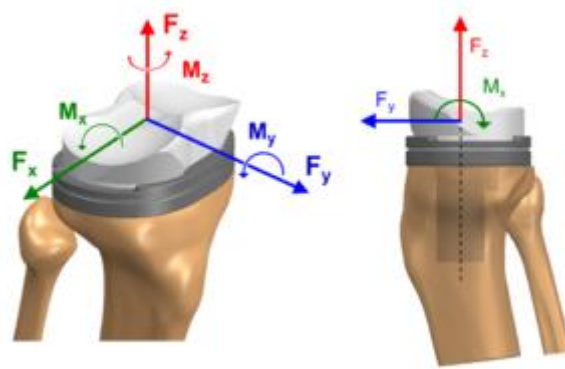
Figure 10: Coordinate system of OrthoLoad data, with the origin in the middle of the keel at the height of the lowest point condyle (Bergmann et al., 2014; OrthoLoad Database, 2021)

Table 3: loads applied to the model in percent body weight

activity	Medial and Lateral X (AP) [%BW]	Medial Y (PD) [%BW]	Lateral Y (PD) [%BW]	Medial and Lateral Z (ML) [%BW]
No14 Gait	-0.70	238.82	27.60	-2.91
No14 Knee bend	2.43	89.54	173.53	-0.52
No14 Stairs down	-0.49	225.81	112.91	2.59
No15 Gait	0.70	222.46	43.96	-2.91
No15 Knee bend	-2.43	96.05	167.02	-0.52
No15 Stairs down	0.49	217.07	121.66	2.59
No16 Gait	0.70	217.56	48.86	-2.91
No16 Knee bend	-2.43	97.99	165.07	-0.52
No16 Stairs down	0.49	214.45	124.28	2.59
No19 Gait	0.70	207.24	59.18	-2.91
No19 Knee bend	-2.43	102.10	160.97	-0.52
No19 Stairs down	0.49	208.93	129.79	2.59
No20 Gait	0.70	229.99	36.44	-2.91
No20 Knee bend	-2.43	93.05	170.02	-0.52
No20 Stairs down	0.49	221.09	117.63	2.59

Simulation

Pre-operative simulation

First, all pre-operative models were simulated via a custom Fortran subroutine. These simulations were performed to create a baseline measure for the remodeling algorithm. With the input BMD values and the applied load cases, the BMD values and Youngs moduli per element were calculated and with those, the reference strain energy density for the post-operative simulation was calculated in this simulation. The BMD values and Young's moduli per element are output and used as an input for the post-operative simulation.

Post-operative simulation

In the post-operative simulation the BMD and Young's modulus calculated in the pre-operative simulation were assigned to each of the elements. During the simulation, the load case of three alternating activity levels was applied repeatedly. With the strain adaptive algorithm, in each iteration, the strain energy density is calculated for each element and compared to the reference value of the pre-operative simulation. If the difference passes the threshold value of 35%, remodeling takes place. If remodeling takes place, the bone properties are adjusted and the new Youngs modulus and the strain energy density are calculated for this new situation. Then, after another increment, the new BMD is again compared to the reference value and new properties are calculated per element. As explained before, 150 CTU is simulated to resemble 5 years of clinical time. In the simulations, the computational time that passes per increment is dependent on the maximum difference between the current SED and the reference value. If the difference is in SED is small, larger time steps are used, but if the difference is small, the time passing per increment is decreased, to assure for detailed bone remodeling calculations.

Three simulations were performed per post-operative model. In each of those three simulations of each model the point loads were placed differently. In the first, original simulations denoted with (1), the node in the middle of the pre-operative springs was chosen, like displayed in Figure 9. In the second simulation (2), the point loads were both placed about two elements distance posterior compared to the first simulation. In the third simulation (3), the point loads were placed about two elements distance lateral to the tibial axis, compared to the first simulation. The different simulations are all shown in one image in Figure 11.
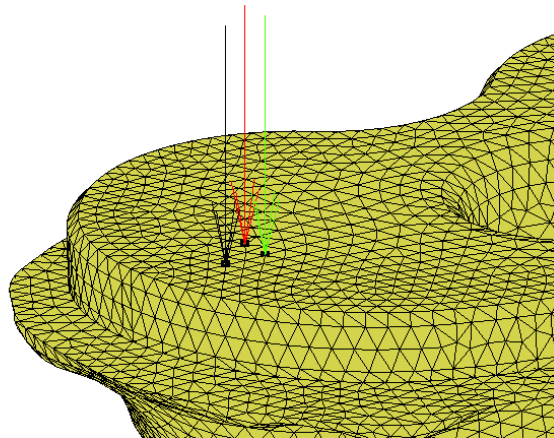
Figure 11: Different positions of the point loads in 3 simulations. The original placement of point load (1) in green, two elements posterior (2) in red and two elements lateral (3) in black

Post-processing

The virtual DEXAs were made by creating a three dimensional matrix in which BMD values of the elements were given. The model was converted to a matrix by using voxels of 0.2 x 0.2 x 0.2 mm. Then, all BMD values in anteroposterior direction were summed, resulting in a two dimensional matrix. By plotting this matrix in grey values a virtual DEXA in AP direction was created. To allow for the assessment of the BMDs in posterior and anterior regions, virtual DEXAs in mediolateral directions were created as well.

Then, the virtual DEXA scores in three regions of interest were extracted to compare with clinical DEXA scores in those same regions of interest (ROIs). Those regions of interest were in agreement with the definition of Minoda et al., 2010. In this definition, the regions of interest are all taken in anteroposterior direction. ROI 1 is 1 cm under the medial side of the tibial tray, ROI 2 is in the center of the tibia, under the keel, 4 cm under the tibial tray and ROI 3 is 1 cm distal to the lateral side of the tibial tray. All regions of interest are 1 cm^2. The regions of interest are visualized in Figure 12.
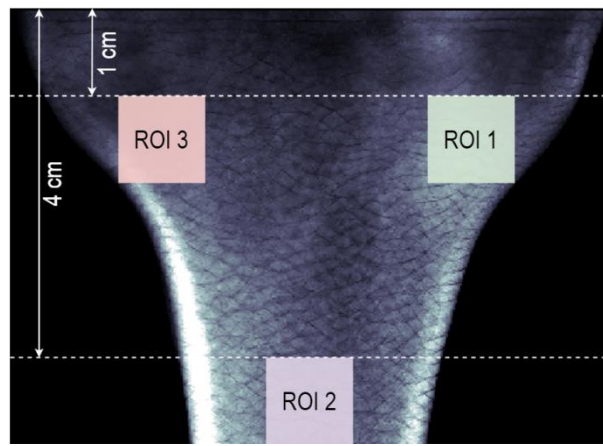
Figure 12: Visualization of regions of interest (ROIs) in a virtual DEXA scan used in post-processing, with ROI 1 medial, ROI 2 distal and ROI 3 lateral.

3 – Results

Model

The models resulting from using the created workflow are displayed in Figure 14. Models No14 and No19 are made of the right tibia of the corresponding patients and No15, No16 and No20 are made of the left tibia. For the descriptions of the angles of the tibial components on the tibia, the convention as described by Watanabe et al., 2021, is used, see Figure 13. Angle beta (β) is the medial angle in AP view between the tibial tray and the anatomical axis of the tibia. Angle delta (δ) is used to describe the posterior angle in ML view between the tibial plateau and the anatomical axis. From the AP views Figure 14 can be seen that models No14 and No19 were placed with an angle β smaller than 90 degrees. No16 and No20 have a β angle slightly smaller than 90 degrees. The implant in model No15 was placed with a β angle a bit larger than 90 degrees. Also, in mediolateral view, it is shown that models No15 and No16 have a δ angle smaller than 90 degrees, while No14 and No19 have a δ angle of more than 90 degrees and No20 has an angle of 90 degrees.
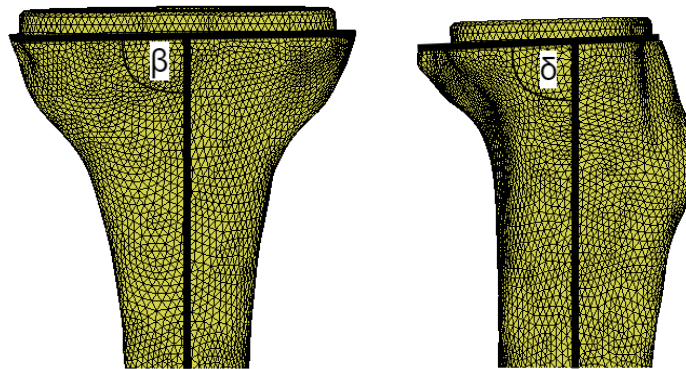
Figure 13: Visualization of beta (β) and delta (δ) angle as described by Watanabe et al.

In the anteroposterior (AP) view (second column) the placement of the implant is shown to be skew to the medial side for both models No14 and No19. In both models the implant protrudes from the tibial surface on the lateral side of the bone and the keel is close to the lateral cortex.

In the third column, the placement of the control node and the attachment of the springs in the pre-operative model are shown. These attachments were manually chosen on the lowest sites of both the medial and lateral condyle of the tibial surface. The amount of nodes selected varied between 75 (No19) and 126 (No16) nodes. The nodes were selected by hand, and approximately the same area was covered in all models. Some of the areas contained more nodes than others, since the elements were locally smaller in some of the models, leading to more nodes in the same area. In model No15 and No19 the nodes selected are more to the edges of the tibial surface, as the lowest points of the condyles were located more towards the edges. In the other three models, de areas selected are closer to the center of the surface. The control node is approximately in the middle of the two attachment areas in all models.

In the fourth column, the locations of the point loads are depicted. The point loads in the post-operative model were placed in the center of where the selected nodes for spring attachment in the pre-operative model were. In most models, the medial point load is about as close to the keel as the lateral point load, except for model No14 and No19, where the lateral point load is closer to the keel than the medial one. This was necessary since the implant is placed skew to the lateral side in these models, when the orientation of the implant is extracted from the post-operative CT scans. The lateral point load would have been placed very close to the edge of the tibia if it was placed at the same distance from the keel as the medial point loads. The point loads are all a little posterior to the middle of the keel, with the lateral point load a bit more posterior compared to the medial one in No14, No16 and No19.
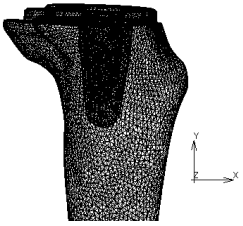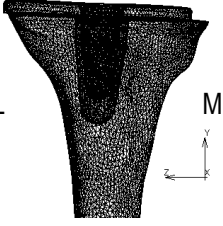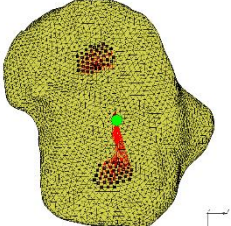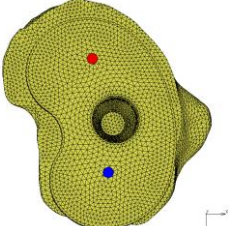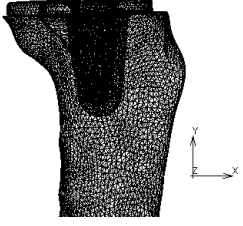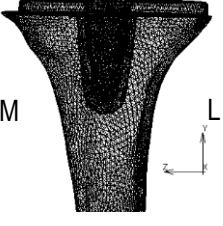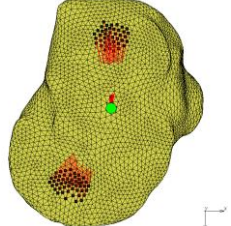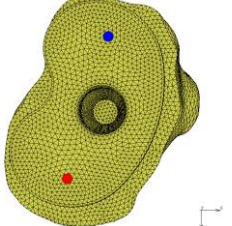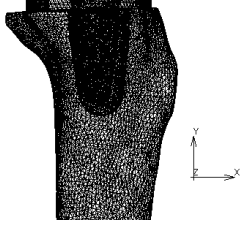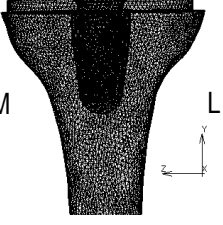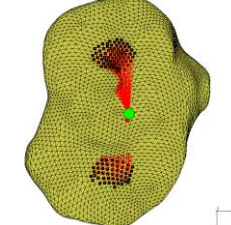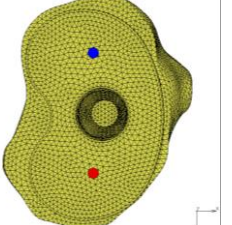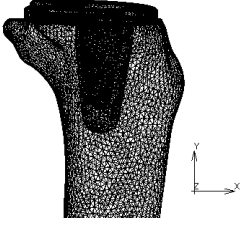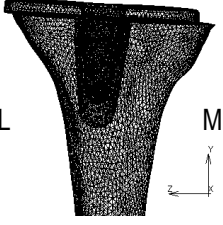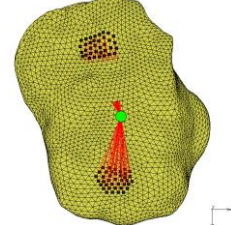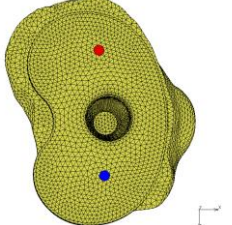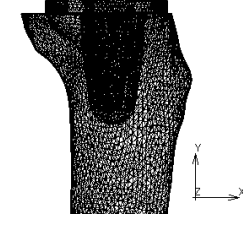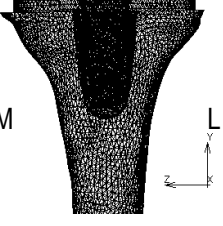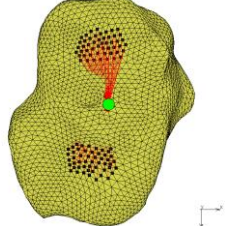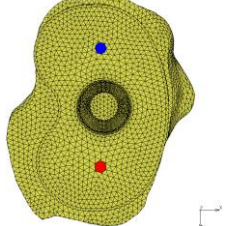
	Implant orientation ML view	*Implant orientation AP view*	*Pre-operative control node and spring attachment*	*Post-operative placement point-loads*
No14		L M	Number of nodes used: 87	
No15		M L	Number of nodes used: 95	
No16		M L	Number of nodes used: 126	
No19		L M	Number of nodes used: 75	
No20		M L	Number of nodes used: 102	

Figure 14: Model workflow outcomes; from left to right: ML and AP view of the implant orientation on the bone, the pre-operative model in PD view with the control node in green and nodes at the surface used to connect the springs in black, the posterior model in PD view with the medial point load location in red and the lateral point node location in blue.

18

Virtual DEXA scans

For the analysis of the simulation outcomes, virtual DEXA images were created. These virtual DEXA images could be used to both analyze the bone remodeling visually and acquire BMD values from the same regions of interest as used in the clinical data. These virtual BMD values could then be used to compare FE results with clinical outcomes.

The virtual DEXA scans were created at the same time intervals the clinical DEXA scans were created, so at 2 weeks, 6 months, 12 months, 24 months, 3 years and 5 years post-operatively. Also, for comparison with the pre-operative situation, a virtual DEXA of the pre-operative situation, was created. All virtual DEXA images are shown in Appendix D. As the BMD in the distal region is highest, the grey values were scaled such that differences in the proximal medial and lateral region were also visible. In the Figures 15 – 29 on the next page, the virtual DEXA scans of all patients in anteroposterior view at three time intervals are displayed. The virtual DEXA images of the pre-operative tibia, 6 months post-operation and 3 years post-operation are shown. At these time intervals the changes in BMD are most clearly visible. The higher the intensity of the pixel shown, the higher is the BMD value of that pixel. In these figures, the medial sides is marked with "M" and the lateral side is marked with "L".
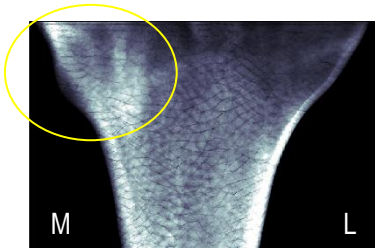
Figure 15: pre-operative
No14 AP view
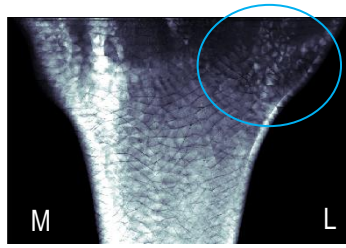
Figure 16: 6 months
No14 AP view
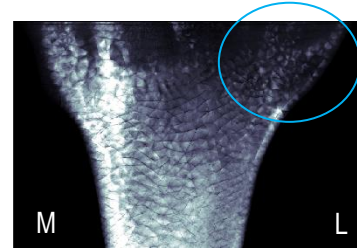
Figure 17: 3 years
No14 AP view

Figure 18: pre-operative
No15 AP view
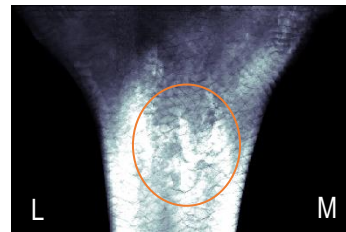
Figure 19: 6 months
No15 AP view

Figure 20: 3 years
No15 AP view

Figure 21: pre-operative
No16 AP view

Figure 22: 6 months
No16 AP view

Figure 23: 3 years
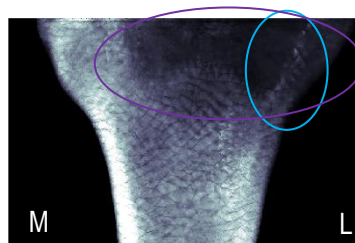*No16 AP view*
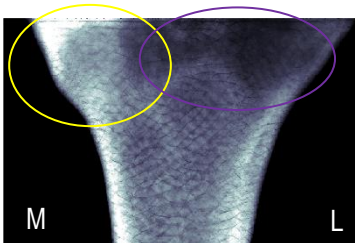
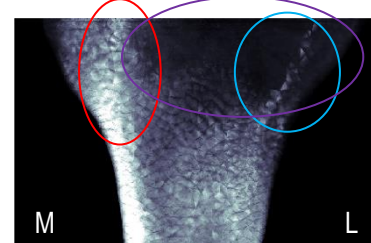*Figure 24: pre-operative*
No19 AP view

Figure 25: 6 months
No19 AP view

Figure 26: 3 years
No19 AP view

Figure 27: pre-operative
No20 AP view

Figure 28: 6 months
No20 AP view

Figure 29: 3 years
No20 AP view

As shown in the virtual DEXA results in Figure 15 – 29, the bone mineral densities in each of the tibiae develop differently over time. Some changes are apparent in multiple tibiae, while other changes are only found in a single tibia. In all five models, in the proximal tibia, directly under the tibial tray, the bone mineral density decreases over time. This may be partly due to the cavity created in the bone for placement of the implant. The darker areas may also be due to stress shielding, in which the loads are mostly distributed via the cortical bone, leading to unloading and loss of BMD below the tibial tray. In all tibiae a high density at the medial, proximal side is present in the pre-operative tibiae. This is most clear in No14, No15, No19 and No20, but also in No16 a slight increase in brightness is shown on the medial side (see yellow circles). The pre-operative tibiae No15 and No20 are the brightest of all five tibiae and thus have the highest initial BMD values in the simulations. Both models show similar behavior in the distal area over time. Some areas with higher density appear over time in these models, spread over the distal part of the tibia (shown with orange circles). In No15 however, these areas are larger and brighter than in No20.

Also, in all five pre-operative tibiae the bone mineral density is high along the lateral and medial cortex. In No14, No15 and No16 the lateral side is thicker and higher in density. In No14, however, after 6 months, the medial side has become higher in density than the lateral side. After 3 years, the density in the medial side looks unchanged, while the lateral side shows a decrease in density. In No15 the lateral cortex is very thick already and after 6 months, the whole distal area had an increase in density. The cortex is still highest in density, but the rest has gained density as well. After 3 years, this density decreases a bit in the center of the distal tibia, but the medial cortex remains high in density, as well as the area on the lateral side. For No16, this persists at the lateral, distal site, but proximally, it vanishes. On the medial side, the more proximal cortex becomes thicker and higher in density. In No19, the medial side is a bit higher in density, but the lateral side is larger pre-operatively. After 6 months, the medial side has become higher in density around the cortex and after 3 years this has not changed. In No20, not only the cortex but the complete distal area is high in density. After 6 months the highest density is found on the medial cortex in No20 and after 3 years the lateral density has decreased even more.

In No14, the area with higher density at the proximal, medial side becomes higher in density over time, while the lateral region gets a bit darker, but still has brighter spots in the area (see blue circles).
In No15, this same medial density is decreasing in density over time, and the lateral side is decreasing as well. More distally, an increase in density is seen.
In No16, the initial density over the shown part of the tibia is lower than the other models, since the image is darker. The density in the medial region is decreasing, while in the center, close to the lateral side (green circle) over the years, some increase in density is seen. This may be due to the tibial tuberosity at this point, so more bone is present and thus the DEXA value at this area is higher.
In No19 the darker area present proximally in the pre-operative tibia becomes darker and spreads out to the lateral side, so the density decreases (purple circles). On the medial side, the high density in the corner of the image vanishes, but closer to the cortex, the density increases over time, this behavior was also seen in No14 (red circle). Some brighter spots appear in the lateral proximal area (blue circle) laterally, like was seen in No14.
In No20 the initial density is high compared to the other tibiae. Over time, the density at the proximal surface of the tibia decreases, mostly on the lateral side.

In the Figures 30 – 44 below, the virtual DEXA scans of all patients are shown in mediolateral view.
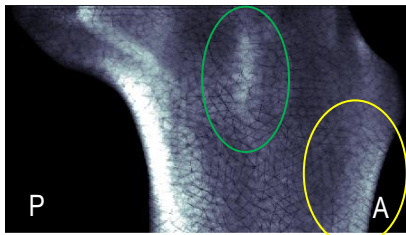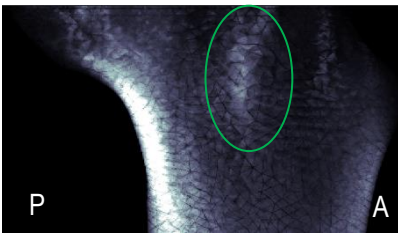

Figure 30: pre-operative
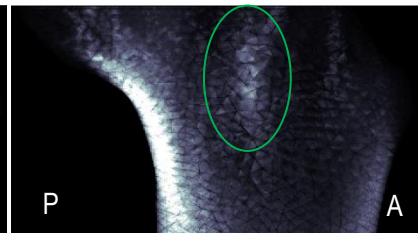*No14 ML view*

Figure 31: 6 months
No14 ML view
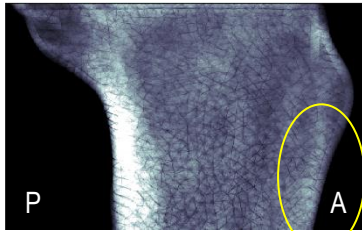
Figure 32: 3 years
No14 ML view

Figure 33: pre-operative
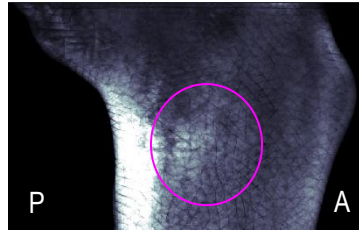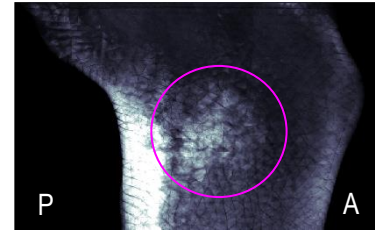*No15 ML view*

Figure 34: 6 months
No15 ML view

Figure 35: 3 years
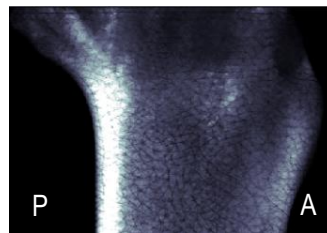*No15 MLview*

Figure 36: pre-operative
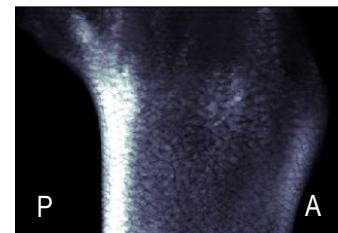*No16 ML view*

Figure 37: 6 months
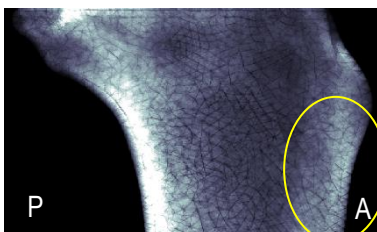*No16 ML view*

Figure 38: 3 years
No16 ML view

Figure 39: pre-operative
No19 ML view
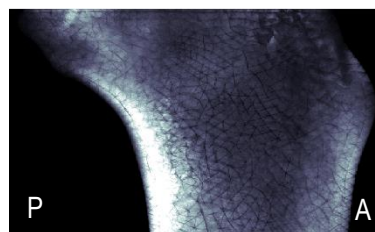
Figure 40: 6 months
No19 ML view

Figure 41: 3 years
No19 ML view

Figure 42: pre-operative
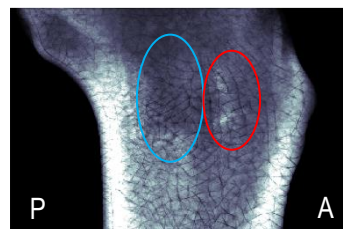*No20 ML view*

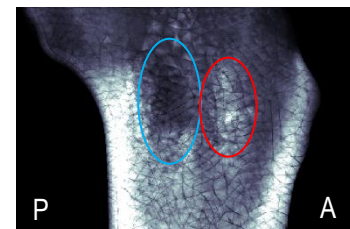*Figure 43: 6 months*
No20 ML view

Figure 44: 3 years
No20 ML view

In mediolateral view (ML) in Figures 30 – 44, the dense posterior cortex is visible in all five pre-operative tibiae (on the left side on all images). In No14, No16 and No19 this area remains approximately the same density and is stable in size. In No15, the area becomes thicker over time and moves distally. In No20 the area thickens as well. The thickening might indicate a posterior shift of the load distribution after TKR. Anteriorly, a denser cortex is also shown in all tibiae, shown in yellow circles. The density is highest in No20. Over the years, this density is not affected by the implant. Also, in all tibiae the overall decrease in density in the proximal region, which was seen in AP view, is visible in this view as well.

In No14, proximally, a bright area is apparent (green circle). Over time the whole proximal tibia becomes darker, meaning a loss in density, but this area persists over the years. In No15, anteriorly from the posterior dense cortex, an area with higher density compared to the rest of the bone develops over the years (pink circle). In No20, in the proximal half of the figures (Figures 42 – 44), the density decreases. In the middle of the tibia, encircled with blue, the density loss is highest, and right to that area, more anteriorly (in red) a brighter area appears over time. All density changes described in this paragraph are at the location of the implant, so these might be due to the effects the implant has on the load distribution in the bone

Quantitative results

In Figure 45 the measured bone mineral densities in both simulation results and clinical results are shown. All data points for each of the five patients are plotted, as well as the averages of all five patients.
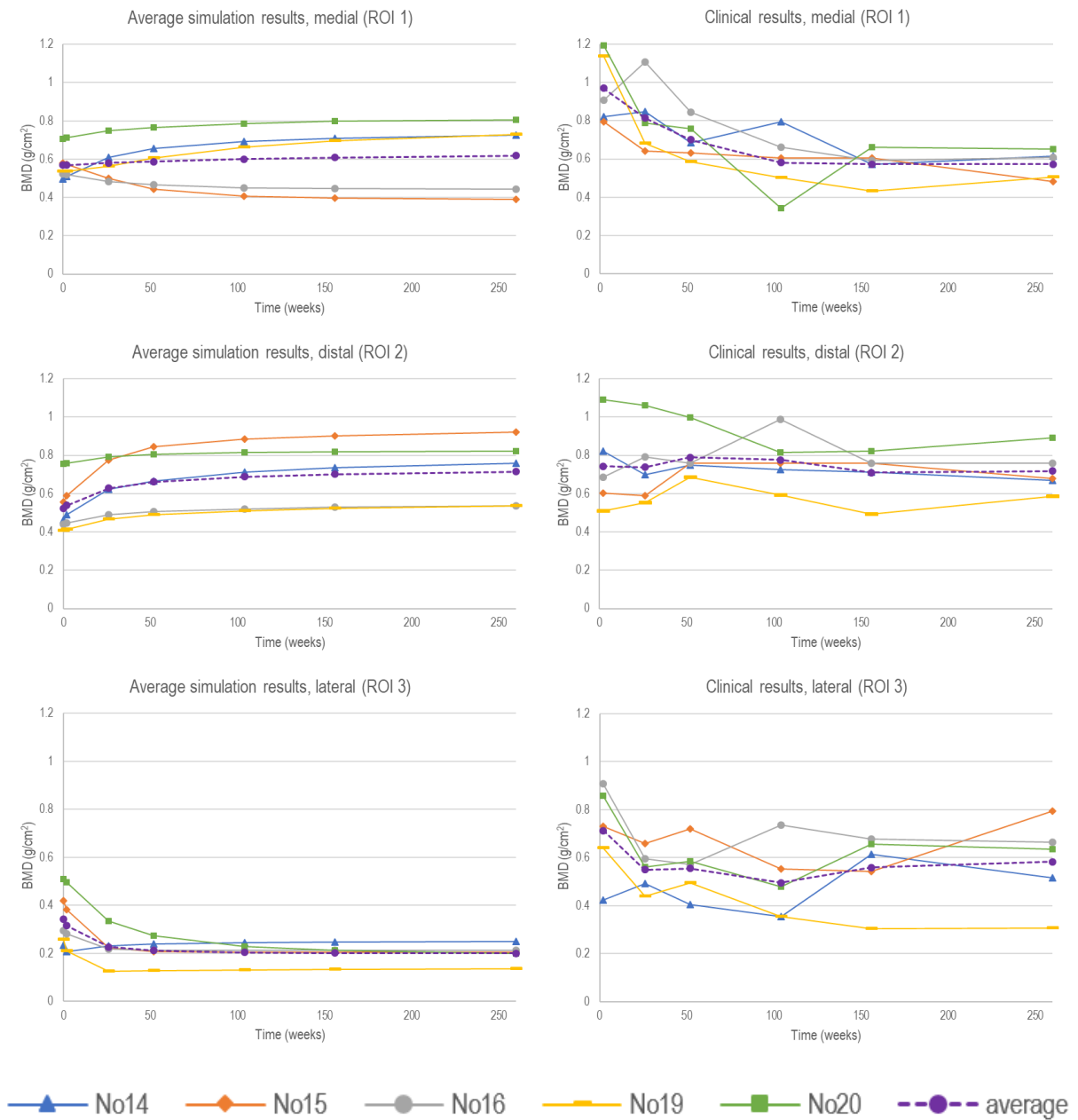

Figure 45: Absolute average BMD values measured from virtual DEXA scans (simulations, left) and BMD values measured from clinical DEXA scans (clinical, right), and averages for 3 ROIs medial, distal and lateral; pre-operatively (FE only), 2 weeks, 6 months, 12 months, 24 months, 3 years and 5 years post-operatively.

In all FE plots, the BMD of No15 and No20 start with the highest initial BMD values, which is in accordance with the visual DEXA images, in which No15 and No20 are the brightest images.

In all regions of interest and for all models, the initial BMD values in the clinical results are higher than in the FE results. For all three regions of interest the initial BMD values in the clinical results, at 2 weeks post-surgery, are higher than the used initial BMD values in the simulations. The average clinical BMD in the lateral ROI is 2.06 times the BMD value used in the model, and the medial BMD is 1.70 times the model BMD. Since the distal clinical values vary a lot, the initial average BMD does not tell much.

In ROI 1, the medial ROI, the FE results show a slight increasing BMD level on average. However, this is caused by the increase of BMD in patients No14, No19 and No20 and a decrease in BMD for No15 and No16. The clinical results for the medial ROI show a decrease in BMD as well, with values from 0.97 to 0.57 g/cm^2 over time. Each of the five patients follow this behavior although some of the datapoints; 6 months for No16 (grey), 24 months for No14 (green) and No20 (blue) do not follow the expected course.

In the distal region of interest, ROI 2, the simulation results shown an increase from 0.53 to 0.72 g/cm^2. This trend of an increasing BMD appears for all five models. On average the clinical result remains constant at about 0.75 g/cm^2. Here, No16 (grey) shows an unexpected peak value at 24 months, which is an outlier in the data and patient No20 (green) shows a large decrease in BMD in the 24 months.

For the third region of interest, ROI 3, on the lateral side, the simulation results show low starting BMD values, 0.35 g/cm^2 on average and a decrease in BMD value in the first year after which it remains constant, on average 0.20 g/cm^2. The average of the five patients shows a small decrease from 0.71 to 0.58 g/cm^2, however, each of the patients show different behavior. No19 (yellow) shows a clear decrease in BMD, while No14 (green) and No15 (orange) increase over time, although not constantly, and No16 (grey) and No20 (blue) show a decrease in BMD at first and an increase later on.

Sensitivity analysis point load placement

Three simulations per model were performed to test the effect of the location of the point load on the remodeling simulation. In Figure 46 the results of each of the simulations are shown per model. The second simulation, in which the point loads are placed posterior compared to the first, original simulations, show a higher distal BMD value over time compared to both the first and third simulation in all models. The BMDs in the medial region are very close to the original trends. For the lateral region (in green), the BMD values resulting from the second simulation are equal or a bit lower than the original simulations, but these are also comparable. In each of the models the medial BMD increases more in the third simulation, when the point loads are placed more towards the edges of the implant, compared to the original, first simulation. In the distal and lateral regions, the trend of the BMD is also a bit higher or similar to the BMD found in the first simulation. However, the difference is smaller compared to the differences in the medial region. The BMD per region follows the same trend for all simulations in each of the models.
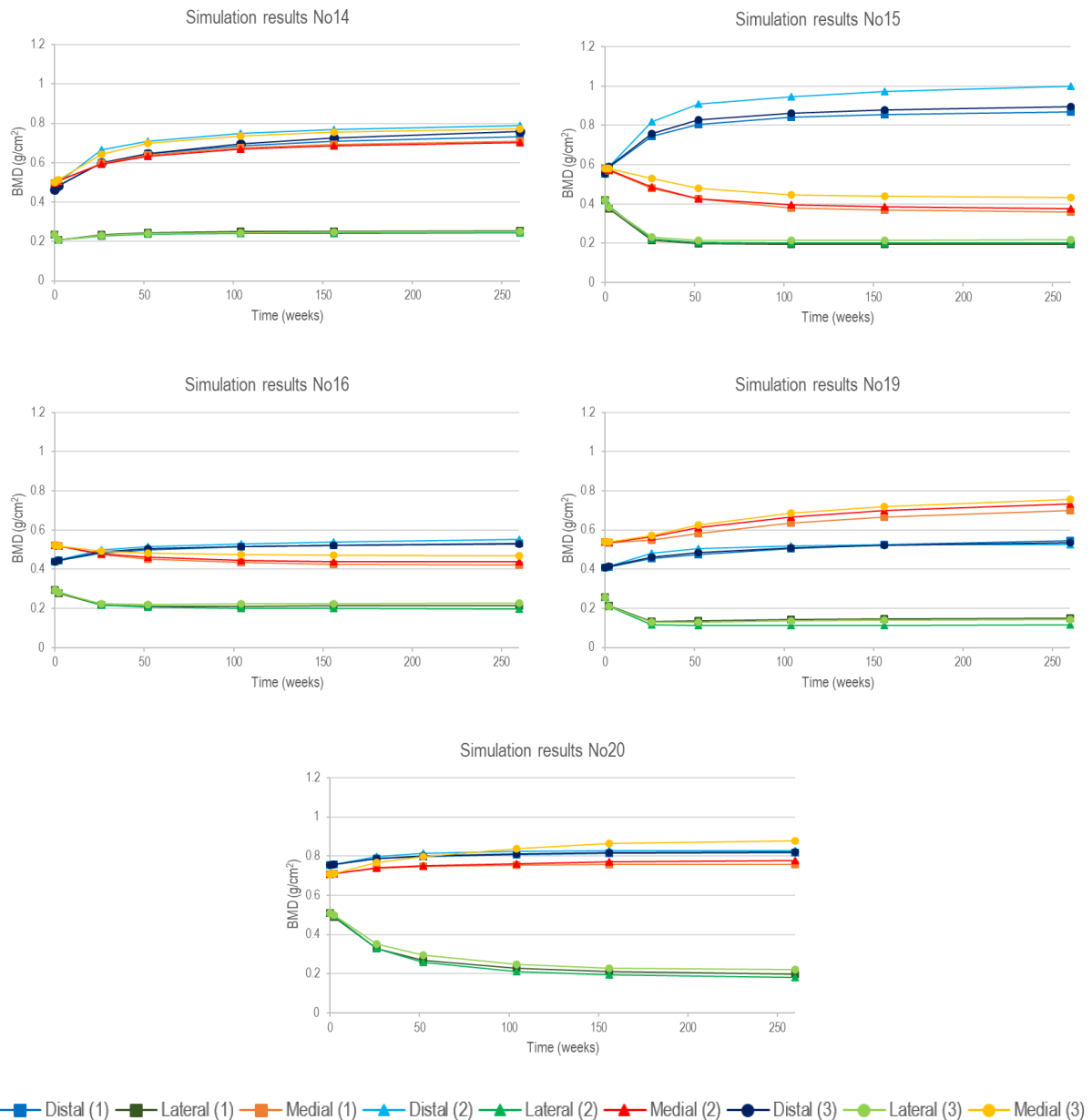

Figure 46: Simulation results of sensitivity analysis per model

4 – Discussion

The goal of this study was to create patient-specific finite element models which could be used to study bone remodeling in the proximal tibia after total knee replacement. Those models could be made with use of an unique data set containing pre- and post-operative CT scans. This dataset is unique since it contains both the pre- and post-operative CT scans of the same patients so that the post-operative scans can be used to extract the exact orientation of the implant on the tibia.
Moreover, the goal was to validate the stain adaptive algorithm by comparing the simulation results with available DEXA data from the same dataset. The results did unfortunately not match and thus the algorithm could not be validated.

Those differences between the simulation results and the DEXA data could be due to numerous limitations in both the computation and in the clinical data set available. In the clinical data, uncertainties are due to the low level of models, the unknown initial BMD values, body weights and activity levels, measurement errors in DEXA scans and unknown loads and load distributions. In the model and simulation of the model, the uncertainties are due to the possible segmentation errors, the placement of the implants, the used alignments, the way loads were applied, neglecting part of the moments from the load cases, not using soft-tissues in the models and the remodeling algorithm.

On the proximal, medial side of the pre-operative virtual DEXA (yellow circles in Results) and the calculated BMD of the medial ROI, a relatively high BMD value is found. This medial densification has been linked to varus alignment in OA patients in multiple clinical studies (Hulet et al., 2002; Jaroma et al., 2016; Li & Nilsson, 2000b). As the mechanical load is higher on the medial side compared to the lateral region due to varus alignment, bone densifies at this proximal, medial region.
The remodeling simulations in the medial ROI show an increase in BMD for three of the five models, and a decrease in the other two. In the clinical data however, the BMD decreases over time for all patients. This was expected, since medial bone loss post-operatively has been linked to the correction from varus alignment to mechanical alignment, as the mechanical load shifts from a medial to a neutral distribution (Jaroma et al., 2016; Yoon et al., 2018). The increase in BMD in the three models has no unambiguous explanation.

In the distal region of interest, an increase in BMD is found for all patients, while in the clinical data, no clear conclusion can be taken from each of the patients data. The average BMD in clinical data is stable. The increase in BMD in the distal region was unexpected, but can be explained by multiple factors.
In the model results, an increase in strain energy density at the distal end of the keel is seen. This results in an increasing distal BMD. In the model, the cement layer was glued perfectly to the implant and fits perfectly into the hole created in the tibia. The connection between the cement layer and the bone is thus fixed at all sites and the cement layer has an equal thickness. In clinical situations, however, the cement is not bonding to the complete surface of the tibia and is not an equal thickness either (Gebert De Uhlenbrock et al., 2012). Anijs et al., 2021, found similar results in their models with an evenly distributed, perfectly fixed cement layer as well and argued that this 'perfect' cement layer could be the cause of a concentration of strains under the keel, leading to bone formation, while in a clinical cement layer, not all sites are bonded well, causing a decrease in peak SED values. Another cause of the distal BMD increase could be the interdigitation of cement into bone in clinical TKR. In the models, the cement layer stays between the bone and the implant, while, in vivo, it has been shown that interdigitation of cement into trabecular bone leads to a decrease in strains in the bone-cement interface (Srinivasan et al., 2017).
In both the virtual DEXA data of No15, and to a lesser extent in No20, in AP view and the plot of the BMD data, over time, the distal region becomes very dense compared to the other models. This brightness is caused by the increase in density at the posterior side of the tibia, as shown in the virtual DEXAs with mediolateral view. The increase in density is caused by an increase in strains posterior to the keel, leading to bone formation posterior to the keel, at the cortex.

In the lateral region, both the clinical data and simulation results show an average decrease in BMD. In the clinical data, however, two of the patients show an increase in BMD level after 5 years and many outliers are present in this data. This might indicate measurement errors in the clinical data. In the simulation data, a decrease is shown for four out of five patients.

In all models for all regions of interest, the initial BMD value in the clinical data was higher than in the FE results. In the models, the air-fat-muscle calibration tool (Eggermont et al., 2019) was used to assign BMD values to the elements of the model. This calibration tool may thus underestimate the BMD values. In the scanners used in the development of the air-fat-muscle calibration tool, certain settings were used. However, in this project different scanners with probably also different settings were used in both the pre- and post-operative CT scans.

Another factor which might explain the discrepancies between the initial BMD values in the models and those in the clinical data is that the clinical BMD values were obtained by DEXA scanners. DEXA scanners were used which do not make a difference between bone and soft tissue. The soft tissues were thus also scanned and their densities were added in the clinical DEXA scans, while the virtual DEXA scans were created out of the model only and thus only contained densities of the bone.

Calibration with the data used in this project would thus be recommended to obtain the same initial BMD values in the simulations as were found by DEXA measurements in the clinical data. The initial BMD levels are important for the remodeling of the bones. It was shown that the initial BMD values were determining for the remodeling rate and should therefore match the clinical situation as good as possible. A computational study showed that for the first two years post-operatively, regardless of the joint alignments, higher density bones were shown to have less relative proximal bone loss compared to bones with lower densities, while after two years, the relation was reversed, with higher density bones having an increased bone loss compared to lower density bones (Anijs et al., 2020). Another, clinical study showed that bones with a relatively high initial BMD value showed a relative decrease in overall BMD while bones with a relative low BMD showed a relative increase in BMD in the first 2 years post-operatively (Li & Nilsson, 2000a). In some of the simulated and clinical data in this project, this behavior can also be seen, although because of all uncertainties in the model, it is not said that the trends of these BMD values are trustworthy and if links with bone remodeling behavior seen in other studies can be applied to these results. In the simulations, the medial BMD of No20 is the highest and this model shows the least relative increase in the first two years. No15 and No16, which both show a decrease in BMD values, also match this. No15 has a higher initial BMD value than No16, and shows a higher relative decrease in BMD, which is in line with the computational study. In the distal ROI, No20 has the highest initial BMD but shows the least relative increase. However, the models with the lowest initial BMD, No16 and No19, do not show the most relative increase in BMD. In the lateral BMD of No20, which has the highest initial BMD value, has a higher relative loss of BMD in the first 2 years, compared to all of the other patients.

In the simulation results, the BMD values in all three regions of interest stabilize after two to three years post-operation. In the clinical data the average BMD in the medial region also stabilizes after 2 years, although the separate measurements of the patients show different behavior. In the distal and lateral region, the clinical results are very different per patient, so no conclusion can be drawn about the stabilizing of the BMD due to the implantation in this regions. In other clinical studies, different results were found. It was shown that the BMD significantly changed within the first year and remained stable in the following 5 years (Saari et al., 2007), but also, it was also shown to go on up to two years (T. Soininvaara et al., 2008). In other long term follow-up studies, the bone remodeling was even shown to go on for 7 years (Jaroma et al., 2016) and 10 years (Small et al., 2013).

The simulation results are not resembling the clinical results. The differences between those can be explained by uncertainties and assumptions in the clinical data and by uncertainties and assumptions made in the creation and simulation of the models.

Uncertainties and assumptions in clinical data

Patient data

First of all, the dataset of CT scans available contains data of 30 patients. In this study, the data of 13 could have been used, which, when using data with both fixed bearing and mobile bearing implant, could have led to 26 models. However, due to time restrictions, only 5 tibiae, all with mobile bearing implants, were used in this study. This is a limitation of this study, as a greater number of models could have given more reliable results. In later research, all available and suitable data could be used to get more trustworthy results.

The patients in the dataset all had bilateral surgery with a mobile bearing in one knee and a fixed, posterior stabilized bearing in the other knee. This data could be used to even expand this current research to two types of implants and to study the difference between those implants for bone remodeling within the same patient.

Secondly, is that CT scans made at the day of surgery were not available for the used patients. These scans could have been used for determining the bone mineral densities before surgery. Since those scans were not available, it is assumed that there was no bone mineral density change in the tibia in the period between the pre-operative scan available and surgery. However, the time between the pre-operative CT scan and surgery varies widely between patients, between 1 day and 5 months. In the time between the pre-operative CT scan and the surgery, bone properties can have changed, due to decrease in activity because of pain for example. The assumption could thus have affected the results, since all simulation results are based on the difference in strain energy in the pre-operative and post-operative bone, assuming that the pre-operative scan is depictive for the situation on the day of surgery. However, the periods between the scan and the surgery are at maximum 5 months, so it is not expected the BMD can have changed a lot.

Thirdly, all loads applied to the model, pre- and post-operatively were scaled to the body weight reported in the dataset. It is not known at what moment this bodyweight was measured and how the body weight developed over time after surgery. In case, for example, the body weight decreases as a result of more physical activity after TKR, the loads would also change and simulations would give different remodeling results. Clinically, it was shown that there is a positive correlation between the body weight and the BMD in the proximal tibia, years after surgery,(Hvid et al., 1988; T. A. Soininvaara et al., 2004) so, the body weight is an important parameter to take into account when modeling.

Relating to that, the unknown physical activity level of each patient, required the assumption of equal activity levels in all patients and over the whole follow-up period. The activity levels chosen, an evenly distributed amount of gait, knee bend and stairs down, were chosen as an average level of activity. However, the actual activities of each of the patients as well as the level of activity is different and could lead to different bone remodeling results. The activity level however, is impossible to know precisely for each patient at each pre- and post-operative time interval. What could be done is to ask the patients for their activities during daily live, during follow-ups, to make an estimation of their activity levels. This is suboptimal, but gives a better indication of the activity level per patient than assuming all patients have the same activity level and that those activity levels are constant over time.

Another point of discussion are the regions of interest used in both the clinical data and in post-processing the simulation results. The regions of interest chosen in the clinical data were according to the definitions from Minoda et al., 2010, and were taken in anteroposterior view 1 cm under the tibial plateau and as close to the cortex as possible on both lateral and medial side. In the clinical data, the measured BMD values in these ROIs vary a lot over time. As shown in Figure 45 outliers are present in the data, especially in the lateral ROI. Those outliers are too large to be due to change in activity levels of the patients and are thus probably caused by measurement errors. As the ROIs are determined on the bone manually, those measurement errors can occur. The outliers in the clinical data make the comparison of computational BMD values with clinical data more difficult or even impossible.

For the two-dimensional measurement of BMD values in the tibia, the tibia might also have been rotated compared to the model. Protocols for densiometric scanning of tibiae exist (Trevisan et al., 1998), but it is unknown what protocol was followed in the clinical measurements in this study. So it could be that the orientation of the tibia in the DEXA scans was different than the models from which the virtual DEXA scans were created,

leading to different results.

Another drawback of the use of the current used ROIs is that the proximal ROIs are both very close to both the cortex on one side and the implant keel on the other side. The cortex is high in density, which can give an overestimation of the BMD in the ROI. On the other side of the ROI, in the surroundings of the keel in the clinical bones, cement can be present due to interdigitation. If the ROI is taken such that cement is present in there, the cement will also give deviations from the actual bone densities in the measured ROIs. Therefore, it is important that the ROIs are chosen in between the cortex and the keel, and most importantly, on the same area in the clinical and model data.

Implant data

The implant geometries to be meshed before use. This has led to simplifications of the implant geometries. The mesh was made such that it was computationally possible to calculate outcomes, but still resembles the actual shapes as good as possible.

Loading conditions

As described before, in this project the OrthoLoad Standard Loads Knee Joint data set was used. Although the data from OrthoLoad was the best available option, the use of it brings some uncertainty into the models. First of all, the implant used in the OrthoLoad data, the INNEX knee system (Zimmer, Warsaw, IL, USA), is different from the Vanguard RP Total Knee System implant used in this project. As described in the introduction of this thesis, the type of implant, the design and material choices all influence the mechanics of the knee joint. So the loads from OrthoLoad cannot be copied to the implant in this project one-to-one.

Besides the implant system there are more differences between these studies. In the OrthoLoad study, German patients, mostly male, with a higher body weight were studied, whereas in this project the tibiae of Japanese, all female and lower body weight patients were studied. These factors have an influence on the bone strength (Naganathan & Sambrook, 2003; Zengin et al., 2015) and shape (Nieves et al., 2005; Roy et al., 2005), which all could affect the load cases.

Besides all these limitations, the loads were applied in a similar way as in the OrthoLoad dataset to the lowest surface area on the tibial plateau, and the load was scaled to the patient's body weight, leading to a representative load case. Moreover, the same load cases were used for the pre- and the post-operative simulations, and since the bone remodeling algorithm uses the difference between the two model results, the effect of not completely fitting load cases might be limited.

Uncertainties and assumptions in the models

In the models, the uncertainties and assumptions can be split up over the different parts of the workflow in which the models were created.

Segmentation

During the segmentation step, the segmentation of the tibia from the CT scans was done mostly automatic and the last part was done manually. This might have led to small errors in the resulting tibial mesh, especially for the post-operative tibial mesh. As the presence of the implant led to artifacts in the CT scan as well as a large contrast, see Figure 47, the post-operative tibia was hard to distinguish from the soft tissue at some points. The auto segmentation program was not able to segment the post-operative tibia as good as the pre-operative tibia, so many adjustments to the automatic segmentation had to be made by hand. This might have caused small errors in the resulting post-operative segmentation. As the post-operative tibia is used for the placement of the implant on the pre-operative tibia, the errors in the post-operative mesh might have caused small deviations of the implant orientation in the model with the clinical implant orientation. The implant in the post-operative scan could easily be segmented manually by using a high threshold value. The registration of the implant geometry to the segmented implant was therefore less sensitive to errors. The largest error in the orientation of the implant on the bone, is from the segmentation of the post-operative tibia. However, the post-operative tibia was used only for the registration and rotation towards the pre-operative tibia, which was performed with the coherent point drift

algorithm, which aligns the two point clouds with each other. Small mistakes in the segmentation lead to small differences between the point clouds of the pre-operative and post-operative tibiae. Most of the points however, are in the correct place and thus, both tibiae still have largely the same shape. The algorithm will thus still be able to calculate the transformation between the two models and the effect of the misplaced points in the post-operative tibia will be minimal.
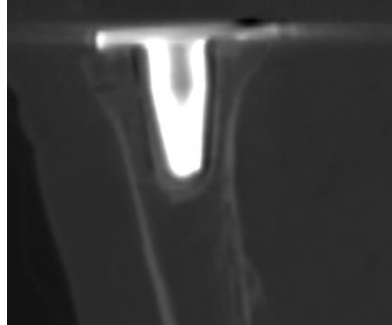

Figure 47: The metal implant causes artifacts and high contrast in the CT image

Rotation

In the rotation step of the workflow, the implants were placed onto the tibiae. In one of the five cases, in No19, the implant does not fit the tibia very well. The tray size used seems too large for the tibia and is also placed skew to the lateral side of the bone. In the model, it is clear that a large part of the tray and cement does not connect to the underlying tibia, see Figure 48.
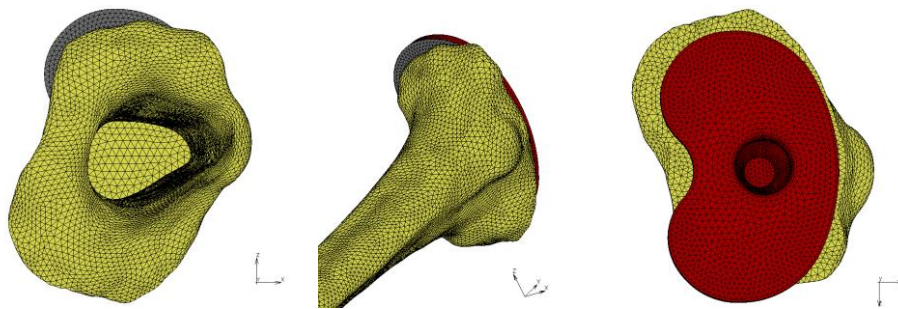
Figure 48: The cement layer (grey) and tray (red) do not fit the tibia (yellow) in model No19

It was checked in the CT images, but, because of the large contrast between the implant and the bone in posterior-distal view, it was hard to see if the implant was indeed placed a skew as it is in the model, or that there was a mistake in the placing of the implant onto the model. On the mediolateral and anteroposterior view however, the orientation of the keel could be compared to the models. Those are shown in Figures 49 - 52, in which can be seen that the implant in the CT is indeed close to the lateral side in AP view and is also rotated towards the posterior cortex a bit. No indications were thus found that placement of the insert in the model was incorrect. It could be that the implant used in surgery was too large for the tibia and would therefore have some overhang.

Figure 49: No19 CT AP view   *Figure 50: No19 model AP view*   *Figure 51: No19 CT ML view*   *Figure 52: No19 model ML view*
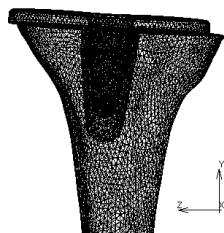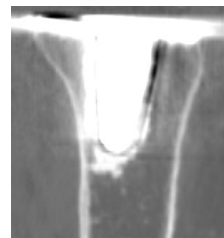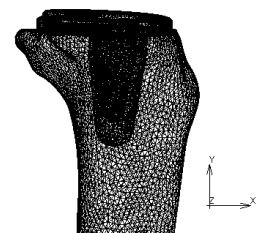
In the virtual DEXA scans of No14 and No19 a brighter speckle pattern appeared in the proximal lateral region over time. No explanation for this behavior was found. It could be due to an effect of the skew placement to the lateral side of the tibial tray in those models. On the medial side of both No14 and No19 a clear increase in BMD along the cortex and proximal (encircled in red in the Results section) was observed. This was unexpected since a study has shown that the lateral shift of an implant leads to a decrease in stress in the medial region, so bone formation was unexpected (Innocenti et al., 2009). The high density in the medial region was already present in the pre-operative scan, but in the post-operative years, the surrounding bone showed a decrease in density. The remaining high density area could be caused by the realignment of the knee and beta angle of the implant. It was already suggested that the high proximal, medial density was caused by the pre-operative varus alignment. After correction to mechanical alignment, the bone is loaded less medially, and it is expected to lead to bone resorption on the medial side. However, the β angles in No14 and No19 are small in the models, which leads to uneven distribution of the loads in the bone. In No20 however, the local higher medial density is also apparent, but in this model, the beta angle is approximately 90 degrees. So the different load distribution due to the small beta angle is not the only possible cause of this result.

In mediolateral view it was also shown that models No14 and No19 have a δ angle of more than 90 degrees, while No15 and No16 have a δ angle smaller than 90 degrees. It could be expected that the distal tip of the keel would be closer to the posterior cortex for that reason. In the models however, the distance between the posterior cortex and the keel of the implant is similar in all models. In all models, the rate of change SED was high at the posterior distal tip of the keel, leading to bone remodeling, especially clearly visible in No15 and No20, as described before.

Bonecutting

Although a high accuracy is wanted in the proximal resection of the tibia, in surgery, errors in the cutting during TKR still appear (Bäthis et al., 2005). This can result in a misfit between the bone and the implant, which is fixed by a cement layer of unequal thickness in between the implant and the bone. In the models however, the bone was cut in the exact shape of the implant, creating a perfect fit with an equal layer of bone cement between the bone and the implant. Since the surgical cutting plane is not visible in the post-operative CT scan, due to the artifacts of the implant, the actual cutting plane could not be used. Being able to create models which mimic the actual surgical cutting planes would be optimal in creating patient-specific models, however, the difference is small and is not expected to create large differences in model results.

Model set-up

In this study, both the pre-operative model and post-operative model are simulated in their orientation in the ERC reference frame and thus the known pre- and post-operative HKA and FTA angles of the patients were not applied to the models. This was done to put the loads from OrthoLoad in the same orientations onto the bone and implant. So the magnitude and distribution of the loads as applied, were directly copied from the patients measured in the OrthoLoad study, even though this was different from the clinical situation of patients in this project. Moreover, endo- or exorotation of the tibia relative to the femur was not reported in the used data. Therefore, it was assumed there was no relative axial rotation between femur and tibia/tibial implant in both pre- and post-operative situation. Rotating the modeled pre- and post-operative tibia could have led to a different load distribution on the model, mostly in the pre-operative situation. In the pre-operative situation, all tibiae were in varus, meaning a higher part of the loads was exerted onto the medial condyle, compared to the lateral condyle, while in the model, the pre-operative tibia was modeled in the alignment of the ERC reference frame. In the post-operative tibia, mechanical alignment was applied in surgery, which makes the difference between the orientation of the modeled tibia in ERC frame and the actual orientation of the post-operative tibia in mechanical alignment smaller, although there still is a difference in alignment in AP view and the discrepancy in exo- or endorotation still creates a different load distribution.

Moreover, due to computational issues in the simulations of the models, it was decided to leave out the insert in the models. The insert, made of polyethylene had a relatively low Young's modulus of 588 MPa, while the tray

and cement layer had a much higher modulus, of 210 GPa and 2551 MPa, respectively. The effect of the insert on the loads distributed onto the boned is therefore expected to be limited.

The loads were applied to the model in line with the loads in the implant in the OrthoLoad study. The nodes at the surface of the pre-operative tibia were chosen at and around the lowest node of the condyle, as it was assumed the femoral component would touch the surface there in all load cases. Also, on the post-operative model, it was chosen to put two point loads directly on the tray. The position of these point loads was chosen to be in the middle of the surface of selected nodes for spring attachment in the pre-operative situation. It was tested what the effect of the placement was in a sensitivity analysis. For all models, both the lateral and medial point loads were placed onto three different positions, all close to each other. As shown in the Results section of this thesis, the small displacements of 2 elements distance, approximately 4 mm did not affect the bone remodeling results of the simulations a lot, the results are still comparable. To test what the effect of the displacement of only the medial node was, three extra simulations were performed with model No20, see Appendix E. These simulations all showed similar behavior for the bone remodeling in the distal and lateral region. In the medial region however, development of the BMD differed between the simulations, showing three different behaviors. Four of the point placements led to an increase in BMD, of which two had a large and two a more moderate increase. The other two point placements showed a very small decrease in BMD over time, see Figure E.3 . The placements of the point loads is thus determinative for the remodeling outcomes, at least in the medial region. It is recommended to perform more analyses on the placement of point loads in both the medial and lateral region to test sensitivity. As one point loads at each condyle do not resemble the clinical situation, other manners to place loads onto the model should be investigated as well.

In the models created, three load cases of different activities were used from the OrthoLoad database. From each of these activities only the measured peak loads were used. However, applying full load cycles of these activities would resemble the bone loading in daily life better. Moreover, during the simulations the three peak loads of activity levels, gait, knee bend and stairs down were applied to the model continuously, without unloading, which is also different from daily life. These simplifications of the activities in daily life may have affected the remodeling outcomes.

Moreover, only the forces and the varus-valgus moment from the OrthoLoad dataset have been used. The other moments were not used. In the version of Marc Menta used, the moments on the nodes were not saved to the .dat file. Since those files were used and adjusted for use in the simulations, the moments had to be left out. The varus-valgus moment was used to calculate the division of the axial load on the tibia over the medial and lateral condyle and thus encorporated in the loads, but was not applied as moment on the nodes directly. For the calculation of the division of the axial load over the medial and lateral side, the varus-valgus moment was added. The moment arm used was the distance between the middle of the implant and the control node at the medial side. So, the load placed on the medial and lateral side have been scaled with the position of the control nodes. Moreover, in the pre-operative models, the load cases from the instrumented implants from OrthoLoad were used as well, while the pre-operative load distributions are different from the post-operative loads.

The effects of soft-tissue surrounding the knee joint, were not taken into account in the models. Soft-tissues play an important role in the transfer of femoral loads onto the tibia and do thus distribution of loads and during surgery, soft-tissue balancing is applied to create an optimal mechanical balance in the operated joint(Hohman et al., 2015; Mihalko et al., 2009). In this project, all knees had pre-operative varus alignment, which is related to laxity of the lateral collateral ligament (LCL). During surgery, mechanical alignment was applied to all knees, and thus an imbalance of the soft tissues may have occurred, leading to different load distributions, since the LCL could not provide the stability on the lateral side of the knee joint needed. This could both lead directly to bone remodeling since the loads on the tibia are change, but also, due to pain or feeling of instability change the activity levels of patients, leading to bone remodeling. However, it was shown that post-operatively, laxity in the lateral collateral ligament would decrease spontaneously over time (Sekiya et al., 2009), so the effect of the lateral collateral ligament specifically is limited. Moreover, in the load data used, soft tissue were present in the measurements So the effect of soft-tissue was already in the load case, and it was thus not completely neglected.

Remodeling algorithm

The used remodeling algorithm was based on the strain adaptive remodeling theory of Huiskes et al., 1987, in which it was applied to femoral bone remodeling after total hip replacement (THR). The parameter values used in the remodeling algorithm, the dead zone values and the time units, were based on results of a validation study on femoral remodeling after hip replacement was performed (Tarala et al., 2011). However, for bone remodeling in the tibia, these parameters could differ. The strain adaptive remodeling algorithm used in this project uses a dead zone of 35%. If the relative change between the strain energy value in an element is smaller than 35%, the remodeling enters a dead or lazy zone and no remodeling takes place. Different dead zones were studied on finite element models of the femur by Bingzhi et al., 2009. It was found that with a dead zone of 35%, most of the bone elements would remodel slowly and would reach their lazy zone fast, they recommended a dead zone between 0 and 35%. In simulations in the same study with dead zones of 10%, 35% and 60%, it was found that the dead zone value had a lot of effect on the bone remodeling and that a dead zone of 60% lead to a lazy zone for most of the elements too soon. Another study however, found a dead zone of 60% to be fitting their models of bone remodeling in the periprosthetic femur after THR (Turner et al., 2005). So, there is no consensus on what dead zone can be chosen best. Moreover, studies have shown that bone formation is a slower process than bone resorption, which suggests that bone cells are less reactive to relative loading compared to relative unloading (Leblanc et al., 1990; Sibonga et al., 2007). To model this properly, a different dead zone for bone formation and bone resorption should be implemented.

Apart from the discussion what dead zone values to use, the bone adaptivity may be different per individual and be also related to factors like age, sex or ethnicity. In some patients bone remodeling might happen at a faster rate or need a higher or lower threshold to start.

Future research

In this project the workflow created by Anijs et al., 2020 was largely adapted to be able to create patient-specific models including the implant orientation from the post-operative CT scans. The current workflow contains some manual steps in the segmentation of the bones, the cutting of the bone and the set-up of the model. The cutting of the bone and the set-up of the model, could be automated to spare time and to avoid mistakes made by hand. Moreover, one script in which all used functions in the complete workflow are run one by one would improve the ease of use of the workflow for other research. The workflow is however shown to work for the creation of patient-specific models. In this study, these models were used to study bone remodeling, but the models created by workflow could be used for studies as well.

Furthermore, this project, the element size of the tibia and the implants and the distal cutting distance were chosen based on earlier research (Anijs et al., 2020, 2021). Also, the ERC orientation of the tibia was chosen to be the neutral orientation of the tibia. In future research, convergence tests on these parameters could be performed to test the effects of those parameters on the modeling outcomes.

In this project, patients with mobile bearing implants were researched. In reality, the insert of a mobile bearing implant is able to rotate and adjust to the geometry and loads from the femoral component pressing on it. This could possibly minimize the effect of slightly misplaced loads in the model as the insert could freely rotate. In the current model, the loads are placed on a node which is fixed. So, a recommendation is to test the effect of leaving out the insert in the model on the load distribution onto the tibia, both with the insert fixed to the tray to test the effect of the addition of the material and geometry of the insert and with the insert being able to rotate to test the effects of the loads distribution of that.

One of the drawbacks of the current research was that the load cases are not patient-specific. To be able to create patient-specific simulations and perform validation of the strain adaptive algorithm, more patient-specific load cases should be made. Those patient-specific calculations could be made with for example musculoskeletal models in which the patient is modeled and activities can be simulated from which loads in the knee can be extracted. Another option is to use in vivo joint loads and joint kinematics and calculate joint loads by inverse

dynamics, as was done by Fitzpatrick & Rullkoetter, 2014. Still, the actual activity level of the patients is not known, but the load cases will be closer to reality than the load cases used now.

In the current modeling, only the tibia and its implants are simulated with forces directly on the tibial insert. However, to resemble the anatomical situation better, the femur and/or femoral component could also be placed onto the tibia/tibial insert. The forces can be exerted on the femoral component, which distributes the forces onto the tibia or the tibial component in a more natural way. During this study, it was already tried to put the femoral component onto the tibial insert and to extract the resulting forces on the insert to use those in the model. However, it turned out to be computationally hard to simulate the contact between the femoral component and the insert, so it was not used in the end. Nonetheless, this would be an opportunity for future research. In this way, by first putting the femoral component on the insert, extracting the resulting forces and using those in the bone remodeling simulation, the femoral component is not used in the final bone remodeling simulation, which would make the simulations very computationally hard, but the forces can be used anyway. Another advantage of using the femur or the femoral component is that rollback of the femur during knee functioning is simulated. In this project all forces were on one fixed place while in reality, during activity, the load is of course a cyclic parameter. With adding the femur and femoral rollback, these effects would be added to the model.
This approach could be extended even more by also adding the patella, and tendons, ligaments and muscles surrounding the knee joint. Those tissues also affect the load distribution on the tibial surface, and by adding those, the simulations would resemble the clinical situation better. However, this would create very complex models which may be hard to solve with the finite elements method. Another option would be to create musculoskeletal models of each of the patients, pre- and post-operatively, put in the implant components in the way it was clinically done and extract the forces on the tibia for the pre-operative situation and the tibial component for the post-operative situation for use in bone remodeling FE simulation.

As the bone is cut, the bone has plastic deformations, which directly after surgery, leads to different properties in the periprosthetic bone. The change in bone properties at the cutting surface was not taken into account in the material assignment for the simulations. This could however be implemented in the simulations in later research to test what the effect is on bone remodeling.

Since for this dataset the pre- and post-operative CT scans and DEXA results at multiple timepoints are available, this data could be used to perform validation of the strain adaptive algorithm in future studies. Clinical post-operative BMD data is available for some regions of interest and by creating patient-specific models out of these CT scans and simulating those, the variables needed to resemble the actual clinical situation with the algorithm could be tuned. When the remodeling algorithm is validated, it can be used to examine the influence of several factors on bone remodeling. For example, the implant components can be made of different materials, one can test the effect of a smaller or larger sized implant component on the remodeling or with different forces or other load cases the effect can be studied.

If the remodeling algorithm is validated for 5 years, predictions of the remodeling behavior of the bone on the long term, for example 10 years, can be made to see whether there is a chance the remodeling will result in failing of the implant, because of aseptic loosening or instability on the long term. On the other hand, a validated remodeling algorithm can also function as a tool which can be used pre-operatively, to test which implants of which materials and in which orientations should be used to get the best results, looking at bone mineral densities, on the long term. However, when using this data set for validation of the bone remodeling algorithm, it should be taken into account that patients studied in this project were elderly female, which have different bone properties than average people (Finkelstein et al., 2008), which, might lead to faulty conclusions if this data is used for validation.
Of course, other effects, like breakdown of the implant or malalignment, should also be taken into account for this, as remodeling is not the only cause of TKR failure. Moreover, for example in knees with mechanical alignment, factors like the gait pattern, force distribution and activity level have been shown to affect the strength of bone more than bone mineral densities (Li & Nilsson, 2000b). So, bone remodeling and BMD are of importance, but other factors should not be overlooked.

5 – Conclusion

In this project, two goals were stated. The first goal was to create patient-specific finite element models based on pre- and post-operative TKR CT data. In this project a workflow was created, in which, with the available CT data, models can be created in which the patient-specific implant orientation is added on the model. This workflow can be used in future computational research on total knee replacements.

The second goal was to validate the strain adaptive remodeling algorithm by simulating the created models and comparing those to clinical DEXA data. The remodeling algorithm could not be validated since the results of the patient-specific models used in the strain adaptive remodeling algorithm did not compare with the clinical data.

In general, more parameters should be known to able to perform validation of the used strain adaptive remodeling algorithm. As there are too many uncertainties and too many assumptions had to be made, it was not possible to resemble the clinical remodeling situation with the created finite element models. More data about the relevant parameters; the body weights of the patients, the activity levels of the patients, the magnitude of the loads, the distribution of the loads and exact pre- and post-operative joint alignments is necessary for validation, as well as information about the effect of each of small changes of these parameters on the remodeling outcomes.

Some of the parameters could already be used to perform validation of the model. The correct initial bone mineral densities could already be obtained by recalibrating the air-fat-muscle calibration tool. By calibrating this tool and creating an initial bone mineral density which is similar to the clinical initial values, the model could already be validated. Also, the HKA and FTA angles of the patients in the data are available and could be used in the model to imitate the clinical situation more. The available loads do not match those alignments, but the effect of applying those alignments to the models could already be tested.

When validated, the created models would be very valuable for research on the tibial bone remodeling after total knee replacement and the prevention of failure this procedure.

6 – References

Adachi, T., Tomita, Y., Sakaue, H., & Tanaka, M. (1997). Simulation of Trabecular Surface Remodeling based in Local Stress Nonuniformity. *JSME International Journal Series C Mechanical Systems, Machine Elements and Manufacturing*, *40*(4), 782–792.

Anijs, T., Eemers, S., Minoda, Y., Wolfson, D., Verdonschot, N., & Janssen, D. (2021). Computational tibial bone remodeling over a population after total knee arthroplasty: A comparative study. *Journal of Biomedical Materials Research - Part B Applied Biomaterials*, *October*, 1–11. https://doi.org/10.1002/jbm.b.34957

Anijs, T., Wolfson, D., Verdonschot, N., & Janssen, D. (2020). Population-based effect of total knee arthroplasty alignment on simulated tibial bone remodeling. *Journal of the Mechanical Behavior of Biomedical Materials*, *111*(July), 104014. https://doi.org/10.1016/j.jmbbm.2020.104014

Au, A. G., James Raso, V., Liggins, A. B., & Amirfazli, A. (2007). Contribution of loading conditions and material properties to stress shielding near the tibial component of total knee replacements. *Journal of Biomechanics*, *40*(6), 1410–1416. https://doi.org/10.1016/j.jbiomech.2006.05.020

Bailey, O., Ferguson, K., Crawfurd, E., James, P., May, P. A., Brown, S., Blyth, M., & Leach, W. J. (2015). No clinical difference between fixed- and mobile-bearing cruciate-retaining total knee arthroplasty: a prospective randomized study. *Knee Surgery, Sports Traumatology, Arthroscopy: Official Journal of the ESSKA*, *23*(6), 1653–1659. https://doi.org/10.1007/s00167-014-2877-9

Barrett, W. P., Mason, J. B., Moskal, J. T., Dalury, D. F., Oliashirazi, A., & Fisher, D. A. (2011). Comparison of radiographic alignment of imageless computer-assisted surgery vs conventional instrumentation in primary total knee arthroplasty. *Journal of Arthroplasty*, *26*(8), 1273-1284.e1. https://doi.org/10.1016/j.arth.2011.04.037

Bäthis, H., Perlick, L., Tingart, M., Perlick, C., Lüring, C., & Grifka, J. (2005). Intraoperative cutting errors in total knee arthroplasty. *Archives of Orthopaedic and Trauma Surgery*, *125*(1), 16–20. https://doi.org/10.1007/s00402-004-0759-1

Berend, M. E., Ritter, M. A., Meding, J. B., Faris, P. M., Keating, E. M., Redelman, R., Faris, G. W., & Davis, K. E. (2004). Tibial component failure mechanisms in total knee arthroplasty. *Clinical Orthopaedics and Related Research*, *428*, 26–34. https://doi.org/10.1097/01.blo.0000148578.22729.0e

Bergmann, G., Bender, A., Graichen, F., Dymke, J., Rohlmann, A., Trepczynski, A., Heller, M. O., & Kutzner, I. (2014). Standardized loads acting in knee implants. *PLoS ONE*, *9*(1). https://doi.org/10.1371/journal.pone.0086035

Bert, J. M., & McShane, M. (1998). Is it necessary to cement the tibial stem in cemented total knee arthroplasty? *Clinical Orthopaedics and Related Research*, *356*, 73–78. https://doi.org/10.1097/00003086-199811000-00012

Bingzhi, C., Yuedong, W., Suming, X., & Wenzhong, Z. (2009). A strain energy criterion for trabecular bone adaptation. *3rd International Conference on Bioinformatics and Biomedical Engineering, ICBBE 2009*, 1–7. https://doi.org/10.1109/ICBBE.2009.5162246

Boskey, A. L. (2013). Bone composition: relationship to bone fragility and antiosteoporotic drug effects. *BoneKEy Reports*, *2*(447), 1–11. https://doi.org/10.1038/bonekey.2013.181

Brihault, J., Navacchia, A., Pianigiani, S., Labey, L., De Corte, R., Pascale, V., & Innocenti, B. (2016). All-polyethylene tibial components generate higher stress and micromotions than metal-backed tibial components in total knee arthroplasty. *Knee Surgery, Sports Traumatology, Arthroscopy : Official Journal of the ESSKA*, *24*(8), 2550–2559. https://doi.org/10.1007/s00167-015-3630-8

Carter, D. R., & Hayes, W. C. (1976). Bone compressive strength: The influence of density and strain rate. *Science*, *194*(4270), 1174–1176. https://doi.org/10.1126/science.996549

Carter, D. R., Van Der Meulen, M. C. H., & Beaupré, G. S. (1996). Mechanical factors in bone growth and development. *Bone*, *18*(1 SUPPL.), S5–S10. https://doi.org/10.1016/8756-3282(95)00373-8

Cawley, D. T., Kelly, N., Simpkin, A., Shannon, F. J., & McGarry, J. P. (2012). Full and surface tibial cementation in total knee arthroplasty: A biomechanical investigation of stress distribution and remodeling in the tibia. *Clinical Biomechanics*, *27*(4), 390–397. https://doi.org/10.1016/j.clinbiomech.2011.10.011

CDC (2013). Prevalence of doctor-diagnosed arthritis and arthritis-attributable activity limitation--United States, 2010-2012. *MMWR. Morbidity and Mortality Weekly Report*, *62*(44), 869–873.

Cherian, J. J., Kapadia, B. H., Banerjee, S., Jauregui, J. J., Issa, K., & Mont, M. A. (2014). Mechanical, anatomical, and kinematic axis in TKA: Concepts and practical applications. *Current Reviews in Musculoskeletal Medicine*, *7*(2), 89–95. https://doi.org/10.1007/s12178-014-9218-y

Chong, D. Y. R., Hansen, U. N., & Amis, A. A. (2011). The influence of tibial prosthesis design features on stresses related to aseptic loosening and stress shielding. *Journal of Mechanics in Medicine and Biology*, *11*(1), 55–72. https://doi.org/10.1142/S0219519410003666

Clark, C. R., Rorabeck, C. H., Macdonald, S., Macdonald, D., Swafford, J., & Cleland, D. (2001). Posterior-stabilized and cruciate-retaining total knee replacement: A randomized study. *Clinical Orthopaedics and Related Research*, *392*, 208–212. https://doi.org/10.1097/00003086-200111000-00025

Cowin, S. C., & Hegedus, D. H. (1976). Bone remodeling I: theory of adaptive elasticity. *Journal of Elasticity*, *6*(3), 313–326. https://doi.org/10.1007/BF00041724

Cross, W. W., Saleh, K. J., Wilt, T. J., & Kane, R. L. (2006). Agreement about indications for total knee arthroplasty. *Clinical Orthopaedics and Related Research*, *446*, 34–39. https://doi.org/10.1097/01.blo.0000214436.49527.5e

Dennis, D. A., Komistek, R. D., Mahfouz, M. R., Outten, J. T., & Sharma, A. (2005). Mobile-bearing total knee arthroplasty: Do the polyethylene bearings rotate? *Clinical Orthopaedics and Related Research*, *440*, 88–95. https://doi.org/10.1097/01.blo.0000185464.23505.6e

Eggermont, F., Verdonschot, N., van der Linden, Y., & Tanck, E. (2019). Calibration with or without phantom for fracture risk prediction in cancer patients with femoral bone metastases using CT-based finite element models. *PLoS ONE*, *14*(7), 1–13. https://doi.org/10.1371/journal.pone.0220564

Enab, T. A., & Bondok, N. E. (2013). Material selection in the design of the tibia tray component of cemented artificial knee using finite element method. *Materials and Design*, *44*, 454–460. https://doi.org/10.1016/j.matdes.2012.08.017

Engh, J., McAuley, J. P., Sychterz, C. J., Sacco, M. E., & Engh, S. (2000). The accuracy and reproducibility of radiographic assessment of stress-shielding: A postmortem analysis. *Journal of Bone and Joint Surgery - Series A*, *82*(10), 1414–1420. https://doi.org/10.2106/00004623-200010000-00007

Finkelstein, J. S., Brockwell, S. E., Mehta, V., Greendale, G. A., Sowers, M. R., Ettinger, B., Lo, J. C., Johnston, J. M., Cauley, J. A., Danielson, M. E., & Neer, R. M. (2008). Bone mineral density changes during the menopause transition in a multiethnic cohort of women. *The Journal of Clinical Endocrinology and Metabolism*, *93*(3), 861–868. https://doi.org/10.1210/jc.2007-1876

García, J. M., Doblaré, M., & Cegoñino, J. (2002). Bone remodelling simulation: A tool for implant design. *Computational Materials Science*, *25*(1–2), 100–114. https://doi.org/10.1016/S0927-0256(02)00254-9

Gebert De Uhlenbrock, A., Püschel, V., Püschel, K., Morlock, M. M., & Bishop, N. E. (2012). Influence of time in-situ and implant type on fixation strength of cemented tibial trays - A post mortem retrieval analysis. *Clinical Biomechanics*, *27*(9), 929–935. https://doi.org/10.1016/j.clinbiomech.2012.06.008

Gill, G. S., & Joshi, A. B. (2001). Long-term results of Kinematic Condylar knee replacement. An analysis of 404 knees. *The Journal of Bone and Joint Surgery. British Volume*, *83*(3), 355–358. https://doi.org/10.1302/0301-620X.83B3.11288

Gong, H., Wang, L., Zhang, M., & Fan, Y. (2014). Computational modeling of bone and bone remodeling. In *Computational Modelling of Biomechanics and Biotribology in the Musculoskeletal System: Biomaterials and Tissues*. Woodhead Publishing Limited. https://doi.org/10.1533/9780857096739.2.244

Grood, E. S., & Suntay, W. J. (1983). A joint coordinate system for the clinical description of three-dimensional motions: Application to the knee. *Journal of Biomechanical Engineering*, *105*(2), 136–144. https://doi.org/10.1115/1.3138397

Hanzlik, J. A., & Day, J. S. (2013). Bone Ingrowth in Well-Fixed Retrieved Porous Tantalum Implants. *The Journal of Arthroplasty*, *28*(6), 922–927. https://doi.org/10.1016/j.arth.2013.01.035

Hart, R. T., Davy, D. T., & Heiple, K. G. (1984). A computational method for stress analysis of adaptive elastic materials with a view toward applications in strain-induced bone remodeling. *Journal of Biomechanical Engineering*, *106*(4), 342–350. https://doi.org/10.1115/1.3138503

Herrera, A., Panisello, J. J., Ibarz, E., Cegoñino, J., Puértolas, J. A., & Gracia, L. (2007). Long-term study of bone remodelling after femoral stem: A comparison between dexa and finite element simulation. *Journal of Biomechanics*, *40*(16), 3615–3625. https://doi.org/10.1016/j.jbiomech.2007.06.008

Hofmann, A. A., Goldberg, T. D., Tanner, A. M., & Cook, T. M. (2006). Surface Cementation of Stemmed Tibial Components in Primary Total Knee Arthroplasty. Minimum 5-Year Follow-up. *Journal of Arthroplasty*, *21*(3), 353–357. https://doi.org/10.1016/j.arth.2005.06.012

Hohman, D. W., Nodzo, S. R., Phillips, M., & Fitz, W. (2015). The implications of mechanical alignment on soft tissue balancing in total knee arthroplasty. *Knee Surgery, Sports Traumatology, Arthroscopy*, *23*(12), 3632–3636. https://doi.org/10.1007/s00167-014-3262-4

Huiskes, R., Weinans, H., Grootenboer, H. J., Dalstra, M., Fudala, B., & Slooff, T. J. (1987). Adaptive Bone-Remodeling Theory Applied to Prosthetic Design Analysis. *Journal of Biomechanics*, *20*(11–12), 1135–1150. https://doi.org/https://doi.org/10.1016/0021-9290(87)90030-3

Huiskes, R., Weinans, H., & Van Rietbergen, B. (1992). The relationship between stress shielding and bone resorption around total hip stems and the effects of flexible materials. *Clinical Orthopaedics and Related Research*, *274*, 124–134. https://doi.org/10.1097/00003086-199201000-00014

Hulet, C., Sabatier, J. P., Souquet, D., Locker, B., Marcelli, C., & Vielpeau, C. (2002). Distribution of bone mineral density at the proximal tibia in knee osteoarthritis. *Calcified Tissue International*, *71*(4), 315–322. https://doi.org/10.1007/s00223-001-2112-9

Hungerford, D. S., & Krackow, K. A. (1985). Total joint arthroplasty of the knee. *Clinical Orthopaedics and Related Research*, *NO. 192*, 23–33. https://doi.org/10.1097/00003086-198501000-00004

Hvid, I., Bentzen, S. M., & Jørgensen, J. (1988). Remodeling of the tibial plateau after knee replacement: CT bone densitometry. *Acta Orthopaedica*, *59*(5), 567–573. https://doi.org/10.3109/17453678809148787

Inaba, Y., Ike, H., Oba, M., & Saito, T. (2016). Evaluation of Adaptive Bone Remodeling after Total Hip Arthroplasty Using Finite Element Analysis. *Perusal of the Finite Element Method*. https://doi.org/10.5772/65031

Innocenti, B., Truyens, E., Labey, L., Wong, P., Victor, J., & Bellemans, J. (2009). Can medio-lateral baseplate position and load sharing induce asymptomatic local bone resorption of the proximal tibia? A finite element study. *Journal of Orthopaedic Surgery and Research*, *4*(1), 1–15. https://doi.org/10.1186/1749-799X-4-26

Jaroma, A., Soininvaara, T., & Kröger, H. (2016). Periprosthetic tibial bone mineral density changes after total knee arthroplasty: A 7-year follow-up of 86 patients. *Acta Orthopaedica*, *87*(3), 268–273. https://doi.org/10.3109/17453674.2016.1173982

Jiang, C., Liu, Z., Wang, Y., Bian, Y., Feng, B., & Weng, X. (2016). Posterior Cruciate Ligament Retention versus Posterior Stabilization for Total Knee Arthroplasty: A Meta-Analysis. *PLoS ONE*, *11*(1). https://doi.org/10.1371/journal.pone.0147865

Jordan, J. M., Helmick, C. G., Renner, J. B., Luta, G., Dragomir, A. D., Woodard, J., Fang, F., Schwartz, T. A., Nelson, A. E., Abbate, L. M., Callahan, L. F., Kalsbeek, W. D., & Hochberg, M. C. (2009). Prevalence of hip symptoms and radiographic and symptomatic hip osteoarthritis in African Americans and Caucasians: The Johnston County osteoarthritis project. *Journal of Rheumatology*, *36*(4), 809–815. https://doi.org/10.3899/jrheum.080677

Keller, T. S. (1994). Predicting the compressive mechanical behavior of bone. *Journal of Biomechanics*, *27*(9), 1159–1168. https://doi.org/10.1016/0021-9290(94)90056-6

Khandaker, M., & Meng, Z. (2015). The Effect of Nanoparticles and Alternative Monomer on the Exothermic Temperature of PMMA Bone Cement Morshed. *Procedia Engineering*, *105*, 946–952. https://doi.org/oi:10.1016/j.proeng.2015.05.120.

Kikinis, R., Pieper, S. D., & Vosburgh, K. (2014). *3D Slicer: A Platform for Subject-Specific Image Analysis, Visualization, and Clinical Support. Intraoperative Imaging Image-Guided Therapy* (F. A. Jolesz (Ed.); 1st ed.). Springer Science+Business Media. https://doi.org/https://doi.org/10.1007/978-1-4614-7657-3

Killen, C. J., Murphy, M. P., Hopkinson, W. J., Harrington, M. A., Adams, W. H., & Rees, H. W. (2020). Minimum twelve-year follow-up of fixed- vs mobile-bearing total knee arthroplasty: Double blinded randomized trial. *Journal of Clinical Orthopaedics and Trauma*, *11*(1), 154–159. https://doi.org/10.1016/j.jcot.2019.03.019

Kim, Y. H., Kim, J. S., Choe, J. W., & Kim, H. J. (2012). Long-term comparison of fixed-bearing and mobile-bearing total knee replacements in patients younger than fifty-one years of age with osteoarthritis. *The Journal of Bone and Joint Surgery. American Volume*, *94*(10), 866–873. https://doi.org/10.2106/JBJS.K.00884

Kim, Y. H., Park, J. W., Kim, J. S., Kulkarni, S. S., & Kim, Y. H. (2014). Long-term clinical outcomes and survivorship of press-fit condylar sigma fixed-bearing and mobile-bearing total knee prostheses in the same patients. *Journal of Bone and Joint Surgery - American Volume*, *96*(19), e168. https://doi.org/10.2106/JBJS.M.01130

Krčah, M., Székely, G., & Blanc, R. (2011). Fully automatic and fast segmentation of the femur bone from 3D-CT images with no shape prior. *Proceedings - International Symposium on Biomedical Imaging*, 2087–2090. https://doi.org/10.1109/ISBI.2011.5872823

Kurtz, S., Ong, K., Lau, E., Mowat, F., & Halpern, M. (2007). Projections of primary and revision hip and knee arthroplasty in the United States from 2005 to 2030. *The Journal of Bone and Joint Surgery. American Volume*, *89*(4), 780–785. https://doi.org/10.2106/JBJS.F.00222

Kutzner, I., Heinlein, B., Graichen, F., Bender, A., Rohlmann, A., Halder, A., Beier, A., & Bergmann, G. (2010). Loading of the knee joint during activities of daily living measured in vivo in five subjects. *Journal of Biomechanics*, *43*(11), 2164–2173. https://doi.org/10.1016/j.jbiomech.2010.03.046

Leblanc, A. D., Schneider, V. S., Evans, H. J., Engelbretson, D. A., & Krebs, J. M. (1990). Bone mineral loss and recovery after 17 weeks of bed rest. *Journal of Bone and Mineral Research : The Official Journal of the American Society for Bone and Mineral Research*, *5*(8), 843–850. https://doi.org/https://doi.org/10.1002/jbmr.5650050807

Li, M. G., & Nilsson, K. G. (2000a). Changes in bone mineral density at the proximal tibia after total knee arthroplasty: A 2-year follow-up of 28 knees using dual energy X-ray absorptiometry. *Journal of Orthopaedic Research*, *18*(1), 40–47. https://doi.org/10.1002/jor.1100180107

Li, M. G., & Nilsson, K. G. (2000b). The effect of the preoperative bone quality on the fixation of the tibial component in total knee arthroplasty. *Journal of Arthroplasty*, *15*(6), 744–753. https://doi.org/10.1054/arth.2000.6617

Luring, C., Perlick, L., Trepte, C., Linhardt, O., Perlick, C., Plitz, W., & Grifka, J. (2006). Micromotion in cemented rotating platform total knee arthroplasty: Cemented tibial stem versus hybrid fixation. *Archives of Orthopaedic and Trauma Surgery*, *126*(1), 45–48. https://doi.org/10.1007/s00402-005-0082-5

Lützner, J., Krummenauer, F., Günther, K. P., & Kirschner, S. (2010). Rotational alignment of the tibial component in total knee arthroplasty is better at the medial third of tibial tuberosity than at the medial border. *BMC Musculoskeletal Disorders*, *11*(57). https://doi.org/10.1186/1471-2474-11-57

Martin, R. B. (1984). Porosity and specific surface of bone. *Critical Reviews in Biomedical Engineering*, *10*(3), 179–222.

Matassi, F., Carulli, C., Civinini, R., & Innocenti, M. (2014). Cemented versus cementless fixation in total knee arthroplasty. *Joints*, *1*(3), 121–125. https://doi.org/10.11138/jts/2013.1.3.121

McEwen, H. M. J., Barnett, P. I., Bell, C. J., Farrar, R., Auger, D. D., Stone, M. H., & Fisher, J. (2005). The influence of design, materials and kinematics on the in vitro wear of total knee replacements. *Journal of Biomechanics*, *38*(2), 357–365. https://doi.org/10.1016/j.jbiomech.2004.02.015

Migliorini, F., Eschweiler, J., Tingart, M., & Rath, B. (2019). Posterior-stabilized versus cruciate-retained implants for total knee arthroplasty: a meta-analysis of clinical trials. In *European Journal of Orthopaedic Surgery and Traumatology* (Vol. 29, Issue 4, pp. 937–946). Springer Paris. https://doi.org/10.1007/s00590-019-02370-1

Mihalko, W. M., Saleh, K. J., Krackow, K. A., & Whiteside, L. A. (2009). Soft-tissue balancing during total knee arthroplasty in the varus knee. *Journal of the American Academy of Orthopaedic Surgeons*, *17*(12), 766–774. https://doi.org/10.5435/00124635-200912000-00005

Minoda, Y., Kobayashi, A., Iwaki, H., Ikebuchi, M., Inori, F., & Takaoka, K. (2010). Comparison of bone mineral density between porous tantalum and cemented tibial total knee arthroplasty components. *Journal of Bone and Joint Surgery - Series A*, *92*(3), 700–706. https://doi.org/10.2106/JBJS.H.01349

Mora, J. C., Przkora, R., & Cruz-Almeida, Y. (2018). Knee osteoarthritis: Pathophysiology and current treatment modalities. *Journal of Pain Research*, *11*, 2189–2196. https://doi.org/10.2147/JPR.S154002

Morgan, E. F., Bayraktar, H. H., & Keaveny, T. M. (2003). Trabecular bone modulus-density relationships depend on anatomic site. *Journal of Biomechanics*, *36*(7), 897–904. https://doi.org/10.1016/S0021-9290(03)00071-X

Mosekilde, L., Mosekilde, L., & Danielsen, C. C. (1987). Biomechanical competence of vertebral trabecular bone in relation to ash density and age in normal individuals. *Bone*, *8*(2), 79–85. https://doi.org/https://doi.org/10.1016/8756-3282(87)90074-3

Naganathan, V., & Sambrook, P. (2003). Gender differences in volumetric bone density: A study of opposite-sex twins. *Osteoporosis International*, *14*(7), 564–569. https://doi.org/10.1007/s00198-003-1422-3

Nieves, J. W., Formica, C., Ruffing, J., Zion, M., Garrett, P., Lindsay, R., & Cosman, F. (2005). Males have larger skeletal size and bone mass than females, despite comparable body size. *Journal of Bone and Mineral Research*, *20*(3), 529–535. https://doi.org/10.1359/JBMR.041005

OrthoLoad Database. (2021). www.OrthoLoad.com/knee-joint/

Park, H. J., Bae, T. S., Kang, S. B., Baek, H. H., Chang, M. J., & Chang, C. B. (2021). A three-dimensional finite element analysis on the effects of implant materials and designs on periprosthetic tibial bone resorption. *PLoS ONE*, *16*(2), 1–12. https://doi.org/10.1371/journal.pone.0246866

Pavone, V., Boettner, F., Fickert, S., & Sculco, T. P. (2001). Total condylar knee arthroplasty: A long-term followup. *Clinical Orthopaedics and Related Research*, *388*, 18–25. https://doi.org/10.1097/00003086-200107000-00005

Perkins, M. R., Arnholt, C. M., MacDonald, D. W., Kurtz, S. M., & Mihalko, W. M. (2020). Retrieval Analysis of Cruciate-Retaining and Posterior-Stabilized Total Knee Arthroplasty and Correlations to Laxity and Wear. *Journal of Arthroplasty*, *35*(8), 2249–2253. https://doi.org/10.1016/j.arth.2020.03.027

Powell, D. (2015). *r3d: Software for fast, robust geometric operations in 3D and 2D - LA-UR-15-26964*.

Powell, D., & Abel, T. (2015). An exact general remeshing scheme applied to physically conservative voxelization. *Journal of Computational Physics*, *297*, 340–356. https://doi.org/10.1016/j.jcp.2015.05.022

Rajgopal, A., Vasdev, N., Pathak, A., Gautam, D., & Vasdev, A. (2014). Histological changes and neural elements in the posterior cruciate ligament in osteoarthritic knees. *Journal of Orthopaedic Surgery (Hong Kong)*, *22*(2), 142–145. https://doi.org/10.1177/230949901402200204

Rivière, C., Iranpour, F., Auvinet, E., Howell, S., Vendittoli, P. A., Cobb, J., & Parratte, S. (2017). Alignment options for total knee arthroplasty: A systematic review. *Orthopaedics and Traumatology: Surgery and Research*, *103*(7), 1047–1056. https://doi.org/10.1016/j.otsr.2017.07.010

Robinson, W. H., Lepus, C. M., Wang, Q., Raghu, H., Mao, R., Lindstrom, T. M., & Sokolove, J. (2016). Low-grade inflammation as a key mediator of the pathogenesis of osteoarthritis. *Nature Reviews Rheumatology*, *12*(10), 580–592. https://doi.org/10.1038/nrrheum.2016.136

Roy, D., Swarbrick, C., King, Y., Pye, S., Adams, J., Berry, J., Silman, A., & O'Neill, T. (2005). Differences in peak bone mass in women of European and South Asian origin can be explained by differences in body size. *Osteoporosis International*, *16*(10), 1254–1262. https://doi.org/10.1007/s00198-005-1837-0

Saari, T., Uvehammer, J., Carlsson, L., Regnér, L., & Kärrholm, J. (2007). Joint area constraint had no influence on bone loss in proximal tibia 5 years after total knee replacement. *Journal of Orthopaedic Research*, *25*(6), 798–803. https://doi.org/https://doi.org/10.1002/jor.20358

Sawaguchi, N., Majima, T., Ishigaki, T., Mori, N., Terashima, T., & Minami, A. (2010). Mobile-bearing total knee arthroplasty improves patellar tracking and patellofemoral contact stress. In vivo measurements in the same patients. *Journal of Arthroplasty*, *25*(6), 920–925. https://doi.org/10.1016/j.arth.2009.07.024

Schroer, W. C., Berend, K. R., Lombardi, A. V, Barnes, C. L., Bolognesi, M. P., Berend, M. E., Ritter, M. A., & Nunley, R. M. (2013). Why Are Total Knees Failing Today ? Etiology of Total Knee Revision in 2010 and 2011. *Journal of Arthroplasty*, *28*(8 suppl), 116–119. https://doi.org/10.1016/j.arth.2013.04.056

Sekiya, H., Takatoku, K., Takada, H., Sasanuma, H., & Sugimoto, N. (2009). Postoperative lateral ligamentous laxity diminishes with time after TKA in the varus knee. *Clinical Orthopaedics and Related Research*, *467*(6), 1582–1586. https://doi.org/10.1007/s11999-008-0588-6

Sharkey, P. F., Lichstein, P. M., Shen, C., Tokarski, A. T., & Parvizi, J. (2014). Why are total knee arthroplasties failing today-has anything changed after 10 years? *Journal of Arthroplasty*, *29*(9), 1774–1778. https://doi.org/10.1016/j.arth.2013.07.024

Sibonga, J. D., Evans, H. J., Sung, H. G., Spector, E. R., Lang, T. F., Oganov, V. S., Bakulin, A. V., Shackelford, L. C., & LeBlanc, A. D. (2007). Recovery of spaceflight-induced bone loss: Bone mineral density after long-duration missions as fitted with an exponential function. *Bone*, *41*(6), 973–978. https://doi.org/10.1016/j.bone.2007.08.022

Skwara, A., Figiel, J., Knott, T., Paletta, J. R. J., Fuchs-Winkelmann, S., & Tibesku, C. O. (2009). Primary stability of tibial components in TKA: In vitro comparison of two cementing techniques. *Knee Surgery, Sports Traumatology, Arthroscopy : Official Journal of the ESSKA*, *17*(10), 1199–1205. https://doi.org/10.1007/s00167-009-0849-2

Small, S. R., Ritter, M. A., Merchun, J. G., Davis, K. E., & Rogge, R. D. (2013). Changes in tibial bone density measured from standard radiographs in cemented and uncemented total knee replacements after ten years' follow-up. *Bone and Joint Journal*, *95 B*(7), 911–916. https://doi.org/10.1302/0301-620X.95B7.30537

Soininvaara, T. A., Miettinen, H. J. A., Jurvelin, J. S., Suomalainen, O. T., Alhava, E. M., & Kröger, H. P. J. (2004). Periprosthetic tibial bone mineral density changes after total knee arthroplasty: One-year follow-up study of 69 patients. *Acta Orthopaedica Scandinavica*, *75*(5), 600–605. https://doi.org/10.1080/00016470410001493

Soininvaara, T., Nikola, T., Vanninen, E., Miettinen, H., & Kröger, H. (2008). Bone mineral density and single photon emission computed tomography changes after total knee arthroplasty: A 2-year follow-up study.

Clinical Physiology and Functional Imaging, *28*(2), 101–106. https://doi.org/10.1111/j.1475-097X.2007.00782.x

Srinivasan, P., Miller, M. A., Verdonschot, N., Mann, K. A., & Janssen, D. (2017). Strain shielding in trabecular bone at the tibial cement-bone interface. *Journal of the Mechanical Behavior of Biomedical Materials*, *66*(november), 181–186. https://doi.org/10.1016/j.jmbbm.2016.11.006

Stock, J. T. (2018). *Wolff's law (bone functional adaptation)* W. Trevathan, M. Cartmill, D. Dufour, C. Larsen, D. O'Rourke, K. Rosenberg, & K. Strier (Eds.)). https://doi.org/10.1002/9781118584538.ieba0521

Stülpner, M. A., Reddy, B. D., Starke, G. R., & Spirakis, A. (1997). A three-dimensional finite analysis of adaptive remodelling in the proximal femur. *Journal of Biomechanics*, *30*(10), 1063–1066. https://doi.org/10.1016/S0021-9290(97)00074-2

Sundfeldt, M., Carlsson, L. V, Johansson, C. B., Thomsen, P., & Gretzer, C. (2006). Aseptic loosening, not only a question of wear: A review of different theories. In *Acta Orthopaedica* (Vol. 77, Issue 2, pp. 177–197). https://doi.org/10.1080/17453670610045902

Swanik, C., Lephart, S., & Rubash, H. (2004). Proprioception, kinesthesia, and balance after total knee arthroplasty with cruciate-retaining and posterior stabilized prostheses. *The Journal of Bone and Joint Surgery. American Volume*, *86*(2), 328–334. https://doi.org/https://doi.org/10.2106/00004623-200402000-00016

Tarala, M., Janssen, D., & Verdonschot, N. (2011). Balancing incompatible endoprosthetic design goals: A combined ingrowth and bone remodeling simulation. *Medical Engineering and Physics*, *33*(3), 374–380. https://doi.org/10.1016/j.medengphy.2010.11.005

Trevisan, C., Bigoni, M., Denti, M., Marinoni, E. C., & Ortolani, S. (1998). Bone assessment after total knee arthroplasty by dual-energy X-ray absorptiometry: Analysis protocol and reproducibility. *Calcified Tissue International*, *62*(4), 359–361. https://doi.org/10.1007/s002239900444

Turner, A. W. L., Gillies, R. M., Sekel, R., Morris, P., Bruce, W., & Walsh, W. R. (2005). Computational bone remodelling simulations and comparisons with DEXA results. *Journal of Orthopaedic Research*, *23*(4), 705–712. https://doi.org/10.1016/j.orthres.2005.02.002

Ueyama, H., Minoda, Y., Sugama, R., Ohta, Y., Nakamura, S., Takemura, S., & Nakamura, H. (2020). Peri-prosthetic bone mineral density after simultaneous bilateral total knee arthroplasty under oral bisphosphonate therapy — A comparison between mobile- and fixed-bearing prostheses. *Knee*, *27*(3), 767–776. https://doi.org/10.1016/j.knee.2020.04.011

Watanabe, S., Tomita, T., Akagi, R., Watanabe, A., Yamazaki, T., Enomoto, T., Nakagawa, R., Kimura, S., Ohtori, S., & Sasho, T. (2021). In vivo kinematics of cruciate-retaining total knee arthroplasty after a change of polyethylene insert configuration. *Asia-Pacific Journal of Sports Medicine, Arthroscopy, Rehabilitation and Technology*, *24*, 1–8. https://doi.org/10.1016/j.asmart.2020.11.002

Xie, J. (2011). *A Systematic Review on Performance of the Vanguard Complete Knee System* (p. 1). Biomet Orthopaedics.

Yoon, C., Chang, M. J., Chang, C. B., Song, M. K., Shin, J. H., & Kang, S. B. (2018). Medial Tibial Periprosthetic Bone Resorption and Its Effect on Clinical Outcomes After Total Knee Arthroplasty: Cobalt-Chromium vs Titanium Implants. *Journal of Arthroplasty*, *33*(9), 2835–2842. https://doi.org/10.1016/j.arth.2018.04.025

Zengin, A., Prentice, A., & Ward, K. A. (2015). Ethnic differences in bone health. *Frontiers in Endocrinology*, *6*(MAR), 1–6. https://doi.org/10.3389/fendo.2015.00024

Zhang, Q. H., Cossey, A., & Tong, J. (2016). Stress shielding in periprosthetic bone following a total knee replacement: Effects of implant material, design and alignment. *Medical Engineering and Physics*, *38*(12), 1481–1488. https://doi.org/10.1016/j.medengphy.2016.09.018

7 – Appendices

A – Total Workflow explanation

In this document the workflow used to create FE models in which the post-operative implant orientation is used is described. Following this workflow leads to models including the insert. The insert was left out in the final simulations done in this project.

1. Data

Data needed to use the workflow

1. Pre-operative DICOM of patient

2. Post-operative DICOM of the same patient

3. Both DICOMs can be either one file or a folder with DICOM slices

4. Model of the implant (tibial implant and insert) , preferably .stp, but .stl works

5. Information about the patient; the body weight, dates of CT scans, pre-operative varus/valgus (preferably), internal/external rotation angles (preferably) and the activity level of the patient (preferably)

6. Material properties of the implant materials

2. Segmentation

In the segmentation step a segmentation of the pre-operative tibia, the post-operative tibia incl implant and the implant itself are created.

MATLAB® : convert DICOM to NIftI

1. Use IvL_dcm2nii_multiple.m for multiple offsets, all the same cropping setting, you need the files:

    a. IvL_dcm2nii

    b. IvL_dcm2nii_2

    c. dcmextread.m *in this file line 81 images = permute(images,[2 1 3]) ; mirrors the leg in the DICOM. Comment this line if you want the nii to be in the same orientation as the DICOM image. If you do not comment this line, the final model (made during 06 Model setup) should be mirrored (mirror lateral and medial)*

2. Use IL_dcm2nii_test to test one file to see if it all works

SSH client: automatic bone segmentation

1. Use batchfile to process multiple .nii files at once (put && between lines), see IL_batchfile_test.bat as example

2. In SSH-client:
   segment-ct ~/home/Inger/IL_CT_files/filename.nii ~/IL_temp ~/IL_masks/mask_filename.nii
   is used to process the .nii files and make masks. The different offsets from dcm2nii are necessary to get a good masks (differs per dcm scan).

3. Download the masks to your own computer

3D Slicer: create .stl files of the autosegmented masks

1. Open the masks and original .nii files in 3D Slicer and compare the masks to find the best fit. If two or more masks are similar make a segmentation of each of them with the tab Segment Editor and compare those with the original scans to see which mask fits the tibia (and/or implant) best.

2. Make a segmentation of the best mask and make sure the fibula and femur parts of the mask are removed. Then, open the original .nii file and adjust the segmentation where needed.

3. Via segment editor,save the file as .stl, you want the coordinate system to be RAS (Right, Anterior, Superior). Do not in any case save the file as .nrrd or another file format first! This changes the origin of the system.

4. About post-op tibia and implant segmentation: First segment the tibia, by changing the contrast in 3D Slicer the tibia gets better visible. Then, in the same session (do not close 3D Slicer or the nii files) create another segmentation for the implant. The implant can be easily segmented by putting the threshold on a high level. Save both segmentations as .stl files.

Run hwremesh.m to remesh the .stl files created by 3D Slicer

This script remeshes the stl to elements of 2 mm, uniformly sized, optimally shaped.

3. Implant

In the workflow, implant geometries are used. Those should be prepared to be used in the workflow. The tray and insert should be converted towards a .stl file and an artificial cementlayer and two cuttingguides have to be created. The tray and insert used in this project are the Vanguard Total Knee System Rotating Platform. This example is made with these geometries. This part of the workflow may be similar for other implants; but will not be completely similar, so use it as a guide.

First, open the .stp files needed in HyperMesh one by one and resize them to mm (the models might be created in inches). To make sure in what measures the models are, automesh them with a triangle element size of 1.5. If the mesh looks fine it is in mm, and scaling is not needed, if the elements are very big, the model is in inches and should be scaled to mm (scale *25.4 in all dimensions).
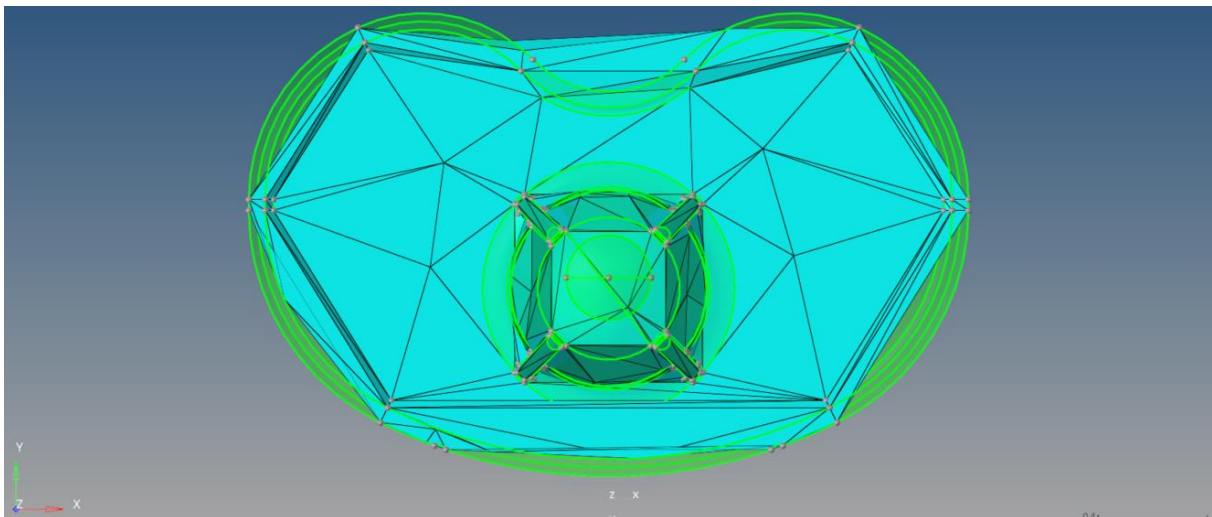
Once scaled, the model should be automeshed. This is done via 2D > automesh. Select all surfaces and the option batchmesh/QI optimize. The element size is 1.5 and the mesh type is trias:
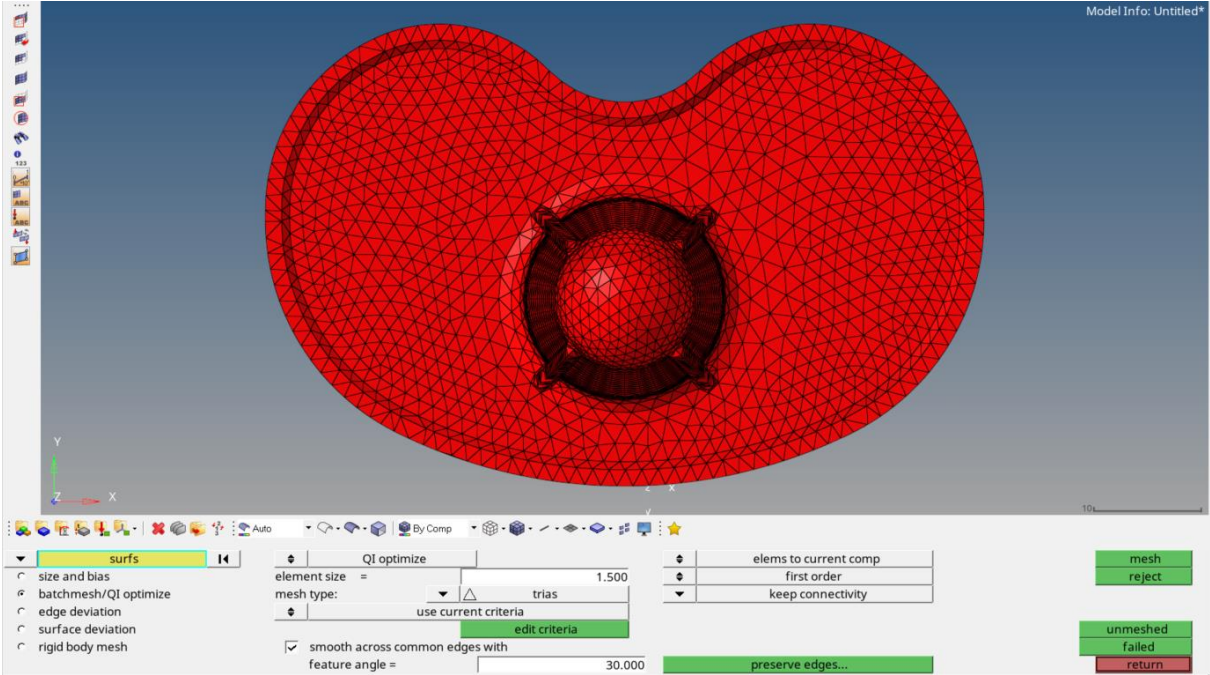
In this mesh, there are some very small elements at the edges. These are deleted and filled with the gap-fill function.
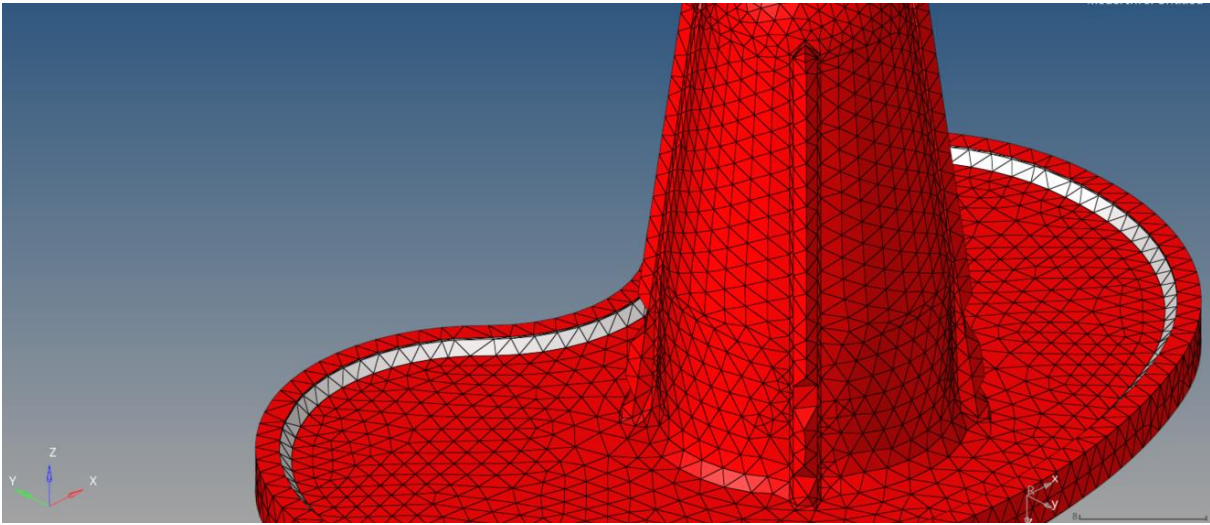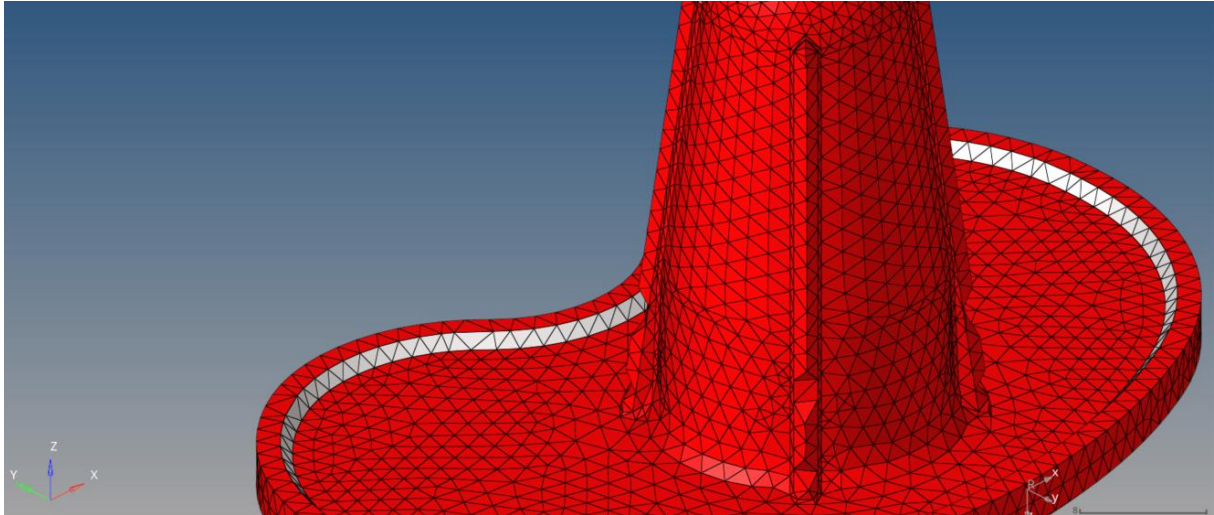
Then, the edges at the keel should also be fixed by hand. There are some gaps in the edges and the sides of each of the four edges contain very small elements. This is fixed by deleting those small elements and the elements in the gaps like shown below, and filling them with patch/hole/gap fill.
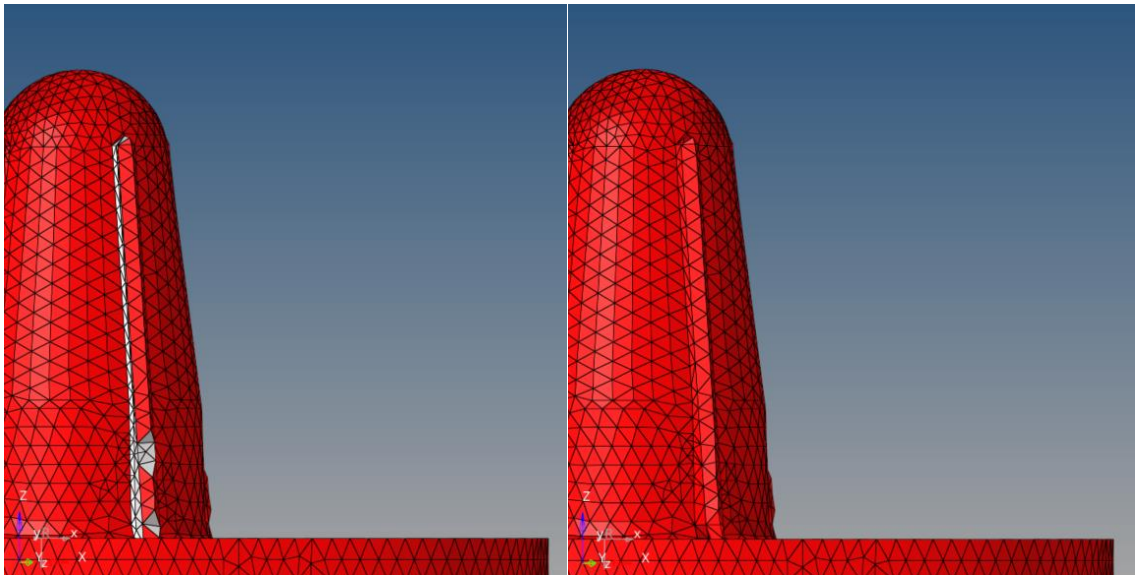
Export the model as .stl. This process is done with all tibial tray sizes.

Then, the tibial tray needed, is imported into MarcMentat. In case of the rotating platform, the mesh is first rotated 180 degrees around Y (Geometry & Mesh > Move > Rotate > rotation angle y = 180 > move elements. This is not needed in case of a PS implant! Save the rotated geometry as _rot.stl.

Then, select the lowest layer of the tray by setting the view to this:
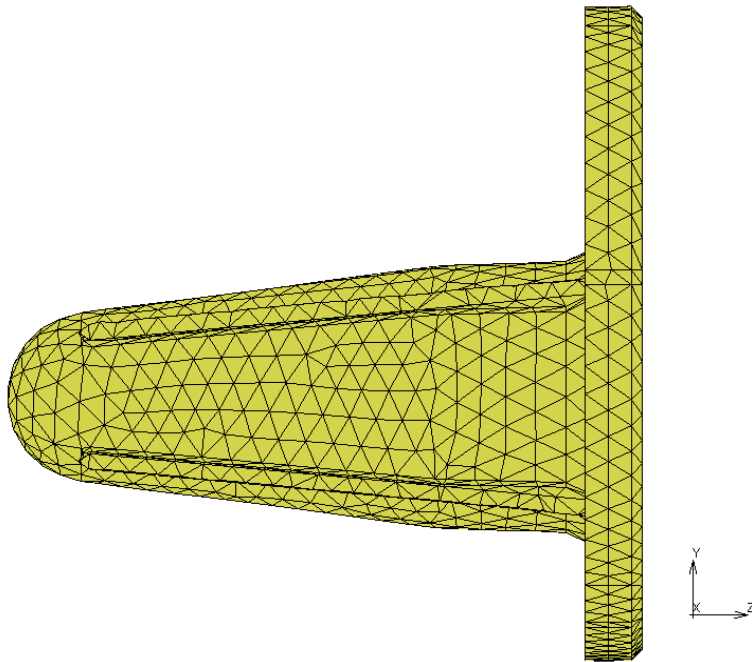
Select > selection control, elements by nodes, all-in-list, the result should look like this:
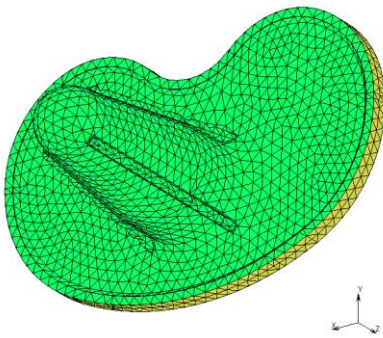
Then, Geometry & Mesh > geometry & Mesh > Elements > Rem > All unselected . And Geometry & Mesh >

geometry & Mesh > Nodes > Rem > All unselected .

Save this file as _onderkant_implant_incl_keel.stl.

Open this .stl in HyperMesh and delete the inner keel and export as _onderkant_implant_excl_keel.stl.
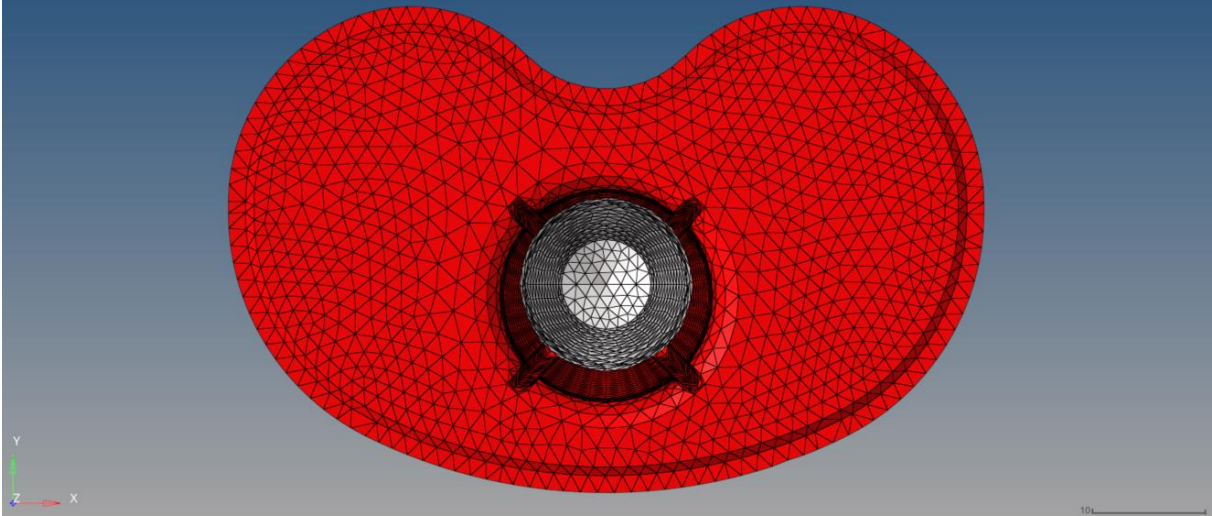
Create a surface in HyperMesh (Geometry > Create > Surface), size 150, at the edges of the geometry:
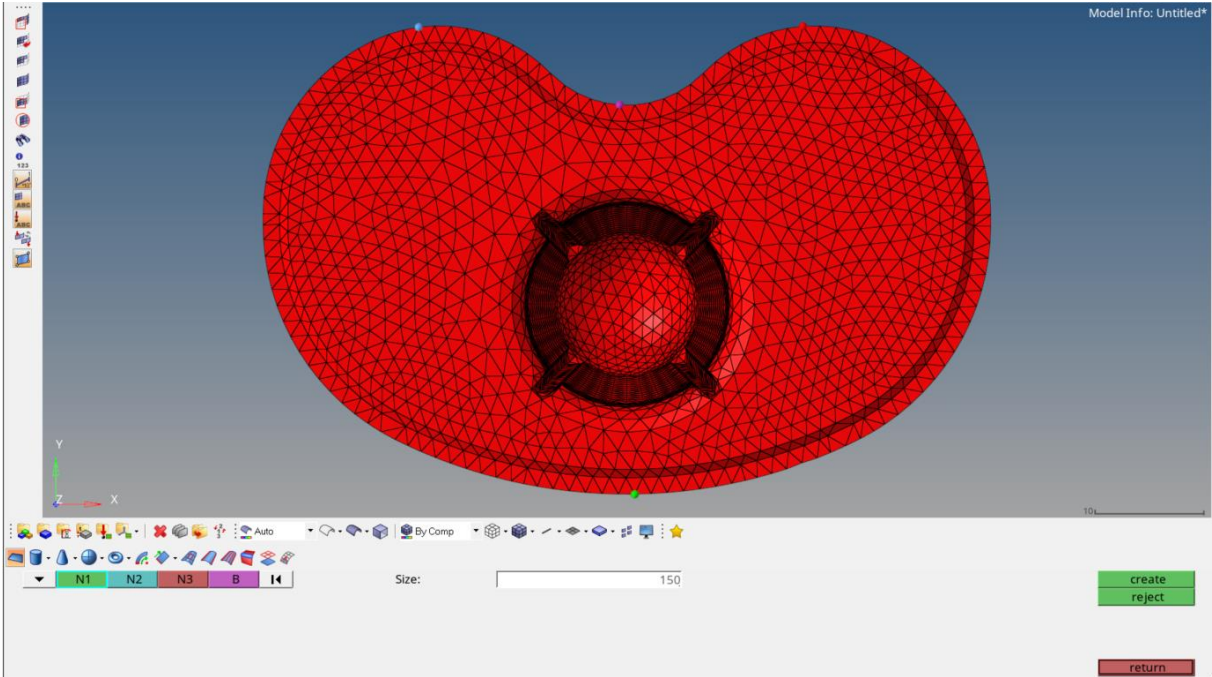
Click on create and return. You should have something like this now:
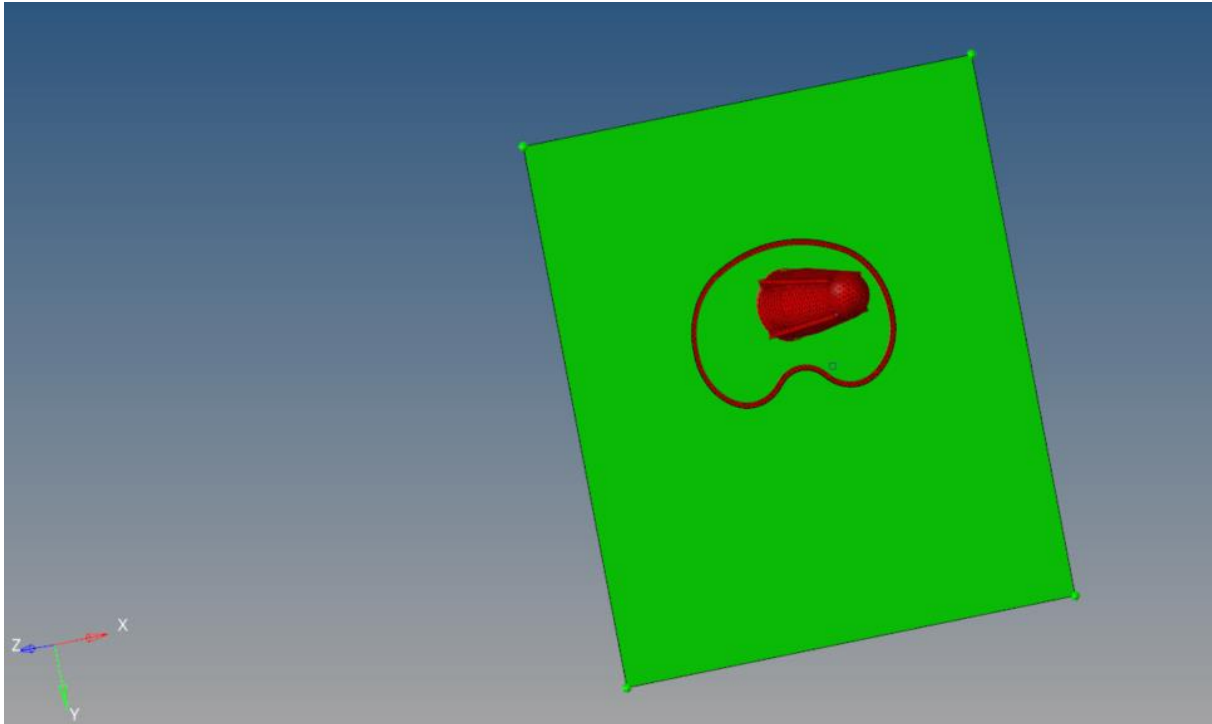
Automesh this surface: 2D > Automesh > Surfs, select surface > size and bias, element size is 1.5, trias elements > mesh > return.

Perform a Boolean operation (Mesh > Boolean Operation). Subtract > All entities for boolean = both components, Master entities = the tray > Run.

Delete the cement pocket, the surface inside the keel and the surface surrounding the tray. Save as cementlayer_bottom_nooffset_2comp.stl
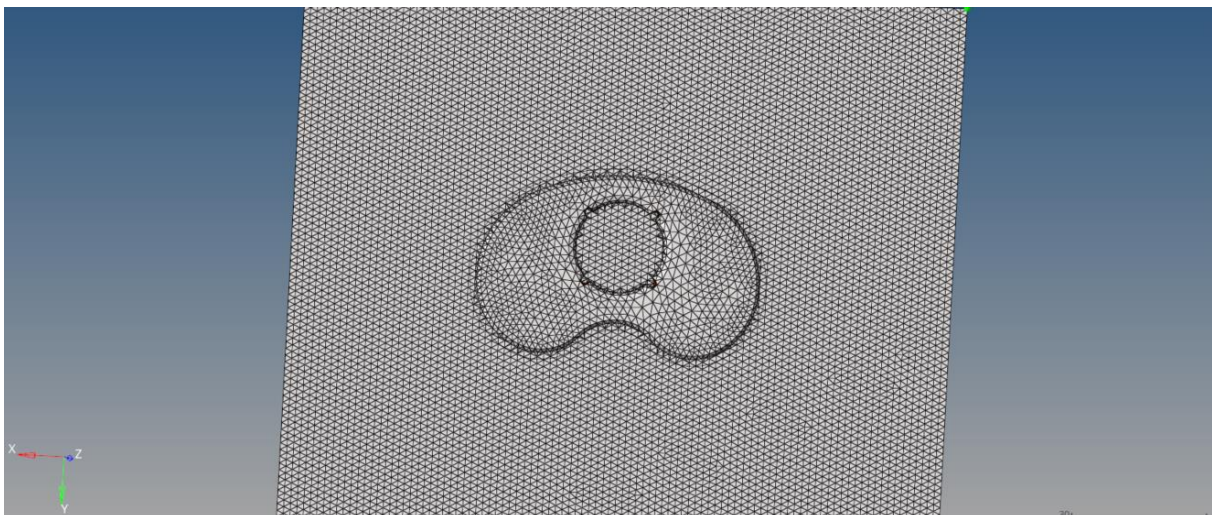
Merge all elements to the same component (the red one) and save as cementlayer_bottom_nooffset_1comp.stl. Then apply a remesh to the component and copy the component. Translate this copy -0.75 mm downwards and hide it.

Then, delete the corners of the cementlayer where the ridges on the keel start. This is needed to perform a good offset. Once the corners are deleted, apply an offset of 0.75 mm to the layer. Then show the copy made earlier to

check how the created holes should be fixed. It looks like this by now, green is the original layer and yellow is the copy:
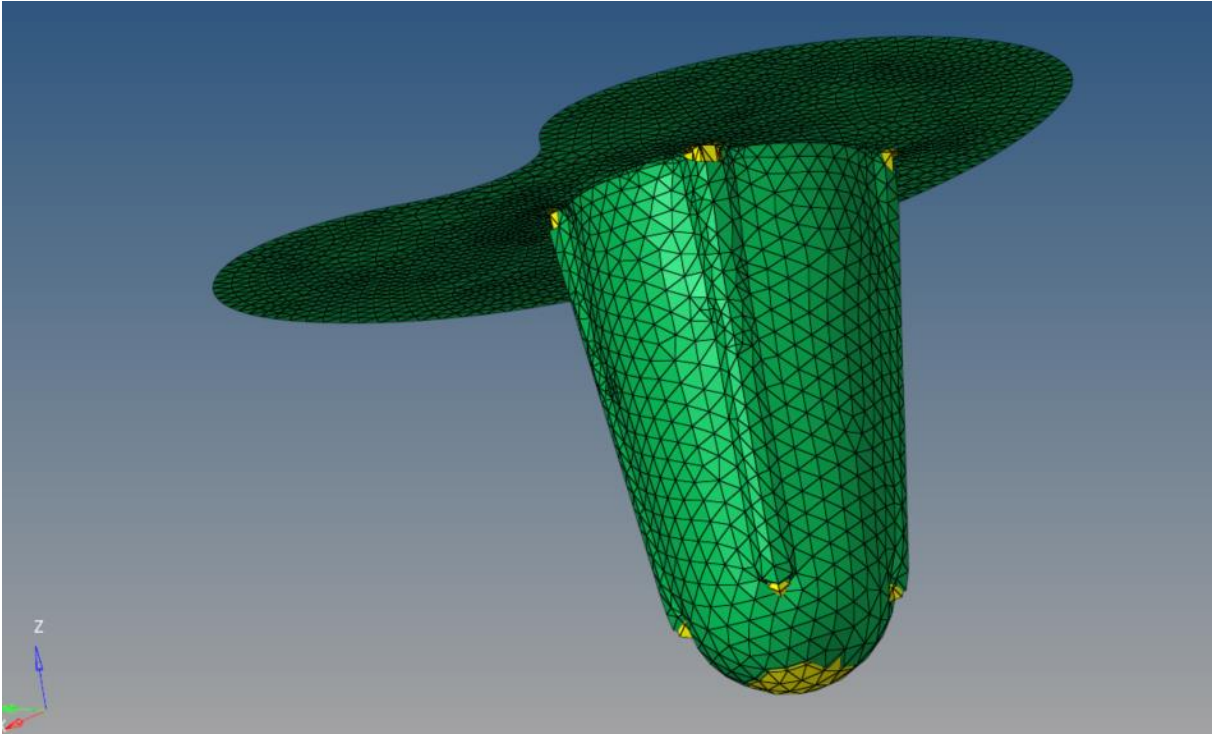
When the holes are filled up, open open the file _onderkant_implant_excl_keel.stl again:
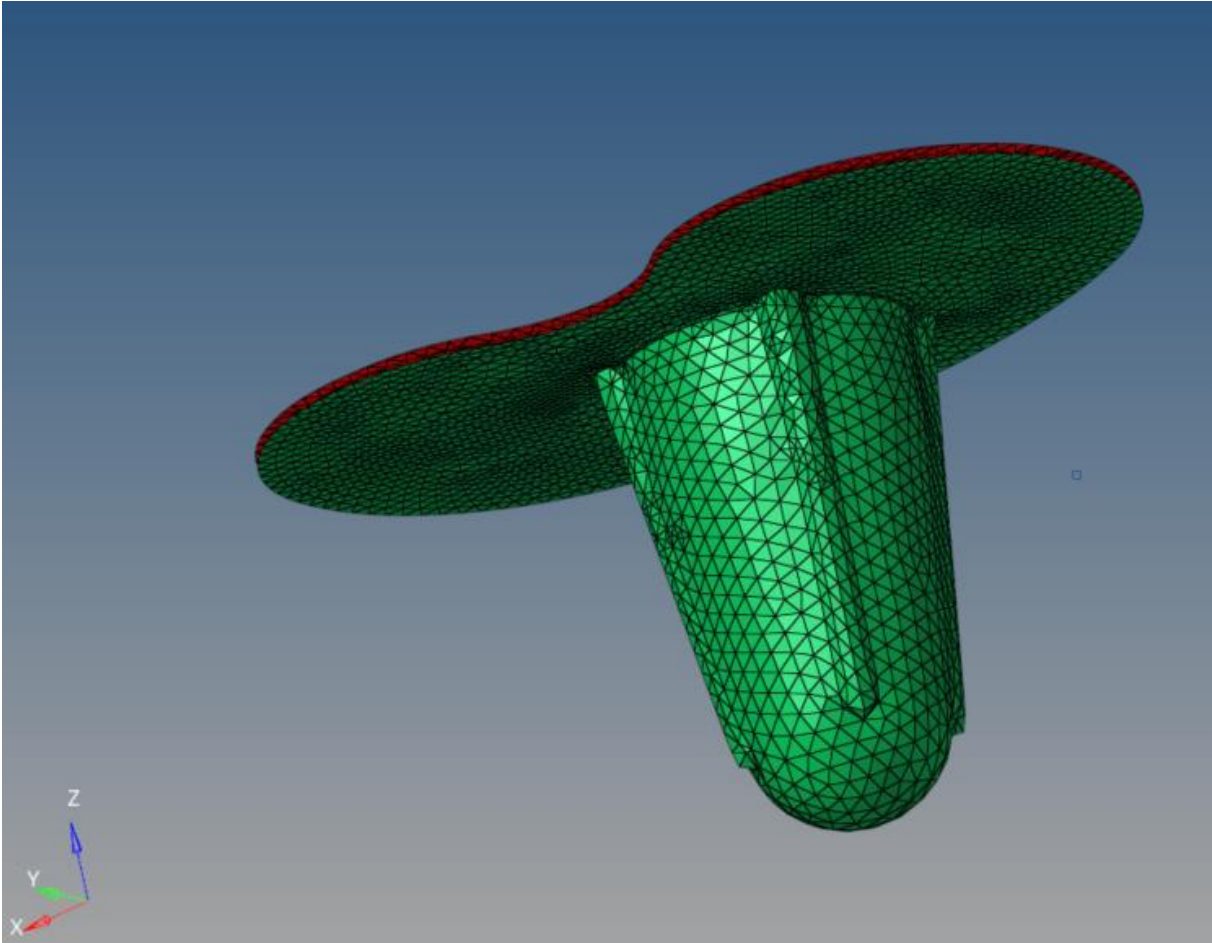
Then, fill the space inbetween with gap fill (Mesh > Hole/Gap fill > Gap Fill, Dest component = new component, Extended Edges > Remesh > Fill). Should look like this:
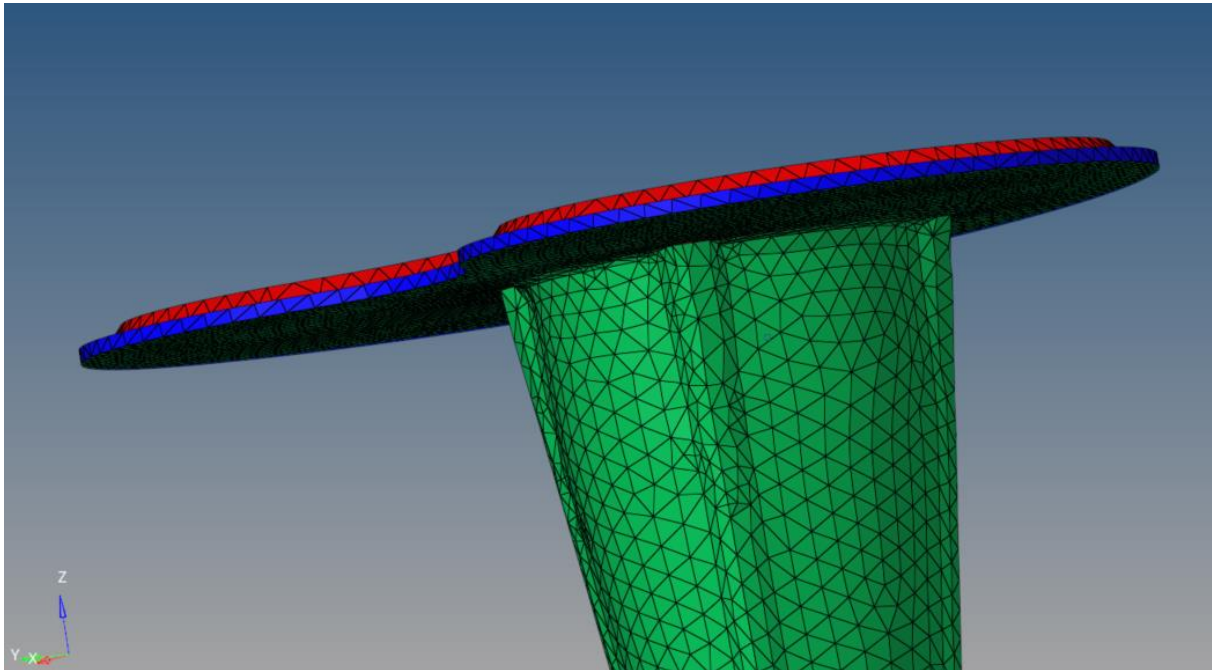
Rename all components with ^ in the name to something without ^. Export file as cementlayer_complete_3comps.stl.

Then, open this file in MM and go to Check and check ID Backfaces. By selecting the sets and clicking flip elements for the elements needed, the cement layer should look like this:
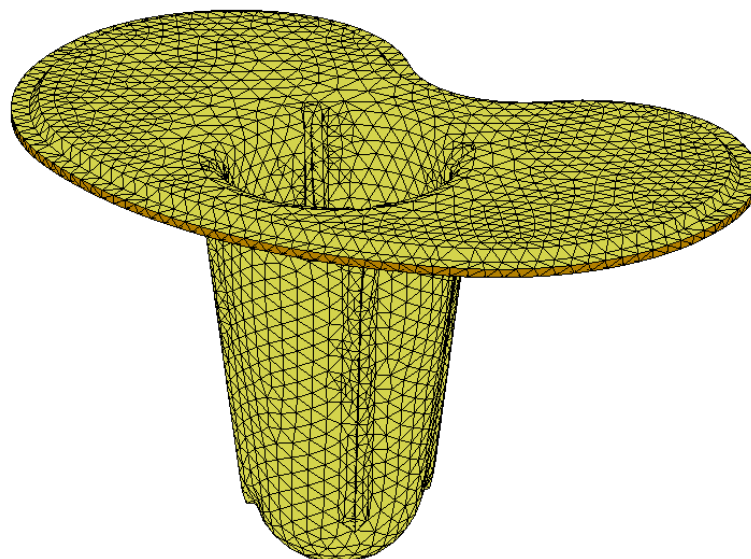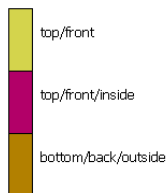
Save the stl as cementlayer_complete_4comps_flipped.stl. Also, delete the sets that are not the bottom and save the bottom as cementlayer_bottom_complete.stl

Open this file in HyperMesh and create lines around it, x: -50 to 50, y = -20 to 60, z = height of the tray (probably 0.127-0.75 but check this!!!).
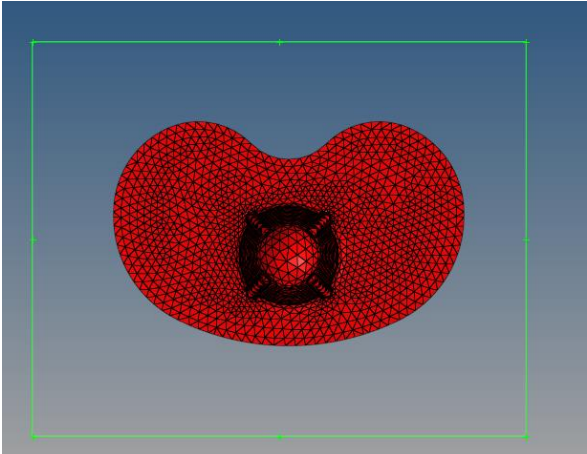
Then, create nodes on these line, 10 per line (Create > Nodes >Extract on line).
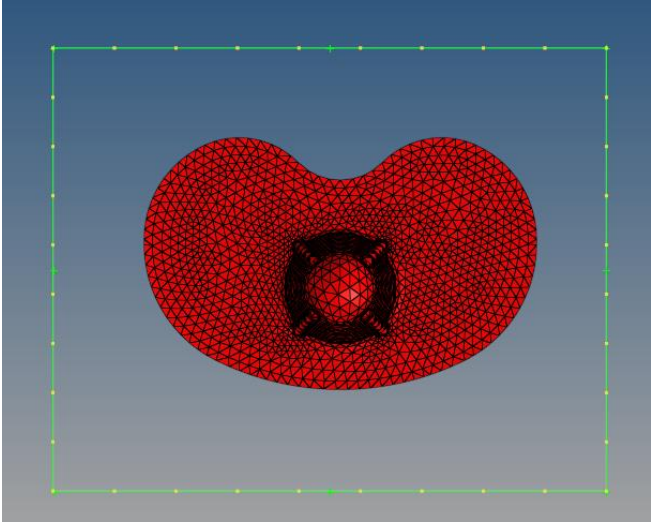
 Then, with gap fill, fill the space between the tray and the lines. Make sure the filling is flat!!!
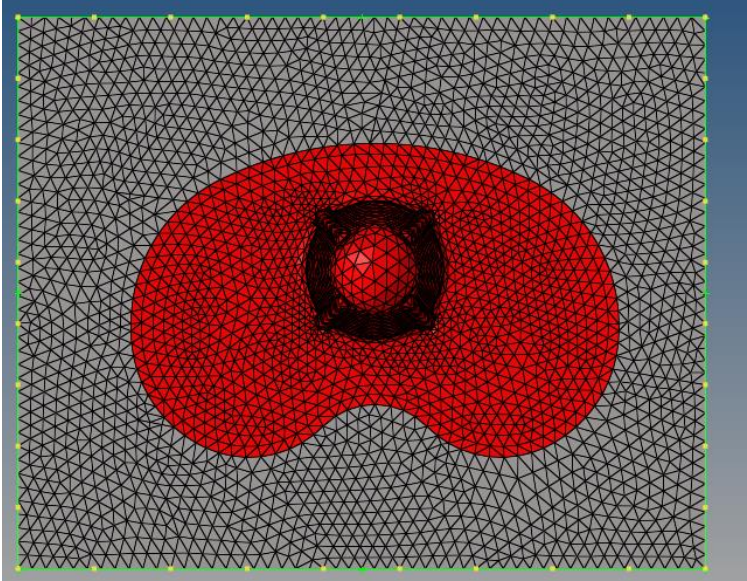
Delete the nodes and the lines and save as cuttingguide_0.75offset_2comp.stl
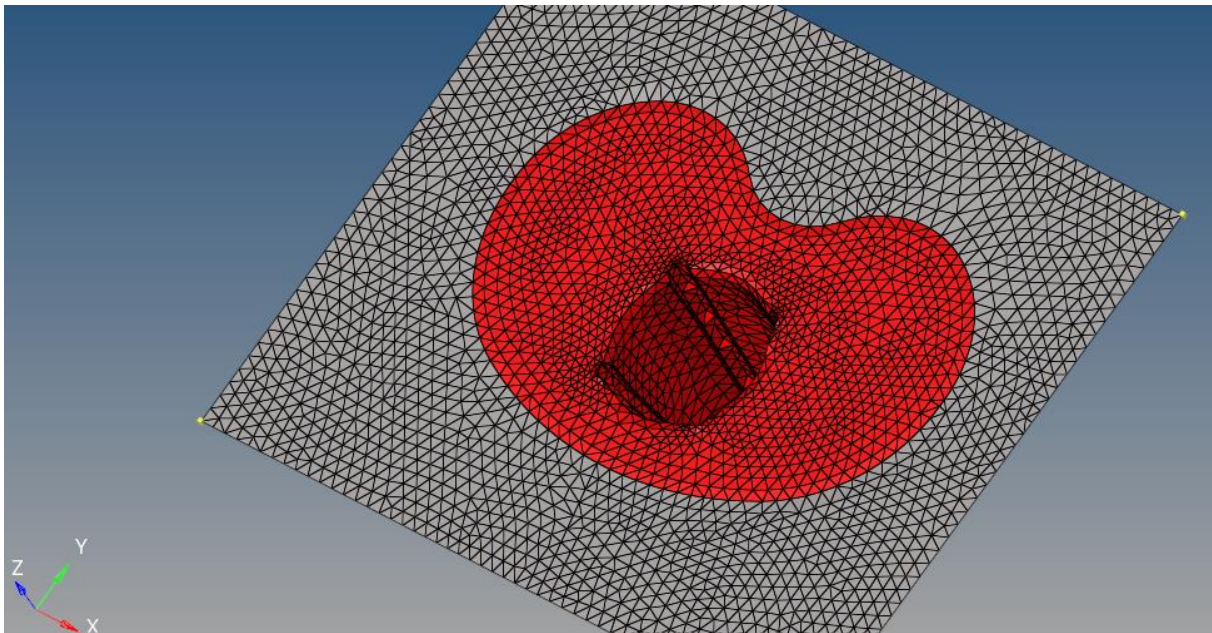
The cement layer is thus called **cementlayer_complete_43comps_flipped.stl**, but will be rotated and renamed in step 04. The cuttingguide is called **cuttingguide_0.75offset_2comp.stl**, but will also be renamed and rotated in step 04.

The insert.stp file can be imported in HyperMesh and via automesh be remeshed (QI is preferable). Then it is moved and rotated such that it is placed onto the tray (see Figure below) and saved as an stl file. This rotation/translation of the insert can be performed in any program (HyperMesh / Marc etc)
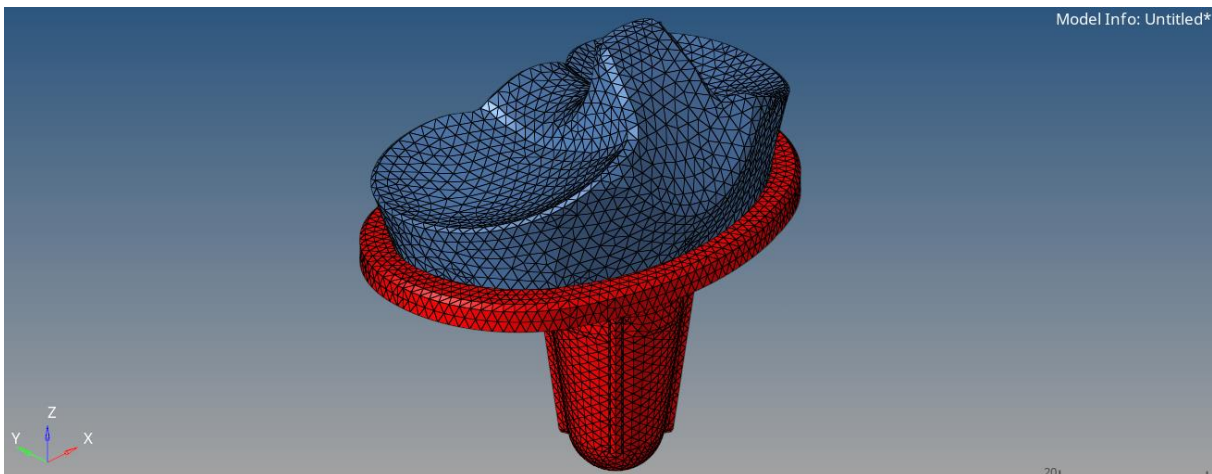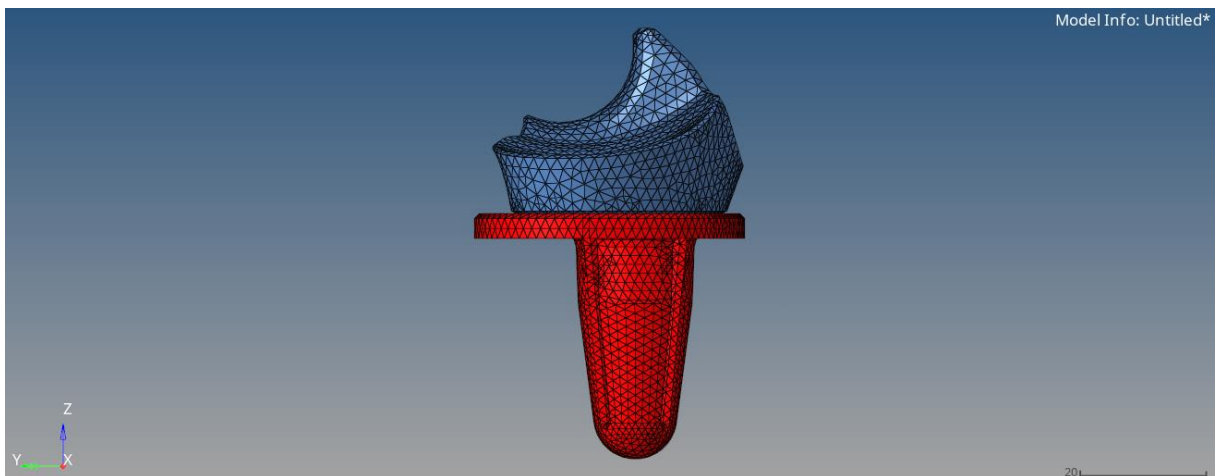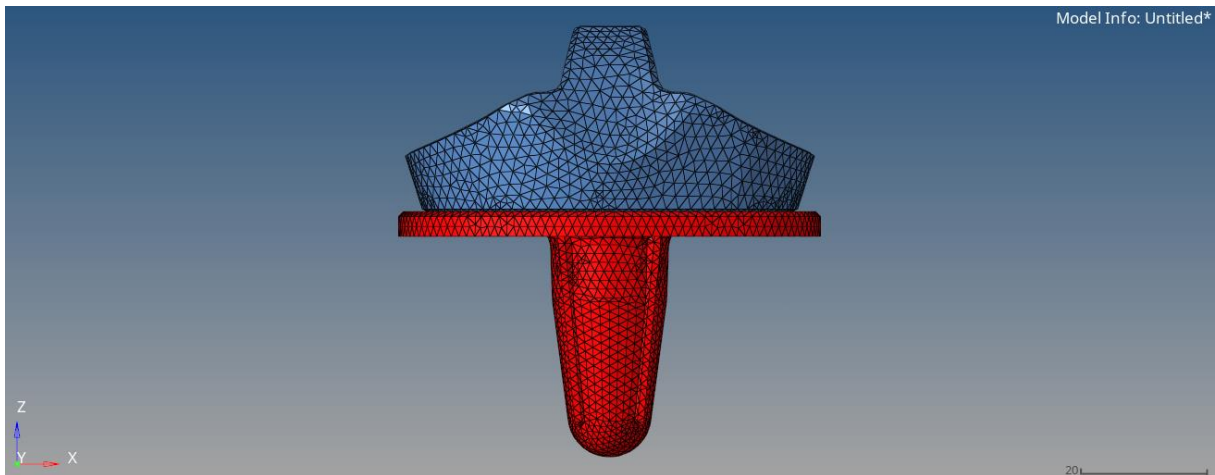
For the distal cuttingguide, create a surface through and parallel to the bottom of the cement layer and translate it 100 / 130 /150 mm (as much as you want), mesh it with automesh and save it as distal cuttingguide

4. Rotation and registration

In the Rotation and registration step, the pre-operative tibia is rotated to the ERC reference frame and the post-operative tibia is registered to the pre-operative tibia, to place the tibial tray onto the pre-operative tibia model in the correct position and orientation. The script used for this part is lvL_registration_complete_func

To do so the .stl files of the half pre-operative tibia (only the superior half), the post-operative tibia including the tibial implant and the implant itself are imported into MATLAB®.

To use this script, it is very important that the post-operative tibia and the segmented implant are in the same coordinate system with the same origin. This can be checked by opening both .stl files in HyperMesh or Marc Mentat. Also, while running, lvL_registration_complete_func.m opens a figure in which both post-operative tibia and the implant are plotted and it can be checked if they align correctly. Then shown point clouds should fall over one another. Keep in mind that the pre-operative and post-operative tibiae do not need to have the same origin!

Once all three .stl files are imported correctly, they are converted into so-called pointClouds, a value type of MATLAB® . First, the half pre-operative tibia is transformed towards the ERC reference frame. The rotation and translation that are made with this are saved in a struct called [tib]. Then, the post-operative tibia and the implant are also rotated with [tib] to get them in a similar orientation to the pre-operative tibia.

Now, the actual registration takes place. This is done with a coherent point drift (CPD) algorithm, built in in MATLAB® . With the CPD algorithm, the transfermatrix to register the post-operative tibia towards the orientation

and position of the half pre-operative tibia is found. This transfermatrix is then used to actually transfer the post-operative tibia and the implant towards the pre-operative tibia. So as a result, the segmented implant is now in the correct position and orientation on the pre-operative tibia.

Then, the implant geometry is loaded and converted to a pointCloud. Rotations around x and y axis are applied to the geometry to give it roughly the same orientation as the segmented implant. This is done to obtain more accurate results with the CPD algorithm. Once the implant geometry is in roughly the same orientation as the segmented implant, the CPD algorithm is used to find the transfer matrix to get to the position and orientation of the segmented implant. This transfer matrix is then applied to the implant geometry so that the pre-operative tibia and the implant geometry are in the correct position and orientation relative to each other.

To place the implant geometry on the tibia later on in the workflow, the cutting guides to cut the pre-operative tibia, the cement layer and the insert have to be rotated as well. Those three models are loaded and first given the same rotations around x and y as was done for the implant. Then the transfer matrix that was applied to the implant is applied to the models. So, the implant, cement layer, cutting guide and insert all have the same rotation and translation.

For the distal cuttingguide, the rotations around x and y are applied as well, but the transfer matrix is not applied. With this, the distal cuttingguide is in the correct position and perpendicular to the length axis of the tibia.

Finally, all rotated components are written to new .stl files.

5. Bone cutting

In this part of the workflow, the .stl files that were created in 3. Implant preparation and transferred to the correct position in 4. Rotation and Registration, are used to created volume meshes of the preoperative tibia.
To perform the bonecutting, tcl scripts are created. These scripts can be run in HyperMesh to almost automatically perform the bonecutting.
First, with the MATLAB® file `IL_cutbone_adjusted` two tcl scripts are created. One for the creation of the volume mesh 'tibia', the pre-operative tibia, cut with both the distal and proximal cuttingguide and one for the 'resect', which is the superior part of the tibia which gets cut of by the proximal cuttingguide. Together, 'tibia' and 'resect' form the pre-operative tibia without the part distal to the distal cuttingguide.
In the MATLAB® script `IL_cutbone_adjusted`, the .stl of the pre-op tibia to be cut, the corresponding, rotated proximal and distal cuttingguides, the template files of the tcl scripts and the locations of the resulting tcl scripts and volume meshes are input.
The script is run and then the created files 'IL_script_tibia.tcl' and 'IL_script_resect.tcl' are opened in Notepad++ or another text editor. HyperMesh is also opened.
First, the tibia is created. To do so, the first half of the tcl script, until the line "*#HIER MOETEN HANDMATIG DE ONDER EN BOVENKANT ERAF WORDEN GEHAALD*", is copied to the command section in HyperMesh. Then, with the delete option of HyperMesh, which is set to the delete faces option, the parts of the tibia under the distal cutting guide and above the proximal cutting guide (shown by lines on the tibia) are deleted. Once this is done, the second half of the tcl script can be copied and pasted into the command section of HyperMesh. With this, the resulting mesh is saved as .stl, converted to a volume mesh and then saved as .dat file.
Then, the resect part is created in a similar fashion. The first part of the `IL_script_resect.tcl` file, until the comment `#HIER MOET HANDMATIG DE ONDERKANT ERAF WORDEN GEHAALD` is copied and pasted into the command section of HyperMesh. Then, with the faces delete option, the lower part of the tibia is deleted, so that only the superior top of the tibia is left. Then the second half of the .tcl-script is copied and pasted into HyperMesh, so that again a .stl-file and a 3D .dat file are created.

6. Model set-up part 1

The created .dat files of the tibia and resect are then opened in MM. First, the jobs are deleted and a set for the tibia with all elements belonging to the tibia and a set resect with all elements of the resect part are created.

Then, all nodes are swept, so no double nodes at the surface between the tibia and resect occur. Then, all nodes are renumbered by Geometry & Mesh > Renumber > Nodes > All. Then, the resect is unselected and the tibia elements are renumbered. Then, the tibia is selected via selection control to see how many elements it has. This number is noted. Then, the elements of the set resect are renumbered starting from the number of elements in the tibia+1. Once this is done, the file is exported as a .dat file (export as Marc Input File in MM) and as .mud (save in MM).

7. Material assignment

To perform the material assignment, first the .dat file just made is loaded into MATLAB® via `IL_importDAT_MM_tibiaANDresect.m`. Then the material assignment script `IL_materass_updated_tibiaANDresect.m` is opened and run. In this file the path to the nii_info file with 00 offset, the rot2ref.mat result (from 4 Rotation and Registration) and the file location of the .restin file which will be made are given, together with the just loaded .dat file of the resect and tibia, which is a struct object.

In this file, the volume meshes of the created tibia model, the resect and tibia part are rotated back towards their original position in the .nii file. This is done by inverting the rotation to the ERC reference frame. Then, with the air-fat-muscle calibration method the info.nii is read and for every element in the volume mesh the bone mineral density is determined and registered in a so-called .restin file.

In this file the tibia+resect is rotated back towards it original position (so the rotation towards the ERC frame is inverted). Then, the greyvalues in the nii file are read out and via a calibration tool AFM-calibration, the greyvalues (HU) are calibrated towards BMD values. To do so, MATLAB® opens a graph in which you have to click on the 3 peaks, 2 with left mouse and the last one with right click. Then, a plot of the nii file in blue and the .dat in red opens. If it all works correctly, those should align. If not, check if the scaling with the voxel size in the registration part of the workflow worked correctly.

The .restin file is saved in the location given by the outputpath.

To make sure this file can be used for both the pre-operative simulation and the post-operative simulation later on, the updaterestin.m file can be run. In this script all values smaller than 0.1 are given the value 0.1 to prevent values in the restout file to become infinite. This is not needed if there are no BMD values that are 0 in the original file, but it is run to be sure.

8. Model set-up part 2
a. Pre-operative model

For the creation of the pre-operative model, the .mud file created before the material assignment is opened and saved as _preop.mud. Then the rotated .stl files of the corresponding implant and insert are opened and the tibia and resect are hidden. Then, the x and z coordinates of the node in the middle of the lowest point of the keel and the y coordinate of the lowest point in the condyles of the insert is written down. Then the model is closed (not saved!) and opened again. Then a new node is created with the x , y and z coordinates written down. This is the control node on which forces will be applied. Apply a point load to this node and apply the loads in x, y and z direction (make sure the M-L, A-P, P-D directions match!). Moreover, add a fixed displacement of 0 in x, y and z on the distal nodes of the tibia.

Then, via selection control, point flood distance 4 or 5 and surface, select the nodes on the surface of the resect on which the loads should be exerted. Then, create a set of the selected nodes. Via links, Springs & Dashpots, create very stiff springs (high spring constant: eg. 1e+09 [kg/s^2]), and a damping coefficient of 1 [kg/s], connect those between the control node and the selected nodes on the surface of the resect.

Create a material with the following properties and add this material to all elements of the bone:
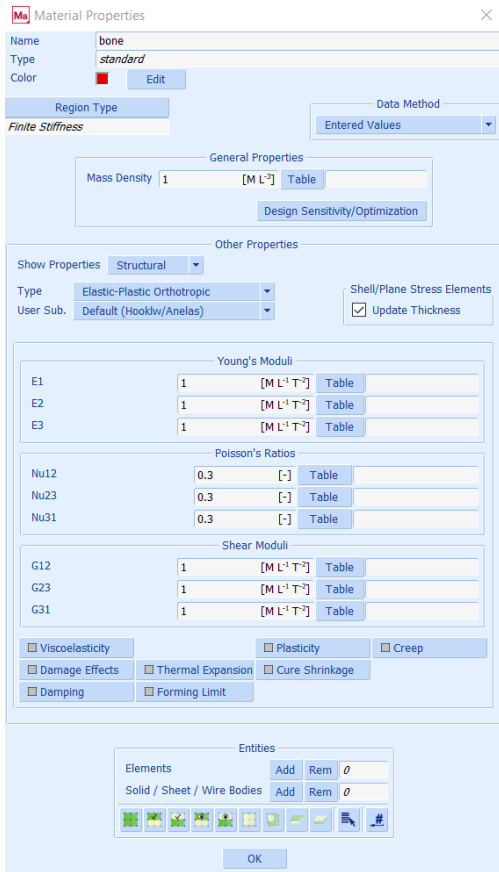
Create a load case in which both loads are selected and the Total Load case Time is 1, with #Steps 3.
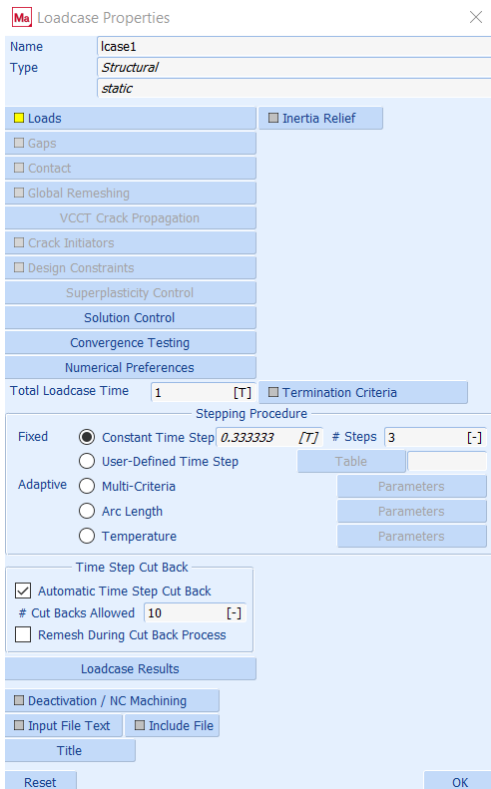
Then, create a job, select Small Strain and the load case just created. In Initial Loads only select the fixed displacement. In Job Results, select the following results

In Output File (under Job Results); select

In Job Parameters set the Version to 2007 and the Style to Old. Click Check to make sure you did not forget anything. Save this file as _preop.mud and export the file as pre.dat.

b. Post-operative model

To set up the post operative model in MM, first, all implant components (in .stl format) are opened in HyperMesh and volume meshed (3D >.Tetra mesh > comps, simple pyramid >mesh). Then saved as .dat file (Export Solver Deck > File Type Marc > Template Marc 3D). This is done via a .tcl script; volumemesh_hypermesh.tcl

Then, in MM preop.mud file is opened again, save as postop.mud. The resect is deleted, as well as all links created in the preop model. The control node with the load on it is retained. Then, the cement layer in .dat format is imported. A set of the elements is created. If needed, the component is mirrored by Geometry & Mesh > Move > Scale, x = 1, y = 1, z = -1 and flipped by Geometry & Mesh > Check > Flip Elements > set of elements of the cement layer. Then, the job of the cement later .dat (probably called job1_1) is deleted. Then the elements of the cement layer are renumbered. The amount of elements in the tibia set is checked and with Geometry & Mesh > Renumber, the cement layer elements are renumbered from the amount of elements in the tibia + 1. Then, the implant/tray is imported, a set of its elements is created and it also mirrored if needed, its job is deleted and the implant is renumbered from the number of elements of the tibia and cement layer +1. The same is then done for the insert.

Once all components are in place, select the nodes on the surface of the insert on which the loads should be exerted. Do this via selection control, point flood distance 4 or 5 and surface. Then, create a set of the selected nodes. Via links, Springs & Dashpots, create very stiff springs (high spring constant: eg. 1e+09 [kg/s^2]), and a damping coefficient of 1 [kg/s], connect those between the control node and the selected nodes on the surface of the insert. In this project this step was left out and two point loads were placed directly on the tray.

Perform a sweep between the lower surface of the tray and the uppersurface of the cementlayer by first selecting the nodes on both surfaces and then sweeping those.

Create three new materials by copying the bone material which already exists. Rename those new materials to cement, tray and insert and assign those materials to the corresponding element sets. Then, in the section Contact, create four contact bodies, tibia, cement, tray and insert (in that order!). Then create a contact table and set all Default Contact to Glued. Then, in jobs, go to Contact Control, uncheck the friction box and select the contact table under Initial Contact.

Save this file as _postop.mud and export as post.dat.

9. Simulation

a. Pre-operative model

For the pre-operative simulation a ptr.ctrl file and a pre.f file are needed next to the created .dat file and the .restin file. The .ctrl file can be created with writectrl.m or by adjusting the file by hand. The correct number of elements in the model has to be filled in and IREMTYP should be set to 0. The pre.f file (Fortran file) contains all subroutines and is ready to use. Make sure all filelocations in the file direct to the correct folders. In the bottom .dat file the three loading conditions are shown. Manually adjust those with the loads in x, y and z you need and save. Those 4 files can then be run on the work station with

```
cd folder_containing_the_4_files && marc2007r1 -j pre.dat -u pre.f
```

b. Post-operative model

For the post-operative model again a post.ctrl file, the post.f file, a new post.restin file and the created post.dat file are needed. In the post.ctrl file, use the pre.ctrl file, but adjust the number of elements to the number of elements of the tibia (without resect) and set IREMTYP to 1. In de post.f file set the filelocations to the correct directories. In the bottom of the .dat file, replace the empty forces with the forces wanted on the point loads, copy this one increment present 600 times and save. For the .restin file, download the pre.restout file and delete the information of the elements you do not have in your postop model (so the same number of elements as in the .ctrl file), then save as post.restin. Those 4 files can then be run on the work station with

```
cd folder_containing_the_4_files && marc2007r1 -j post.dat -u post.f
```

10. Post-processing

In postprocessing, first download all files from the workstation. Then in MATLAB® , run the file IL_selectrestout to select the correct restout for post-operative time interval wanted. Then, to convert the model elements into a matrix, a mask is made. With sedMask.m, select the boundaries of the mask in matrix d, by trial and error. The boundaries are in there like: d = [PD left, AP bottom, AP left; PD right, AP/PD top, AP right].

Then open IL_postprocessing_test, change the name of you files with ctrl+F and set the side of the tibia to 'l' or 'r' (left or right leg). Running this file then creates virtual DEXA images at all time points selected and calculated the DEXA score in 3 regions of interest via subscript IL_minoda_roi.

B – Scripts needed per step in Workflow

1. Segmentation
- **lvL_dcm2nii_multiple.m**
    - **dcmextread.m** the mirroring is deleted in this script!
    - **lvL_dcm2nii.m**
    - **lvL_dcm2nii_2.m**
- Autosegmentation workstation
- Manual adjustments Slicer 3D
- **hwremesh.m** → remesh the .stl output of the segmenations to wanted element size 2 mm

2. Rotation and registration
- **lvL_registration_complete_func.m**

3. Bone cutting
- **IL_cutbone_adjusted.m** for the creations of the .tcl files
    - **IL_template_tibia.tcl**
    - **IL_script_tibia.tcl**
    - **IL_template_resect.tcl**
    - **IL_script_resect.tcl**

4. Model set-up 1
- **sweepandrenumbernodesNOTelements.proc** could be used to import the tibia and resect files from the bone cutting into Marc Mentat and to automatically create sets, perform sweeping and renumber the nodes. The elements have to be renumbered as well, <u>but this has to be performed manually</u>

5. Material assignment
- **IL_importDAT_MM_tibiaANDresect.m**
- **IL_materass_updated_tibiaANDresect.m**

6. Model set-up 2
- In this part of the workflow, no files are needed. Everything is done manually in HyperMesh and Marc.

7. Simulation
- **writectrl.m** to create the .ctrl file, but could also be done by hand
- **writerestin.m** could be used to get post.restin file out of pre.restout, by doing this manually is faster

8. Post-processing
- **IL_selectrestout.m**
- **IL_postprocessing_test.m**
    - **IL_minoda_roi.m**

C – Load cases applied to the post-operative model

In Table C.1 the absolute loads that where applied in the load cases per model are shown. All these loads are peak loads of each of the mentioned activities, scaled to the body weight of the patient. Each of the increments applied in the simulation was a combination of the three peak loads. During simulation, these loads were all repeatedly placed onto the model.

Table C.1: loads applied to the models in absolute values

activity	Medial X (AP) [N]	Medial Y (PD) [N]	Medial Z (ML) [N]	Lateral X (AP) [N]	Lateral Y (PD)[N]	Lateral Z (ML) [N]
No14 Gait	-1.996E+01	-1.635E+03	-4.760E+00	-1.996E+01	-1.890E+02	-4.760E+00
No14 Knee bend	-3.550E+00	-6.131E+02	1.664E+01	-3.550E+00	-1.188E+03	1.664E+01
No14 Stairs down	1.777E+01	-1.546E+03	-3.364E+00	1.777E+01	-7.732E+02	-3.364E+00
No15 Gait	-1.987E+01	-1.517E+03	4.740E+00	-1.987E+01	-2.997E+02	4.740E+00
No15 Knee bend	-3.535E+00	-6.548E+02	-1.656E+01	-3.535E+00	-1.139E+03	-1.656E+01
No15 Stairs down	1.769E+01	-1.480E+03	3.350E+00	1.769E+01	-8.295E+02	3.350E+00
No16 Gait	-1.658E+01	-1.238E+03	3.956E+00	-1.658E+01	-2.780E+02	3.956E+00
No16 Knee bend	-2.950E+00	-5.576E+02	-1.382E+01	-2.950E+00	-9.392E+02	-1.382E+01
No16 Stairs down	1.476E+01	-1.220E+03	2.796E+00	1.476E+01	-7.071E+02	2.796E+00
No19 Gait	-1.547E+01	-1.100E+03	-3.690E+00	-1.547E+01	-3.141E+02	-3.690E+00
No19 Knee bend	-2.752E+00	-5.419E+02	1.289E+01	-2.752E+00	-8.543E+02	1.289E+01
No19 Stairs down	1.377E+01	-1.109E+03	-2.608E+00	1.377E+01	-6.888E+02	-2.608E+00
No20 Gait	-1.515E+01	-1.196E+03	3.615E+00	-1.515E+01	-1.894E+02	3.615E+00
No20 Knee bend	-2.696E+00	-4.838E+02	-1.263E+01	-2.696E+00	-8.840E+02	-1.263E+01
No20 Stairs down	1.349E+01	-1.150E+03	2.555E+00	1.349E+01	-6.116E+02	2.555E+00

D – Virtual DEXA results

In the Figures D.1 – D.70 below, all virtual DEXA results of the five patients are shown. For each time interval, a virtual DEXA in anteroposterior view and a virtual DEXA in mediolateral view was created.

No14
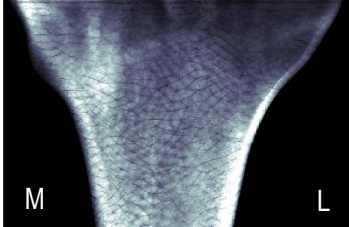

Figure D.1: pre-operative No14 AP view
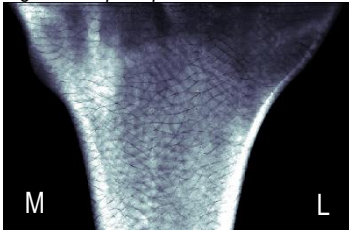

*Figure D.2: 2 weeks No14 AP*
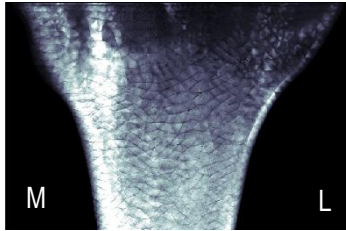
Figure D.3: 6 months No14 AP
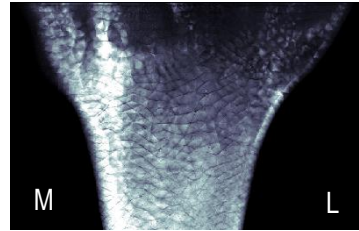
Figure D.4: 12 months No14 AP
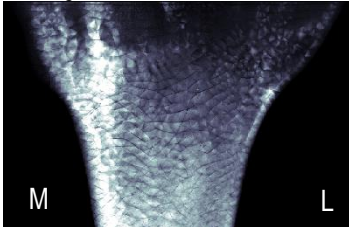
Figure 13: D.5 months No14 AP
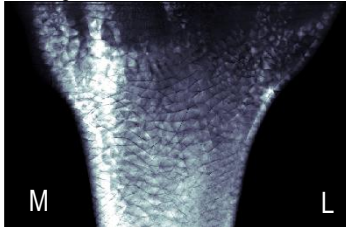
Figure D.6: 3 years No14 AP
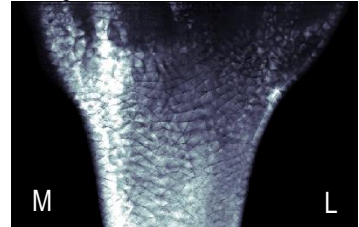
Figure D.7: 5 years No14 AP
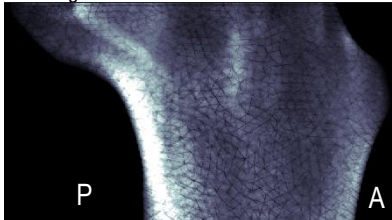
Figure D.8: pre-operative MLNo14 view
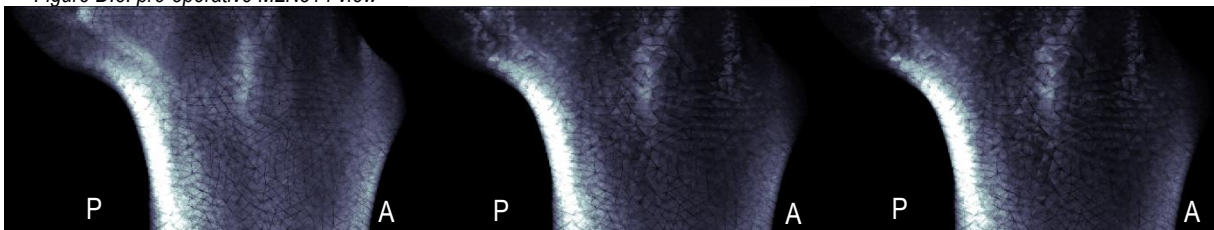
Figure D.9: 2 weeks No14 ML

*Figure D.10: 6 months No14 ML*

Figure D.11: 12 months No14 ML
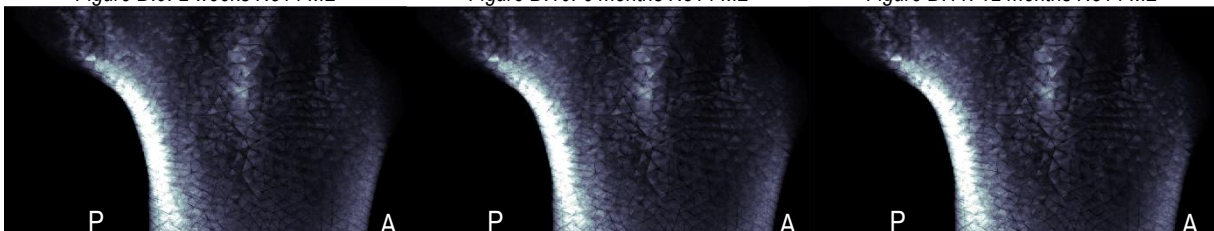
Figure D.12: 24 months No14 ML

Figure D.13: 3 years No14 ML

Figure D.14: 5 years No14 ML

No15
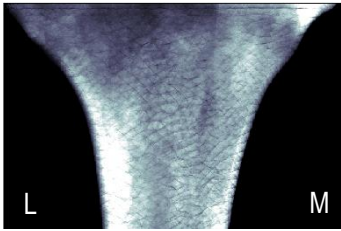
Figure D.15: pre-operative No15 AP view
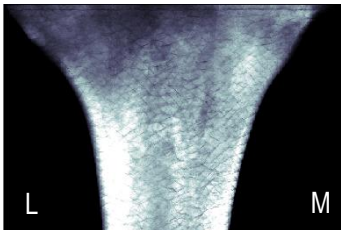
Figure D.16: 2 weeks No15 AP
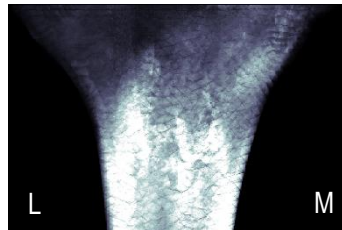
Figure D.17: 6 months No15 AP
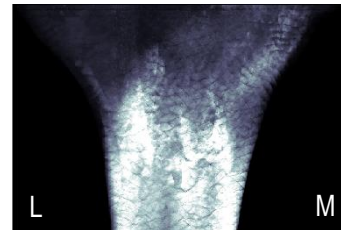
D.18: 12 months No15 AP
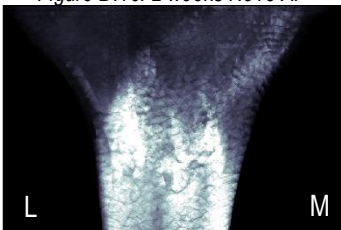
Figure D.19: 24 months No15 AP
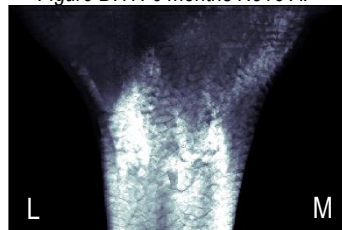
Figure D.20: 3 years No15 AP
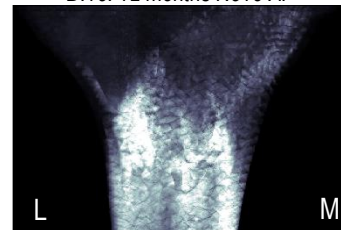
Figure D.21: 5 years No15 AP
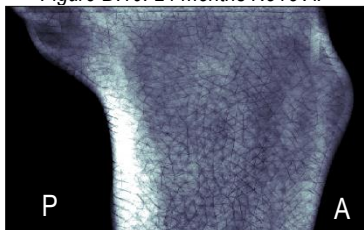
Figure D.22: pre-operative MLNo15 view
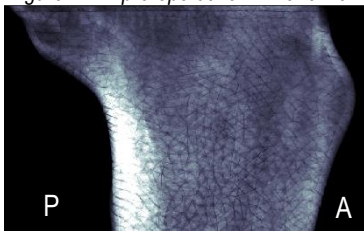
Figure D.23: 2 weeks No15 ML

Figure D.24: 6 months No15 ML

Figure D.25: 12 months No15 ML

Figure D.26: 24 months No15 ML

Figure D.27: 3 years No15 ML
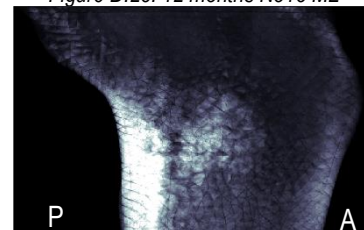
Figure D.28: 5 years No15 ML

No16
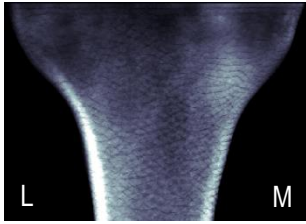
Figure D.29: pre-operative No16 AP view
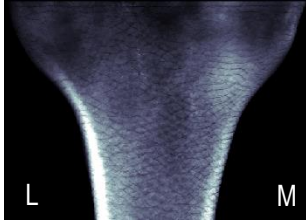
Figure D.30: 2 weeks No16 AP
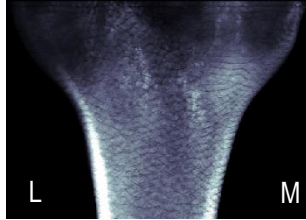
Figure D.31: 6 months No16 AP
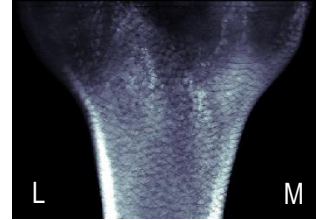
*Figure D.32: 12 months No16 AP*
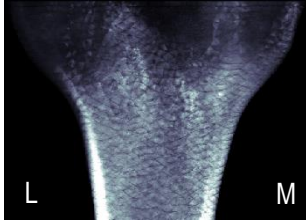
*Figure D.33: 24 months No16 AP*
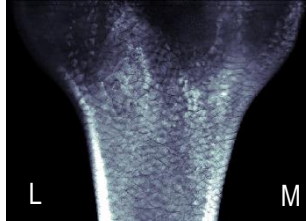
Figure D.34: 3 years No16 AP
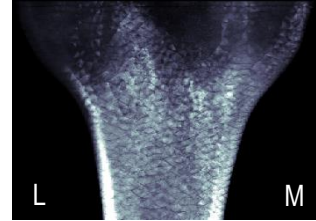
Figure D.35: 5 years No16 AP
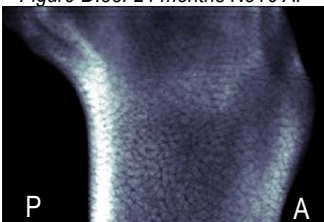
Figure D.36: pre-operative MLNo16 view
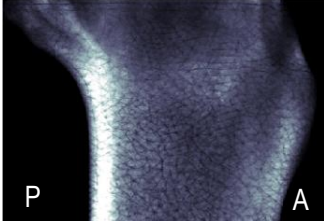
Figure D.37: 2 weeks No16 ML

Figure D.38: 6 months No16 ML

Figure D.39: 12 months No16 ML
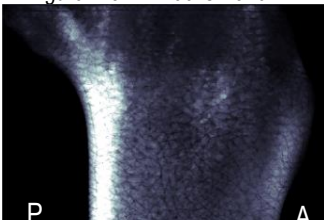
Figure D.40: 24 months No16 ML
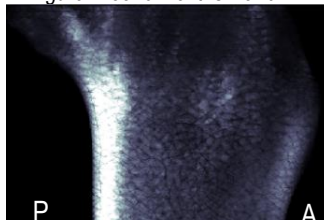
Figure D.41: 3 years No16 ML
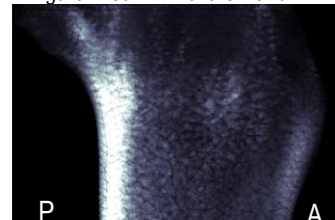
Figure D.42: 5 years No16 ML

No19
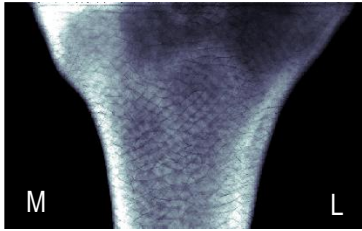
Figure D.43: pre-operative No19 AP view
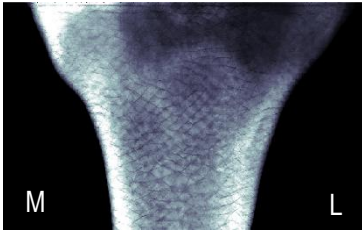
Figure D.44: 2 weeks No19 AP
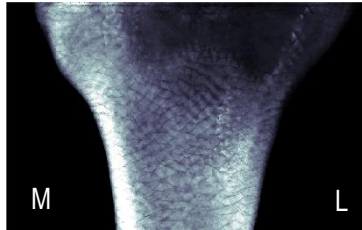
Figure D.45: 6 months No19 AP
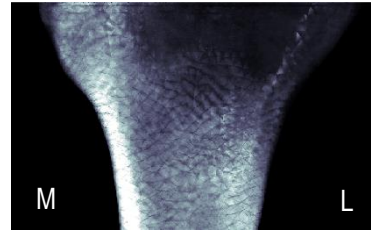
Figure D.46: 12 months No19 AP
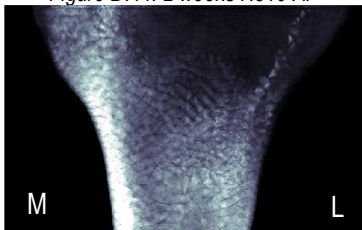
Figure D.47: 24 months No19 AP
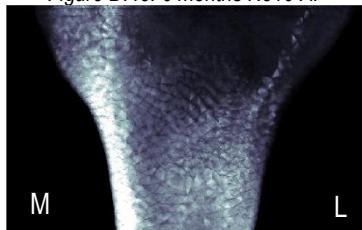
*Figure D.48: 3 years No19 AP*
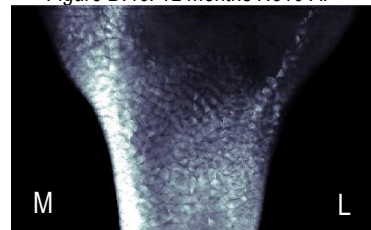
Figure D.49: 5 years No19 AP
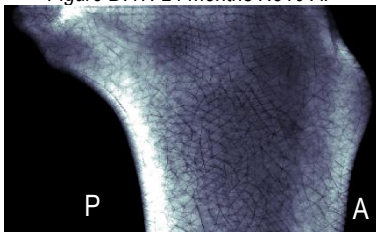
Figure D.50: pre-operative MLNo19 view
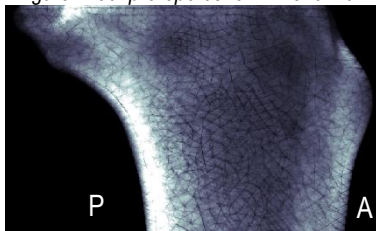
Figure D.51: 2 weeks No19 ML
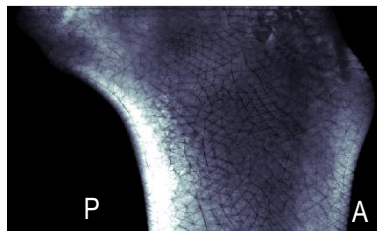
Figure D.52: 6 months No19 ML
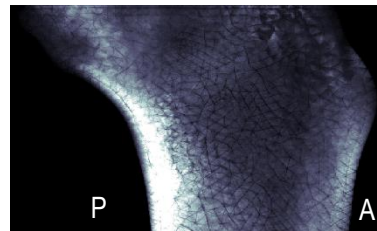
Figure D.53: 12 months No19 ML
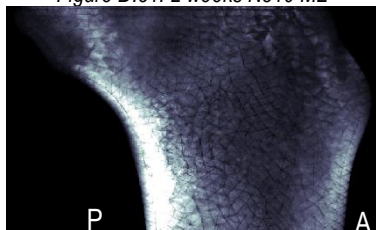
Figure D.54: 24 months No19 ML
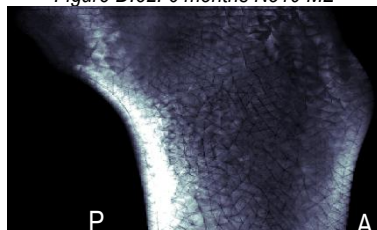
Figure D.55: 3 years No19 ML
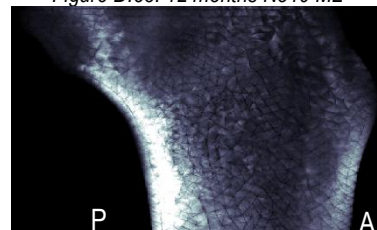
Figure D.56: 5 years No19 ML

No20
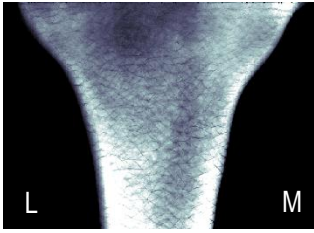
Figure D.57: pre-operative No20 AP view

Figure D.58: 2 weeks No20 AP
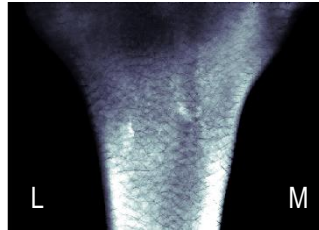
Figure D.59: 6 months No20 AP
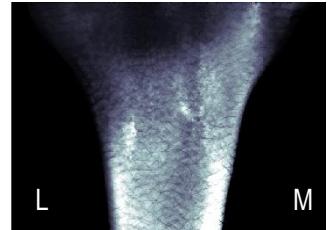
Figure D.60: 12 months No20 AP
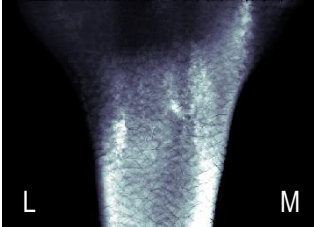
Figure D.61: 24 months No20 AP
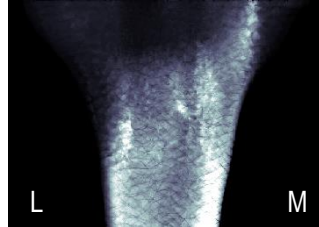
Figure D.62: 3 years No20 AP
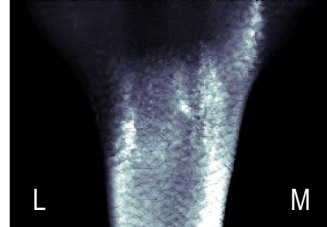
Figure D.63: 5 years No20 AP
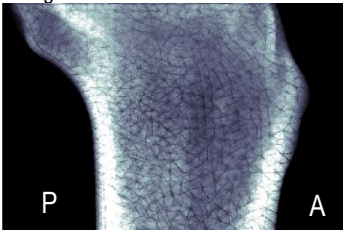
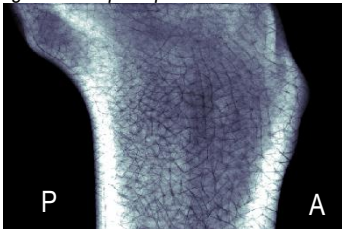*Figure D.64: pre-operative MLNo20 view*
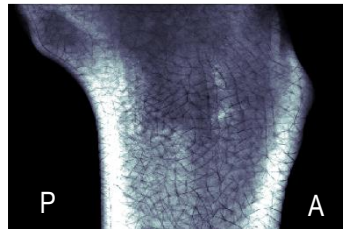

Figure D.65: 2 weeks No20 ML
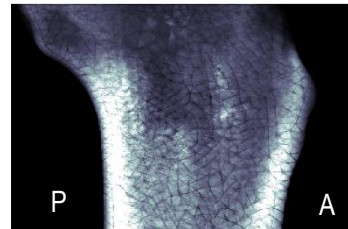

Figure D.66: 6 months No20 ML
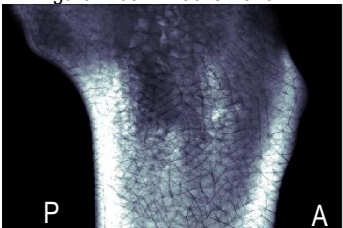

Figure D.67: 12 months No20 ML

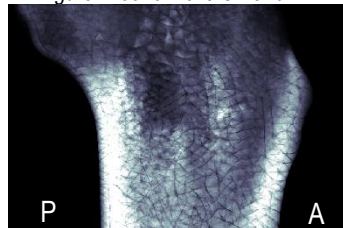*Figure D.68: 24 months No20 ML*
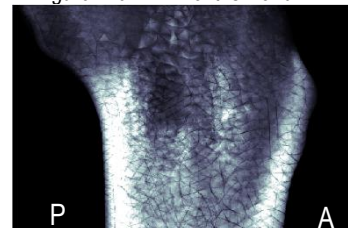

Figure D.69: 3 years No20 ML

Figure D.70: 5 years No20 ML

E – Sensitivity analysis load placement No20

For model No20, six variations in the placement of the point loads were simulated. This was done to see what the effect of the variation of placement of the medial point load is. The first three simulations were the variations decribed in the Methods, the fourth, fifth and sixth are all displacements of the medial point load only. All described displacements are relative to the model in the first simulaiton; the In the fourth simulation, (4) the medial point load is placed 1 element more towards the keel. In the fifth simulation (5), the medial point load is placed one element more towards the keel and 2 elements more posterior. The sixth simulation (6) has the medial point load 4 elements more posterior and 1 element more lateral to the tibial axis, towards the edge of the implant. The exact placement of the point loads in each of those simulations is shown in Figure E.1.
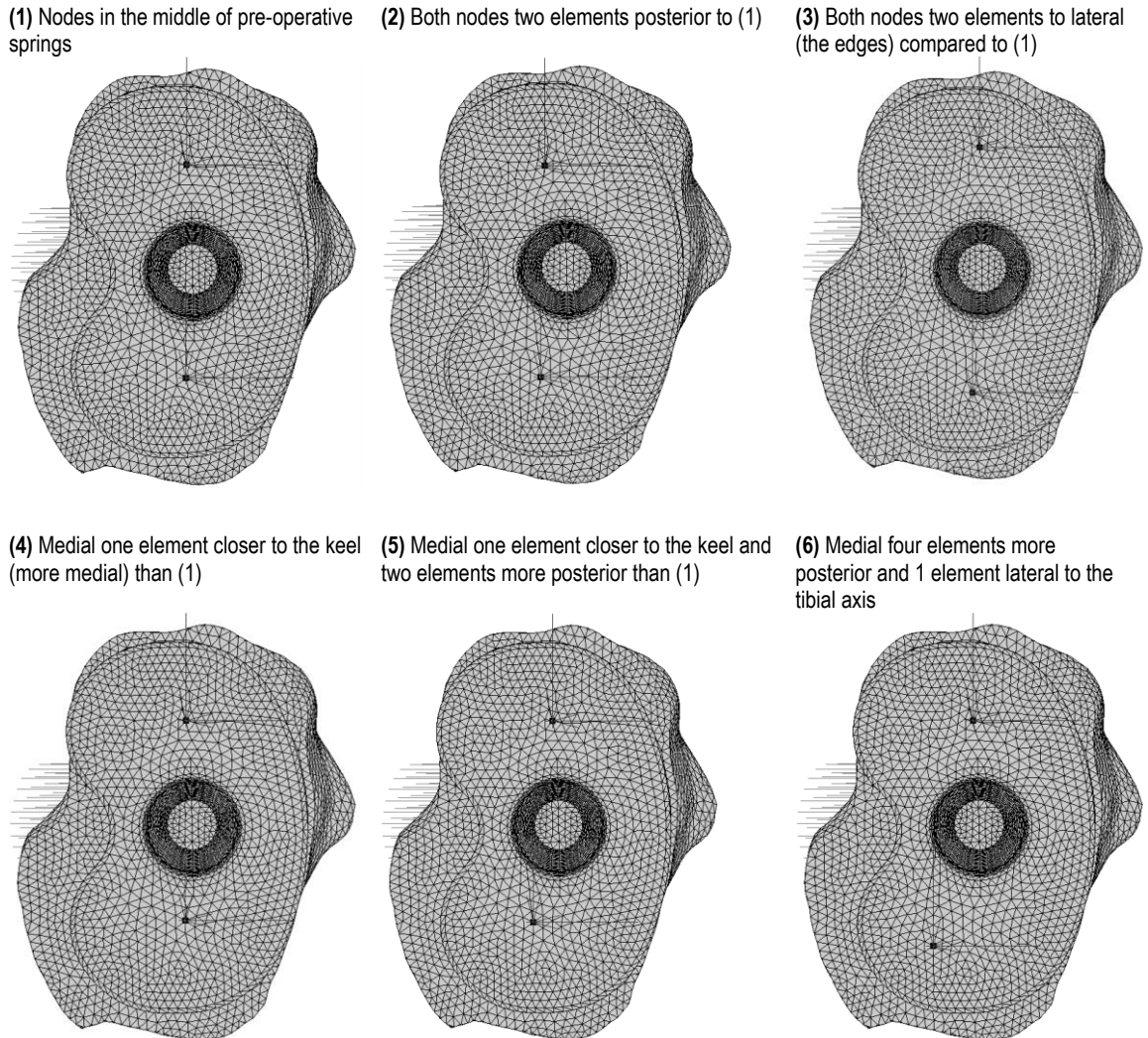
(1) Nodes in the middle of pre-operative springs

(2) Both nodes two elements posterior to (1)

(3) Both nodes two elements to lateral (the edges) compared to (1)

(4) Medial one element closer to the keel (more medial) than (1)

(5) Medial one element closer to the keel and two elements more posterior than (1)

(6) Medial four elements more posterior and 1 element lateral to the tibial axis

Figure E.1: Placement of point loads in all simulations of No20

The results of all 6 simulations are displayed in Figure E.2. In this figure it is clear that the variations in the placements of the point loads affect the medial BMD (in red) most and that the distal and lateral BMD show similar behavior over the years for all six simulations.
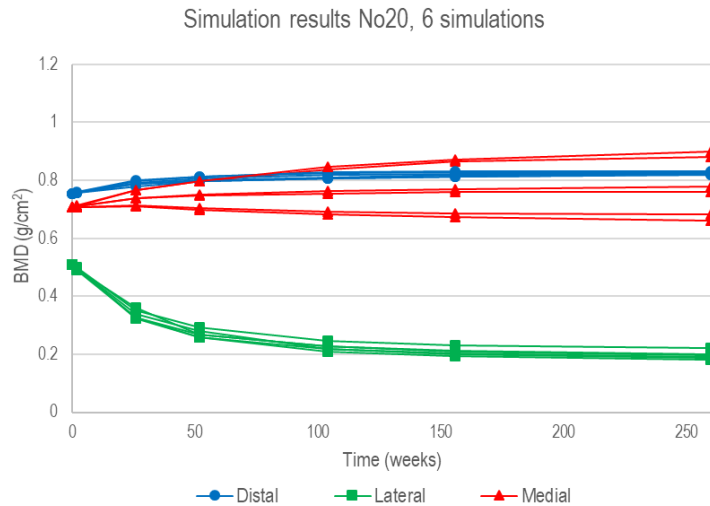
Figure E.2: Simulation results No20 with the results
for the medial ROI in shades of red, the distal ROI in blue and the lateral ROI in green

In Figure E.3 the simulation results of the medial region of interest are zoomed in and shown. In this figure, three different patterns are present. The BMD values from the first (yellow) and second (green) simulation, respectively, show a small increase in BMD of approximately 0.06 g/cm^2 over the years. The third (blue) and sixth (green) variation, show a faster increase and have an increase of 0.20 g/cm^2 average after 5 years. The last two simulations, the fourth and fifth show are almost stable in the first 6 months after which both decrease with 0.03 g/cm^2 average.
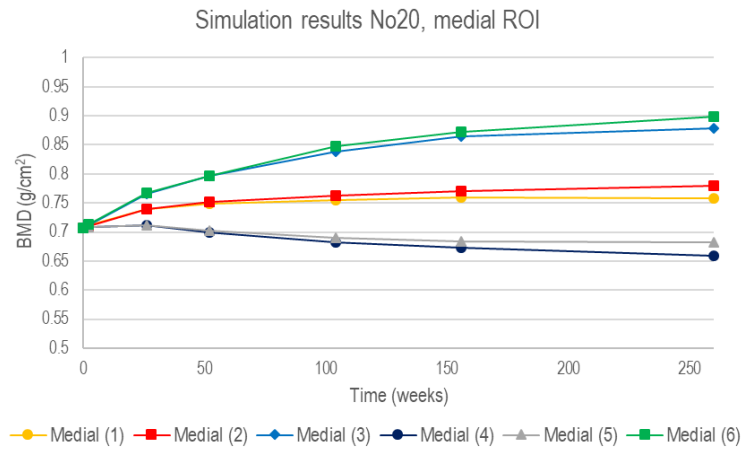

Figure E.3: Results of simulations No20 for the medial region only